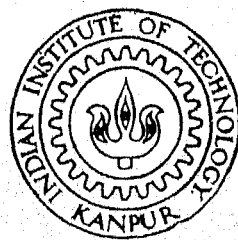


**MATHEMATICAL MODELLING
OF FLOW AND RESIDENCE TIME DISTRIBUTION IN
DIFFERENT TUNDISH DESIGNS**

by
ASHISH ROBERT

MME
1997
M
ROB
MAT



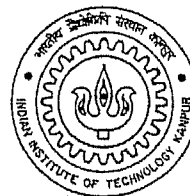
Department of Materials and Metallurgical Engineering
INDIAN INSTITUTE OF TECHNOLOGY KANPUR
DECEMBER, 1997

MATHEMATICAL MODELLING OF FLOW AND RESIDENCE TIME DISTRIBUTION IN DIFFERENT TUNDISH DESIGNS

A Thesis Submitted
in Partial Fulfillment of the Requirements
for the Degree of
MASTER OF TECHNOLOGY

by

ASHISH ROBERT



to the
**DEPARTMENT OF MATERIALS AND
METALLURGICAL ENGINEERING**
INDIAN INSTITUTE OF TECHNOLOGY, KANPUR

January, 1998

CERTIFICATE

This is to certify that the present work '**MATHEMATICAL MODELLING OF FLOW AND RESIDENCE TIME DISTRIBUTION IN DIFFERENT TUNDISH DESIGNS**' has been carried out by Mr. Ashish Robert (Roll No: 9520602) towards his M.Tech, dissertation under my supervision and that this has not been submitted elsewhere for a degree.

January 5th, 1997

Dipak Mazumdar
(Prof. Dipak Mazumdar)

Department of Materials and Metallurgical Engineering
Indian Institute of Technology, Kanpur.

ACKNOWLEDGEMENT

The author wishes to express his profound and sincere gratitude to Professor Dipak Mazumdar for his able guidance, valuable suggestions during the course of this study. The author would also like to take this opportunity to gratefully acknowledge the financial support received from R.D.C.I.S (SAIL), Ranchi, to carry out the research work successfully.

He would also like to thank his friends and well wishers, for making his stay at Kanpur a memorable one.

Finally, he would like to thank his mother and family members for their support and motivation.

TABLE OF CONTENTS

Abstract

List of Symbols

List of Figures

List of Tables

Page No.

CHAPTER 1

INTRODUCTION TO THE THESIS

1.1 Introduction	1
1.2 Characteristics of metallurgical tundish systems	2
1.3 Previous work	8
1.3 Scope of the Present Work	11
1.4 Layout of the Thesis	12

CHAPTER 2

MATHEMATICAL MODELLING

2.1 Introduction	13
2.2 Assumption in modelling	14
2.3 Description of the steady state two phase three dimensional turbulent flow model	
2.3.1 The liquid phase equation of motion	15
2.3.2 The turbulence model	16
2.3.3 Equation of motion of gas phase	18
2.3.5 Estimation of Gas volume fraction	20
2.3.6 Estimation of the interphase drag and the turbulence production due to bubbles	20
2.3.4 Equation of tracer dispersion	22
2.4 The boundary conditions	22
2.5 The general differential equations	27
2.6 The grid arrangement	28
2.7 The numerical solution procedure	31
2.8 Modelling of the inclined tundish wall and flow modification devices	33

CHAPTER3**RESULTS AND DISCUSSION****3.1 Assessment of the computational procedure developed**

3.1.1 Laminar flow in an enclosed cavity	40
3.1.2 Entrance length prediction for laminar flow	46
3.1.3 Prediction of bubble rise in a stagnant liquid	49

3.2 Modelling of flow and Residence Time Distributions in steelmaking tundish systems

3.2.1 Flow and RTD in a single strand tundish	53
3.2.2. Flow and RTD in a two strand slab casting tundish	62
3.2.3 Flow and RTD in the six strand billet casting tundish	76

CHAPTER 4**CONCLUDING REMARKS****CHAPTER 5****RECOMMENDATIONS FOR FUTURE WORK****REFERENCES**

ABSTRACT

Name of student: Ashish Robert Roll No: 9520602
Degree for which submitted: M.Tech. Department: MME
Name of the thesis supervisor: Dr. Dipak Mazumdar, Professor
Month and year of submission: Jan, 1998
Text of Abstract begins here 

Visual opacity of molten metals, relatively large size of the industrial metal processing units and high operating temperatures often preclude direct experimental observations. As a natural consequence of these, mathematical modelling has emerged in recent years as a key process analysis tool in the area of metals and materials processing operations. More specifically, in the area of steelmaking, transport type models have been frequently applied to characterise liquid steel flow in the reactor vessel and to estimate the rates of the associated heat and mass transfer processes such as, melting, dissolution, dispersion, mixing etc. It is rather well known that various unit processes in steelmaking are inherently multi-dimensional (steady or transient) and multi-phase (slag-metal-gas) in nature. Consequently, in many instances, for effective and realistic process simulation two phase three dimensional transport type models are required (for example, fluid flow in tundish, CC mould, degassing units etc.). The present work therefore concerns with the development of a steady state, two phase, three dimensional, turbulent flow calculation procedure with the primary objective of predicting melt flow and RTD characteristic in steelmaking tundish systems. To develop the present two phase model, a combined Eulerian-Lagrangian approach has been adopted in which, the trajectories of the individual bubbles are stochastically determined in space by solving three additional differential equations (essentially Newton's second law of motion).

Thus as the first step, governing equations of liquid phase and gas phase motions together with the equation of tracer dispersion were derived in three dimension in the Cartesian co-ordinate system in conjunction with their associated boundary conditions. To characterise

liquid phase turbulence, the two equation $k-\epsilon$ turbulence model of Launder and Spalding was applied. The governing equations flow, turbulence and tracer dispersion were solved numerically adapting a control volume based finite difference procedure embodying the SIMPLE (Semi Implicit Method for Pressure Linked Equations) algorithm of Patankar and Spalding. Prior to the analysis of melt flow and RTD in tundish, the results from the three dimensional model were evaluated against a set of benchmark solutions. This for example includes, flow in a cubic cavity, entrance length against Reynolds number in ducts, prediction of bubble rise in a stagnant fluid etc. The primary objective of such an exercise was to demonstrate the internal consistency of the software developed and to assess the accuracy of numerical prediction. Comparisons between bench mark and corresponding numerical solutions indicated excellent agreement between the two. Finally, the three dimensional turbulent flow model was applied to predict the flow behaviour and RTD (Residence Time Distribution) in three different tundish designs. This for example included a single strand slab casting tundish, a two strand slab casting tundish and a skewed delta shaped six strand tundish, with or without flow control devices (viz., dams, weirs, dams + weirs etc.). For all the tundish designs, numerically predicted flow and RTD were compared with the available experimental data reported in the literature and reasonably good agreement was achieved between the two. In addition to these, the role of auxilliary gas injection in the two strand tundish was assessed from a purely computational stand point with the aid of the present two phase model.

LIST OF SYMBOLS

$A_P, A_E, A_W, A_N, A_S, A_T, A_B$: coefficients of discretization equation representing the effect of convection and diffusion
A_{nb}	: summation of all neighbour point coefficients
C, C_i	: concentration of the tracer, $kg\ m^{-3}$
C_o	: average concentration of the tracer, $kg\ m^{-3}$
$C_1, C_2, C_\mu, \sigma_k, \sigma_\epsilon$: constants of the k- ϵ model
C_b	: constant defined by Eq.(2.21)
C_D	: drag coefficient
d_b	: bubble diameter, m
E	: roughness parameter
E_θ	: Eotvos number ($= g \rho_l d_b^2 / \sigma$)
F_x, F_y, F_z	: interphase drag forces in the Navier Stokes equations
g	: acceleration due to gravity, $m\ s^{-2}$
G_k	: volumetric rate of turbulence generation
K	: constant of proportionality
k	: turbulent kinetic energy, $m^2 s^{-2}$
L	: depth of the liquid in the vessel, m
N	: number of bubbles in a train in a given control volume
p	: dynamic pressure with respect to the local hydro-static

	pressure, Pa
Pe	: Peclet number
P_b	: volumetric rate of turbulence generation due to bubbles
Q	: gas flow rate corrected to mean height and pressure of the liquid, $m^3 s^{-1}$
Re	: Reynolds number
S	: the source term in the discretization equation
S_p	: the slope of the linearized source term
S_c	: constant part of the linearized source term
S_u	: source term in the equation of motion in x direction
S_v	: source term in the equation of motion in y direction
S_w	: source term in the equation of motion in z direction
t	: time, s
t_{avg}	: average residence time, s
t_{min}	: minimum breakthrough time, s
t_{peak}	: peak concentration time, s
t_r	: nominal residence time, s
$t_{r, m}$: residence time of mth bubble, s
Tu	: intensity of turbulence
u	: x component of velocity, $m s^{-1}$
U	: instantaneous liquid velocity component in axial direction, $m s^{-1}$
U_b	: resultant bubble velocity, $m s^{-1}$

U_f	: resultant instantaneous liquid velocity, $m s^{-1}$
U_r	: relative velocity vector, $m s^{-1}$
u_τ	: friction velocity, $m s^{-1}$
v	: y component of velocity, $m s^{-1}$
V	: y component of instantaneous liquid velocity, $m s^{-1}$
$V_{B,x}$: instantaneous bubble velocity in the x direction, $m s^{-1}$
$V_{B,y}$: instantaneous bubble velocity in the y direction, $m s^{-1}$
$V_{B,z}$: instantaneous bubble velocity in the z direction, $m s^{-1}$
V_d	: dead volume, m^3
V_{dp}	: dispersed plug volume, m^3
V_m	: well mixed volume, m^3
w	: z component of velocity, $m s^{-1}$
W_B	: work per unit time due to buoyancy, $kg m^2 s^{-3}$
W_g	: kinetic energy per unit time of injected gas at orifice of vessel, $kg m^2 s^{-3}$
y^+	: dimensionless distance normal to the wall
Δt	: incremental time step in the trajectory, s
ΔV_{cv}	: volume of the control volume, m^3
$\Delta X, \Delta Y, \Delta Z$: length of control volume faces in three mutually perpendicular directions, m
$\delta X_e, \delta X_w, \delta Y_n, \delta Y_s, \delta Z_t, \delta Z_b$: distance between the various nodes in the three mutually perpendicular coordinate axis, m

α_g	: gas volume fraction
α_l	: liquid volume fraction
ρ_g	: density of gas, $kg\ m^{-3}$
ρ_l	: density of liquid, $kg\ m^{-3}$
ρ_s	: density of the solid, $kg\ m^{-3}$
μ_l, μ_0	: liquid / bulk medium viscosity, $kg\ m^{-1}s^{-1}$
μ_T	: turbulent viscosity, $kg\ m^{-1}s^{-1}$
μ_e	: effective viscosity, $kg\ m^{-1}s^{-1}$
ϵ	: rate of turbulence kinetic energy dissipation, m^2s^{-3}
ϕ	: general dependent variable of the discretization equation
$\phi_P, \phi_E, \phi_W, \phi_N, \phi_S, \phi_T, \phi_B$: values of ϕ at the various nodes in the general discretization equation
ϕ_{nb}	: summation of neighbour point ϕ' s
κ	: van Karmen constant
τ_w	: shear stress close to the wall, $kg\ m^{-1}s^{-2}$
Γ	: diffusion coefficient, $kg\ m^{-1}s^{-1}$

LIST OF FIGURES

Fig.(1.1) : The general methodology of mathematical model development [2].

Fig.(1.2) : Schematic representation of the continuous casting process.

Fig.(1.3) : A typical "C" curve

Fig.(2.1) : Schematic of a section of Eulerian grid network intercepted by a bubble trajectory (2-D representation).

Fig.(2.2) : Schematic of the one quarter of the tundish illustrating the surfaces on which boundary conditions were applied.

Fig.(2.3) : Schematic representation of the procedure applied for the near wall region on flow variables and turbulence parameters.

Fig.(2.4) : A typical three dimensional, scalar control volume and various nomenclature used in the Cartesian co-ordinate system.

Fig.(2.5) : Scalar and staggered control volumes in three dimensional Cartesian co-ordinate system.

Fig.(2.6) : The characteristics of calculation and flow domains in terms of the finite difference grid. (a) calculation domain (b) flow domain.

Fig.(2.7) : A control volume cut by the vessel wall (2-D representation).

Fig.(2.8) : The flow diagram of the computer model.

Fig.(3.1) : Schematic of the cubic cavity with one of the walls moving.

Fig.(3.2a) : Predicted velocity field in longitudinal vertical plane at z/W of 0.5 for cubic cavity test ($Re=100$)

Fig.(3.2b) : Predicted flow field for cubic cavity test ($Re=100$) (a) transverse vertical plane (b) transverse horizontal plane

Fig.(3.3) : Cubic cavity velocity profile for ($Re=100$), (a) vertical centre line (b) horizontal line

Fig.(3.4) : Schematic of the developing velocity profiles and pressure changes in the entrance of a duct flow.

Fig.(3.5) : Schematic of a duct with a square cross-section and the relevant co-ordinate axis to the problem.

Fig.(3.6) : The procedure adopted for modelling the inflow and outflow boundary condition for the prediction of entrance lengths.

Fig.(3.7) : Predicted entrance lengths (L_e / D) as a function of the inlet Reynolds number.

Fig.(3.8) : Comparision of analytical and numerical estimated terminal rise velocity of four different size sherial cap bubbles in water.

Fig.(3.9) : Schematic of the single strand model tundish dimensions[8].

Fig.(3.10) : Predicted flow field in single strand tundish at different elevations in transverse planes at the different dimensionless height of (a)0.95 (b) 0.60 (c) 0.32 (d) 0.045

Fig.(3.11) : Predicted flow field in single strand tundish in longitudinal vertical planes at dimensionless distances (z/W) of (a) 0.5 (b) 0.1 (c) 0.19 (d) 0.045

Fig.(3.12) : Predicted flow field in single strand tundish in the transvese plane at dimensionless distance (x/L) of (a) 0.11 (b) 0.28 (c) 0.67 (d) 0.78

Fig.(3.13) : RTD in single strand tundish

Fig.(3.14) : Schematic of three different configurations of the two strand tundish used for numerical simulation (a) without baffle (b) with a dam (c) with a dam and a wier (c) with a bubbler in place of dam

Fig.(3.15) : Prdicted flow field in the two strand symmetrical tundish without baffle in the longitudinal vertical planes at dimensionless distance (z/W) of (a) 0.99 (b) 0.70 (c) 0.34

Fig(3.16) : Predicted flow field in the two strand symmetrical tundish without baffle in the horizontal transverse planes at different dimensinless height (y/H) of (a) 0.99 (b) 0.50 (c) 0.05

Fig.(3.17) : Prdicted flow field in the two strand symmetrical tundish with a dam in the longitudinal vertical planes at dimensionless distance (z/W) of (a) 0.99 (b) 0.70 (c) 0.34

Fig(3.18) : Predicted flow field in the two strand symmetrical tundish with a dam in the horizontal transverse planes at different dimensinless height (y/H) of (a) 0.95 (b) 0.49 (c) 0.05

Fig(3.19) : Predicted flow field in the two strand symmetrical tundish with a dam & a wier in the horizontal transverse planes at different dimensinless height (y/H) of (a) 0.99 (b) 0.70 (c) 0.34

Fig.(3.20) : Prdicted flow field in the two strand symmetrical tundish with a bubbler in the longitudinal vertical planes at dimensionless distance (z/W) of (a) 0.99 (b) 0.70 (c) 0.34

Fig(3.21) : Predicted flow field in the two strand symmetrical tundish with a bubbler in the horizontal transverse planes at different dimensionless height (y/H) of (a) 0.95 (b) 0.50 (c) 0.05

Fig.(3.22) RTD for two, strand tundish for four different case (a) without baffle (b) with a dam (c) with a weir and a dam (d) with a bubbler located in place of the dam

Fig.(3.23) Schematic of the six strand tundish with all dimensions

Fig.(3.24) Predicted flow field in six strand full scale tundish (no baffle) in longitudinal vertical planes at dimensionless distance z/W of (a) 0.40 (b) 0.3 and (c) 0.4(d) 0.15

Fig.(3.25) Predicted flow field in six strand water model tundish (no baffle) in transverse horizontal planes at dimensionless height y/H of (a) 0.05 (b) 0.50 (c) 0.95

Fig.(3.26) Comparison of RTD for six strand delta shaped tundish without baffle for different outlets

LIST OF TABLES

Table(1.1) : Major research efforts in the field of physiacal modelling of tundish.

Table(1.2) : Major research efforts in the field of mathematical modelling of tundish.

Table(2.1) : Popularly used software packages to study transport phenomena[2].

Table(2.2) : Values of constants used in $k-\epsilon$ model.

Table(2.3) : Definition of Γ , ϕ and S of Eq.(2.28)

Table(3.1) : Characteristic parameters of the single strand model tundish [8].

Table (3.2) : Chracteristics of the RTD in the single strand tundish and their comparison with equivalent measurements reported in the literature[8].

Table (3.3) : Characteristic parameters of the two strand model tundish (13) .

Table (3.4) : Residence Time distribution characteristics in the two strand tundish as a function of various configurations

Table (3.5) : Comparision of flow characteristics of two strand tundish with experimentally observed values.

Table (3.6) : Characteristic parameter of the six strand delta shape water model tundish.

Table (3.7) : Comparision of predicted and experimentally observed values of minimum breakthrough times for different outlets of six strand delta shaped water model tundish

CHAPTER 1

INTRODUCTION TO THE THESIS

1.1 Introduction

Physical modelling was traditionally the preferred tool [1] in metallurgy but of late, mathematical modelling has become more popular because of availability of several software packages, cheaper computational hardware, growing experience with the tackling of a broad range of computational problems and better understanding of the underlying fundamental concepts. With the development of new materials i.e., ceramics, composites etc. and a more challenging market place, the focus of a process metallurgist has undergone substantial reorientation and has shifted to cost control and better product quality. These warrant better process control and process optimisation . Towards this, mathematical modelling, over the last few years has played a key role, as both process control and process optimisation require the representation and understanding of the process/operation in quantitative form.

Apart from lower costs, mathematical modelling has other inherent advantages over conventional forms of investigation *viz.*, pilot plant scale experimentation and physical modelling. They are as follows:

1. **Speed** : With the help of a mathematical model an investigator can study various configurations with ease, at a remarkable speed .
2. **Information**: The data derived from mathematical model are detailed and complete. The values of all possible variables in the domain of interest can be calculated and this information can be put to much more effective use. Mathematical modelling scores over other forms of investigation *viz.* physical modelling and pilot scale experimentation on this aspect.
3. **Simulation flexibility**: With the help of a mathematical model, small scale or cold models can be studied. Further, various theoretical possibilities such as, constant

density and infinite reaction rate options can also be evaluated which at times help the researcher in developing a better understanding of the subject.

The general methodology of a mathematical model development is shown schematically [2] in Fig.(1.1). This involves identifying the problem, carrying out simple calculations and then drawing a plan for detailed experimental and computational work. It needs to be stressed here that mathematical modelling together with physical modelling and pilot plant investigation needs to be carried out in a complementary fashion.

Owing to the distinct advantages mentioned in the preceding paragraph mathematical model has become very popular among researchers in the field of materials and metallurgical engineering. Numerous investigations thus have been carried out and reported in the literature by practising and research engineers alike on various aspects of metals and materials processing, accompanying benification, refining, casting, & solidification etc. In the arena of liquid metal processing operations, mathematical modelling has been extensively applied to investigate liquid steel flows, alloy motion, alloy dissolution, mixing and RTD(Residence time Distribution) etc. This has assumed considerable relevance since visual opacity, relatively large size of the processing units and extremely high operating temperature($\sim 1600^0$) often precludes direct investigations on industrial metal processing units. Thus in the present study an attempt has been made to investigate the melt flow and Residence Time Distribution characteristics in different designs of steel making tundish system, with the aid of a mathematical model, developed by the prent author. Prior to outlining the essence of the mathematical model, it however useful to ellucidate the characteristic features of the metallurgical tundish system.

1.2 Characteristics of metallurgical tundish system

A continuous casting set up essentially consists of three components, the teeming ladle, the tundish and the continuous casting mould. The tundish is the intermediate vessel between the ladle and the mould which functions as a distributor and a buffer vessel and helps

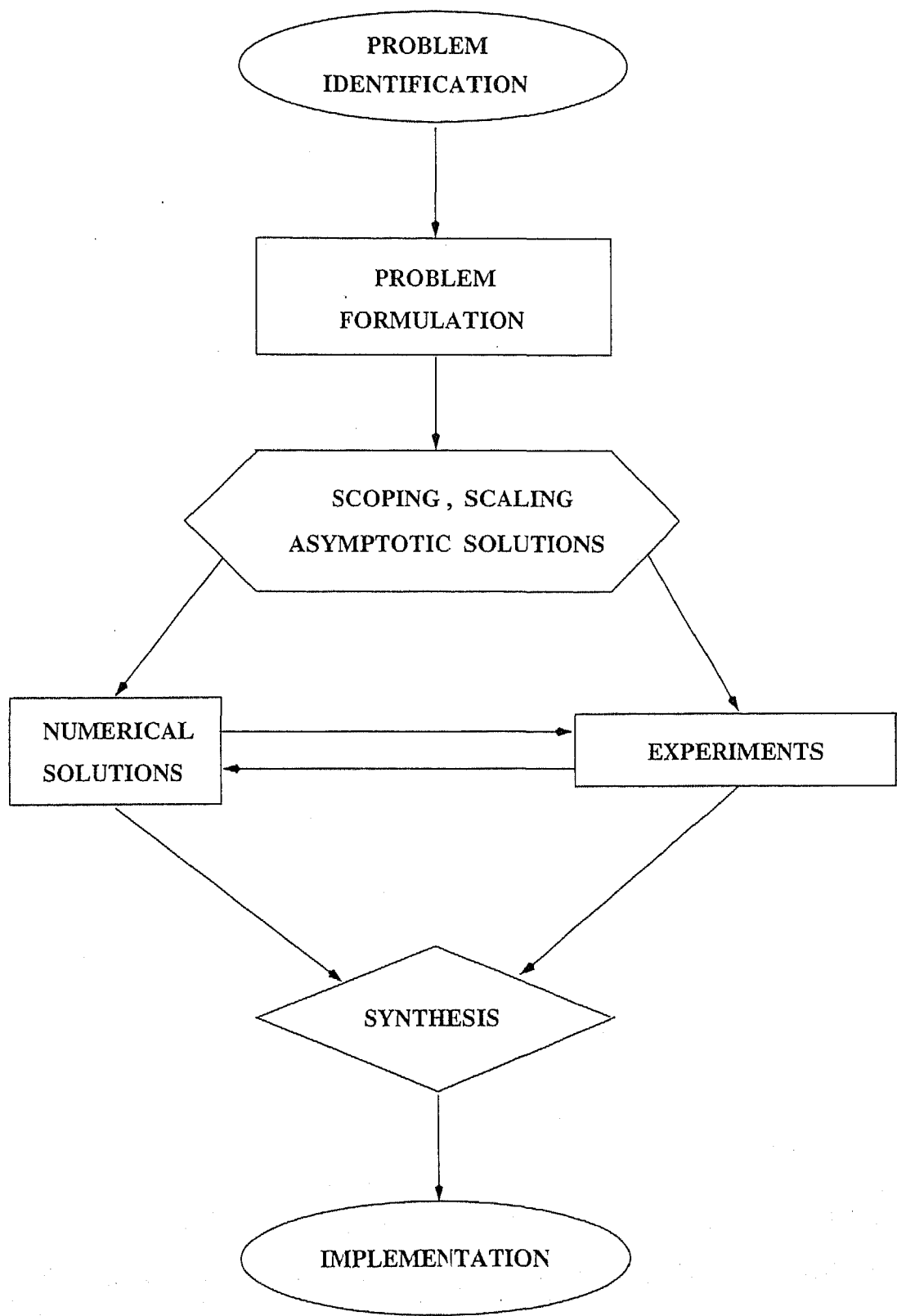


Fig. (1.1) : The general methodology of mathematical model development [2].

maintain a relatively uniform flow as the teeming ladle is being emptied and replaced by a new one. Fig.(1.2) shows a schematic of the continuous casting process. Over the years the quality requirements of the final steel product have become very stringent and the tundish therefore is considered to offer the last opportunity for the removal and modification of impurities and for any adjustment of trim chemical composition by micro-alloying. With the emphasis on the novel casting methods like thin slab and strip casting in a single step, the role of tundish has become even more critical.

The performance of a tundish is very closely related to the nature of steel flow as the basic tundish design as well as flow modification devices affect liquid steel motion profoundly. For example, a well mixed flow in a given tundish would be more suitable for dissolution and alloying whereas a plug flow is more suited for inclusion separation. Therefore, the basic design of the tundish is important towards performing the desired functions effectively. To this end, mathematical modelling can give a reasonable quantitative understanding of the flows and the associated Residence Time Distribution in the tundish and thus, provide useful information on the overall process. This in turn can help achieving an optimal tundish design.

When fluid flows through the tundish it is important to establish the time spent in the system by individual fluid elements. The "*average time*" or the "*nominal holding time*", of the fluid in the system is easily calculated from the definition

$$t_r = \frac{\text{Volume of fluid in vessel}}{\text{Volumetric rate of fluid flow}} \quad (1.1)$$

However, some fluid individual elements may spend a longer, and others a shorter period of time in the system. The minimum amount of time a fluid spends inside the vessel is called the "*breakthrough time*". This departure of actual residence times from the mean i.e., the distribution of residence times is an important characteristic of the tundish system and influences the latter's performance as a reactor.

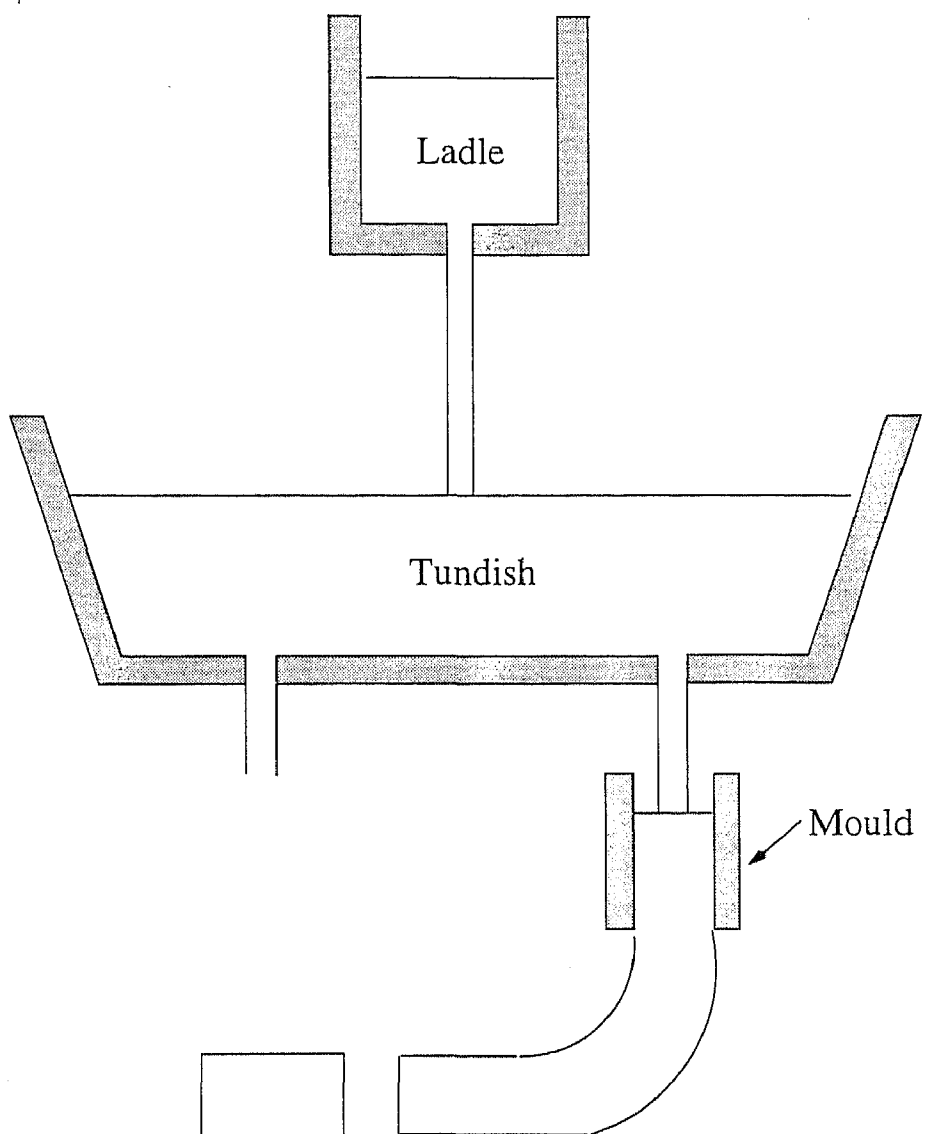


Fig. (1.2) : Schematic representation of the continuous casting proces

The Residence Time Distribution(RTD) of a fluid flowing through the tundish can be determined either experimentally or via mathematical modelling. Experimental determination of RTD involves pulse addition of a tracer in the stream entering the vessel and simultaneously monitoring the tracer concentration at the exit with respect to time. In contrast, RTD can be calculated from the first principles by solving an appropriate species conservation equation. The variation of concentration at the exit as a function of time deduced either experimentally or theoretically is typically plotted in the form of dimensionless concentration vs. dimensionless time. Such a plot is referred to as the "C-curve". A typical C curve is shown in Fig.(1.3). The C curve thus obtained is analysed to assess the hydrodynamic performance of a given tundish. The area under the C-curve is unity as all tracer entering the system should eventually leave it $\int_0^\infty C(t)dt=1$. From the C-curve parameters like the minimum breakthrough time (t_{min}), the time at which the peak concentration is reached (t_{peak}), and the average residence time (t_{mean}) can be obtained.

The mean residence time is calculated from the C-curve as:

$$t_{mean} = \frac{\int_0^\infty tC(t)dt}{\int_0^\infty C(t)dt} \quad (1.2)$$

These can be converted into their equivalent dimensionless forms ($\theta_{min} = t_{min} / t_r$, $\theta_{peak} = t_{peak} / t_r$, $\theta_{mean} = t_{mean} / t_r$) where t_r is the theoretical residence time as defined by Eq.(1.1). To interpret the results from the C-curve quantitatively the vessel volume can be assumed to be made up of three parts namely, a well mixed volume (V_m), a dispersed plug volume (V_{dp}) and a dead volume (V_d). The fractional volumes can be calculated as :

$$V_d = (1 - \theta_{mean}) \quad (1.3)$$

$$V_{dp} = \frac{(\theta_{min} + \theta_{peak})}{2} \quad (1.4)$$

$$V_m = 1 - V_d - V_{dp} \quad (1.5)$$

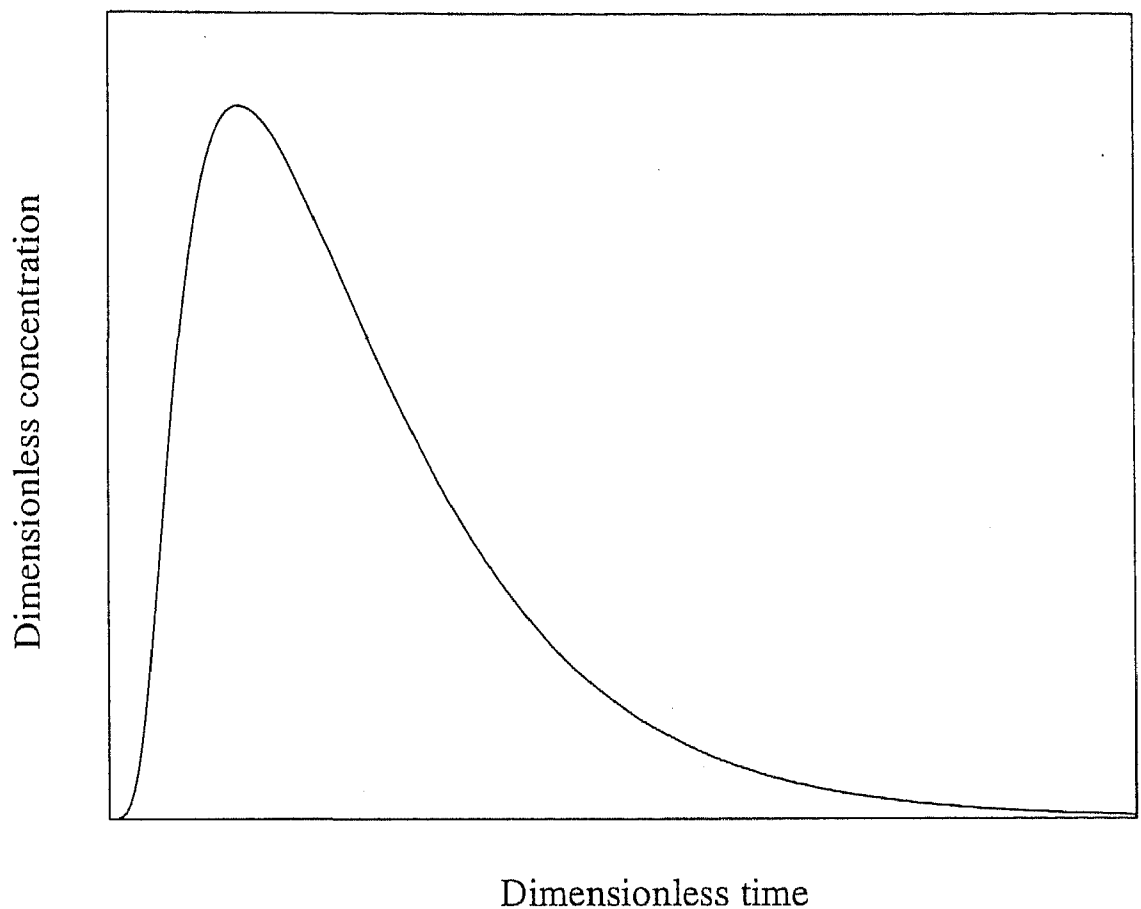


Fig. (1.3) : A typical " C " curve

The relative amounts of these volumes determine the efficiency of a given tundish and can also be used as appropriate criteria for improving the tundish design or for comparative analysis. The preceding formulation assumes that only negligible volume of liquid spends a time greater than twice the theoretical residence time in the tundish.

1.3 Previous work

The subject of fluid flow and Residence Time Distribution phenomena has received considerable attention over the years. Many studies, computational as well as experimental, have been carried out in recent years to investigate the influence of design and operating parameters on the tundish hydrodynamics and the associated process efficiency. In general, two different approaches have been employed by the researcher's to investigate flow and Residence Time Distribution in tundish. These include,

1. Physical modelling using either full scale or reduced scale aqueous models
2. Mathematical modelling

Numerous physical model studies have been carried out to investigate the hydrodynamics, RTD, inclusion separation etc. using aqueous models of steel making tundish system. Both isothermal and non-isothermal conditions were studied through water modelling to primarily investigate the variation of exit temperature(strand to strand) as a function of time. Such aqueous model studies have been carried out either using full scale models or appropriately scaled down models. Often the Froude number based modelling criteria have been applied to maintain dynamic similarity between the model and the full scale tundish systems. Extensive experimental trials were made on flow and RTD embodying various kinds of flow modification devices, such as dams, weirs, slotted dams etc. The principal objective of the experimental studies was concerned with an optimum tundish design together with a set of optimally placed flow control devices. Table 1.1, summarises the work reported to date in various aspects of physical modelling of tundish system. This

includes the group of researchers together with their area of research in a chronological fashion.

Table 1.1 : Major research efforts in the field of physical modelling of tundish .

Year	Researchers	Area of research
1981	F. Kemeny, A. McLean, T. R. Meadowcroft and J. D. Young	Fluid flow studies in a water model tundish of a slab caster with/without flow control devices such as dams, wiers, and slotted dams.[3]
1986	Y. Sahai and R. Ahuja	Fluid flow and mixing of melt in steel making tundishes with flow control devices such as dams, wiers, slotted dams and submerged gas injection. [4]
	T. Robertson and A. Perkins	Physical and mathematical modelling of liquid steel temperature in continuous casting tundish. Water modelling experiments were carried out to develop tundish designs which give optimum temperature over the outlet streams of multistrand tundishes.[5]
1992	Y. Sahai and M. D. Burwal	Validity of Reynolds and Froude similarity criteria for water modelling of melt flow in tundishes.[6]
	Liu Xintian, Zhou Yaohe, Shang Baolu, and Jiag Weiming	Flow behaviour and filtration of steel melt in continuous casting tundish.[7]
1993	S. Singh and S. C. Koria	Water model study of the dynamics of flow in a single strand aqueous model tundish.[8]
	S. Joo and R. I. L. Guthrie	Study of inclusion behaviour and heat transfer phenomena in steel making tundishes via aqueous modelling.[9]
1994	F. Shen, J. M. Khodadadi, S. J. Pien, and X. K. Lan	Mathematical and physical modelling studies of molten Aluminum flow in a tundish.[10]
1995	Dipak Mazumdar, Guler Yamanoglu, Ramani Shankarnarayanan and Roderick I. L. Guthrie	Similarity considerations in the physical modelling of steel making tundish systems illustrating the importance of Froude number based scaling.[11]
1996	Y. Sahai and Toshihiko Emi	Melt flow characterisation in continuous casting tundishes and assessment of mixed flow models of relevance to tundish hydrodynamics.[12]
1997	Dipak Mazumdar, Guler Yamanoglu, and Roderick I. L. Guthrie	A comparative study of hydrodynamic performance of two strand, five strand, and six strand tundish systems with/without flow control devices via appropriately scaled down model tundishes.[13]

Mathematical modelling of melt flow and RTD in steelmaking tundishes were carried out through solution of turbulent Navier -Stokes equations in conjunction with an appropriate species conservation equation. Mostly bench mark CFD codes such as, PHOENICS.

METFLO etc. were applied to this end.

Table 1.2 : Major research effort in the field of mathematical modelling of tundish.

Year	Researchers	Area of research
1986	J. Szekely and N. El-Kaddah	Mathematical modelling of three-dimensional heat flow , fluid flow and turbulence phenomena in tundishes.[14]
	O. J. Illegbusi and J. Szekely	The modelling of fluid flow, tracer dispersion and inclusion behaviour in tundishes.[15]
	K. Y. M. Lai, M. Salcudean, S. Tanaka, and R. I. L. Guthrie	Mathematical modelling of flows in large tundish systems in steelmaking and verification of predicted results with physical modelling results.[16]
1987	K. H. Tacke and J. C. Ludwig	Study of steel flow and inclusion separation in continuous casting tundishes via mathematical model.[17]
	Y. He and Y. Sahai	Study of tundish wall inclination on the fluid flow and mixing via water and mathematical model.[18]
1988	O. J. Illegbusi and J. Szekely	Study of fluid flow and tracer dispersion in shallow tundishes via mathematical model.[19]
1989	O. J. Illegbusi and J. Szekely	Effect of externally imposed magnetic field on tundish performance.[20]
1991	O. J. Illegbusi and J. Szekely	Heat transfer and the role of auxiliary heating in tundishes.[21]
1992	J. L. Yeh, W. H. Hwang, and C. L. Chou	Physical modelling validation of computational fluid dynamics code for tundish design.[22]
	S. Chakraborty and Y. Sahai	Mathematical modelling of transport phenomena in continuous casting tundishes during ladle transfer operations[23]
		influence of varying ladle stream temperature and[24]
		and of holding time and surface cover in ladles on liquid steel flow in continuous casting tundishes.[25]
1993	S. Joo and R. I. L. Guthrie	Inclusion behaviour and heat transfer phenomena in steel making tundishes via mathematical modelling.[26]
	B. Kaufmann, A. Niedermayr, H. Sattler and A. Preuer	Separation of nonmetallic particles in tundishes.[27]
1994	O. J. Illegbusi	Application of the Two-fluid model of Turbulence to tundish problems.[28]
1995	C. Damle and Y. Sahai	The effect of tracer density on melt flow characterisation in continuous casting tundishes via mathematical and water model. [29]

Alternatively Sahai and co-workers developed their custom built model to investigate tundish hydrodynamics. In addition to the studies on flow and RTD the role of auxiliary

heating and electromagnetic stirring on tundish performance were also studied numerically. Some researchers also went on to investigate the floatation characteristic of non-metallic inclusion in tundishes. Some recent computational work includes an assessment study of the applicability of $k-\epsilon$ model to tundish systems. Mathematical modelling studies carried out and reported to date have been summarised in Table 1.2. This show the various group of researchers together with their specific area of research chronologically.

Alternatively Sahai and co-workers developed their custom built model to investigate tundish hydrodynamics. In addition to the studies on flow and RTD the role of auxiliary heating and electromagnetic stirring on tundish performance were also studied numerically. Some researchers also went on to investigate the floatation characteristic of non-metallic inclusion in tundishes. Some recent computational work includes an assessment study of the applicability of $k-\epsilon$ model to tundish systems. Mathematical modelling studies carried out and reported to date have been summarised in Table 1.2. This show the various group of researchers together with their specific area of research chronologically.

1.4 Scope of the present work

The brief introduction to the thesis indicates that mathematical modelling in recent years has become very popular to investigate various aspects of liquid steel processing in the tundish. Despite numerous modelling exercises taken up over the years in widely varying areas, there remains considerable scope in broadening the applicability of the mathematical (better called 'Process') models and their performance. A quick survey of the relevant literature might as well lead one to conclude that mathematical modelling in the area of metals processing has been most exhaustive in 2-D or axi-symmetrical systems. Transient, two phase, 3-D calculations have been few and far between. Since, most metal processing operations do not involve symmetry, consequently the need for a three dimensional transport model can be readily visualized (for example, analysis of asymmetric gas injection, dual plug bubbling, flow in a tundish etc. necessitates a three dimensional turbulent flow calculation procedure).

The purpose of the present work has been primarily to develop steady state, three dimensional, two phase, turbulent flow calculation procedure embodying the two equation $k-\epsilon$ model of turbulence in the Cartesian co-ordinate system. The three dimensional code developed was extensively tested against available benchmark solutions to assess its internal consistency and reliability. Subsequent to these, the 3-D model was applied to predict flow phenomena and Residence Time Distribution characteristics in three different tundish systems with/without flow control devices. For the first time numerical computations were also carried out as exactly as possible to investigate the role of auxilliary gas injection in a tundish. Results thus obtained were also compared with those published already in the literature.

1.5 Layout of the thesis

The main body of the thesis consists of five chapters. Chapter-2 deals with the development of the three dimensional, steady state, two phase turbulence flow model. This include the governing equations, salient features of the formulation ,boundary conditions and the procedure for incorporating inclined walls/flow modification devices in the numerical solution scheme. In chapter-3 a rigorous assessment of the computational procedure has been carried out by performing some benchmark tests. Subsequent to this the model has been applied to predict fluid flow behaviour and Residence Time Distribution for different tundish designs with a gas bubbler and various flow modification devices. Chapter-4 summarises the general conclusions derived from the present work and the thesis concludes with the recommendation for future work in Chapter-5.

CHAPTER 2

MATHEMATICAL MODELLING

2.1 Introduction

The degree of complexity required to mathematically model different metallurgical processes varies from one to another. While, operations like axisymmetric gas injection, axisymmetric pouring and drainage, can be effectively modelled using a two dimensional turbulent flow model, others, like melt flow in tundishes or in a R-H degasser require a three dimensional turbulent flow model for effective simulation. Needless to mention that transport processes in practically all metallurgical operations can be successfully modelled using transient, two phase, three dimensional models. To this end, several software packages are currently commercially available. Some of the popularly used software packages have been listed in Table-2.1.

Table-2.1: Popularly used software packages to study transport phenomena [2].

Name	Application	Technique
<i>PHOENICS</i>	fluid dynamics, Heat Transfer, Chemical Reaction	finite volume
<i>TEACH - T</i>	fluid dynamics	finite volume
<i>FLOW 3-D</i>	fluid dynamics	finite difference
<i>FLUENT</i>	fluid dynamics, Heat Transfer	finite difference
<i>NECTON</i>	fluid dynamics, Heat Transfer	finite element
<i>NISA</i>	fluid dynamics, Heat Transfer	finite difference

However, the key problem lies in the definition of the boundary conditions and the ability to interpret the results in an intelligent manner. Hence, many researchers prefer custom built models from the first principles with consideration of elementary control volumes. Indeed, this later philosophy has been applied in the present investigation to develop a steady, two phase, three dimensional turbulent flow calculation procedure.

Thus, the present chapter deals with the development of a steady state, three dimensional, two phase, turbulent flow model in Cartesian coordinate system. The computer code developed has been subsequently used to study some benchmark conditions together with the fluid flow behaviour in different shapes of tundish with and without flow control devices .

2.2 Assumptions in modelling

The following assumptions and idealisations were made in the present work to computationally investigate fluid flow and RTD behaviour in steel making tundish systems.

- i. The flow is assumed to be turbulent and macroscopically steady i.e., the effect of transience during filling and emptying of tundish was neglected.
- ii. The melt surface is assumed to be flat and phenomena like wave formation, presence of slag layer at the free surface and vortexing during drainage etc. are neglected.
- iii. Entrainment of air or gas through the metal inlet is neglected (the ladle stream is essentially shrouded).
- iv. The flow is essentially Newtonian and incompressible and
- v. The system is isothermal and thus the effect of temperature differential on the induced flow is neglected.

In addition to the above, to model the influence of gas injection in tundishes, the following assumptions were made:

- vi. Discrete monosize bubbles are assumed to form at the lance/tuyere tip. Furthermore, the size of the bubbles forming at the orifice is assumed to be known.

vii. Bubble-bubble interactions were assumed to be negligible and hence, the drag coefficient correlation applicable to a single bubble fluid system is applied for the appropriate range of Eotvos and Weber numbers.

viii. Bubbles within the upwelling gas-liquid plume contribute to the generation of turbulence and the turbulence phenomena affects the bubble motion.

2.3 Description of the steady state, two phase, three dimensional turbulent flow model

The essence of the combined Eulerian-Langrangian two phase, three dimensional turbulent flow model is presented below.

2.3.1 The liquid phase equations of motion

In terms of Cartesian co-ordinate system (x, y, z), the governing flow equations (for the liquid phase) under steady state conditions can be represented as:

Equation of continuity :

$$\frac{\partial}{\partial x}(\alpha_l \rho u) + \frac{\partial}{\partial y}(\alpha_l \rho v) + \frac{\partial}{\partial z}(\alpha_l \rho w) = 0 \quad (2.1)$$

Equation of motion in x direction :

$$\frac{\partial}{\partial x}(\alpha_l \rho uu) + \frac{\partial}{\partial y}(\alpha_l \rho uv) + \frac{\partial}{\partial z}(\alpha_l \rho uw) = - \alpha_l \frac{\partial p}{\partial x} - \frac{\partial}{\partial x}(\alpha_l \mu_e \frac{\partial u}{\partial x}) + \frac{\partial}{\partial y}(\alpha_l \mu_e \frac{\partial u}{\partial y}) + \frac{\partial}{\partial z}(\alpha_l \mu_e \frac{\partial u}{\partial z}) + S_u \quad (2.2a)$$

in which,

$$S_u = \frac{\partial}{\partial x}(\alpha_l \mu_e \frac{\partial u}{\partial x}) + \frac{\partial}{\partial y}(\alpha_l \mu_e \frac{\partial v}{\partial x}) + \frac{\partial}{\partial z}(\alpha_l \mu_e \frac{\partial w}{\partial x}) - F_x \quad (2.2b)$$

Equation of motion in the y direction :

$$\frac{\partial}{\partial x}(\alpha_l \rho uv) + \frac{\partial}{\partial y}(\alpha_l \rho vv) + \frac{\partial}{\partial z}(\alpha_l \rho vw) = - \alpha_l \frac{\partial p}{\partial y} + \frac{\partial}{\partial x}(\alpha_l \mu_e \frac{\partial v}{\partial x}) + \frac{\partial}{\partial y}(\alpha_l \mu_e \frac{\partial v}{\partial y}) + \frac{\partial}{\partial z}(\alpha_l \mu_e \frac{\partial v}{\partial z}) + S_v \quad (2.3a)$$

in which,

$$S_v = \frac{\partial}{\partial x}(\alpha_l \mu_e \frac{\partial u}{\partial y}) + \frac{\partial}{\partial y}(\alpha_l \mu_e \frac{\partial v}{\partial y}) + \frac{\partial}{\partial z}(\alpha_l \mu_e \frac{\partial w}{\partial y}) + F_y \quad (2.3b)$$

Equation of motion in the z direction :

$$\frac{\partial}{\partial x}(\alpha_l \rho uw) + \frac{\partial}{\partial y}(\alpha_l \rho vw) + \frac{\partial}{\partial z}(\alpha_l \rho ww) = -\alpha_l \frac{\partial p}{\partial z} + \frac{\partial}{\partial x}(\alpha_l \mu_e \frac{\partial w}{\partial x}) + \frac{\partial}{\partial y}(\alpha_l \mu_e \frac{\partial w}{\partial y}) + \frac{\partial}{\partial z}(\alpha_l \mu_e \frac{\partial w}{\partial z}) + S_w \quad (2.4a)$$

in which,

$$S_w = \frac{\partial}{\partial x}(\alpha_l \mu_e \frac{\partial u}{\partial z}) + \frac{\partial}{\partial y}(\alpha_l \mu_e \frac{\partial v}{\partial z}) + \frac{\partial}{\partial z}(\alpha_l \mu_e \frac{\partial w}{\partial z}) + F_z \quad (2.4b)$$

Eqs (2.2a) through (2.4b) are the well known Navier-Stokes equations. In these u , v , w and p (gauge with reference to local hydrostatic pressure) are respectively the time averaged velocity components and pressure. α_l is the volume fraction of liquid and F 's are the various forces acting on the fluid which may include buoyancy, drag etc. Finally, μ_e , appearing in Eqs.(2.2a) through (2.4b) is the effective viscosity and is derived from an appropriate turbulence model.

The values of α_l , the volume fraction of liquid in a given control volume, in Eqs(2.2a) through (2.4b) can be obtained from the solution of bubble trajectory equations (see later).

2.3.2 The turbulence model

In the present work, the popular two equation $k-\epsilon$ Model of Launder and Spalding[31] has been used for the estimation of turbulence parameters. The model incorporates an equation for the conservation of turbulence kinetic energy, $k \{ = 1/2(u^2 + v^2 + w^2) \}$ and its dissipation rate, $\epsilon \{ = -dk/dt \}$. The k and ϵ transport equations in terms of Cartesian co-ordinate system can be expressed as following:

Conservation equation for the turbulence kinetic energy, k :

$$\frac{\partial}{\partial x}(\rho_l \alpha_l u k) + \frac{\partial}{\partial y}(\rho_l \alpha_l v k) + \frac{\partial}{\partial z}(\rho_l \alpha_l w k) = \frac{\partial}{\partial x}(\alpha_l \frac{\mu_e \partial k}{\sigma_k \partial x}) + \frac{\partial}{\partial y}(\alpha_l \frac{\mu_e \partial k}{\sigma_k \partial y}) + \frac{\partial}{\partial z}(\alpha_l \frac{\mu_e \partial k}{\sigma_k \partial z}) + S_k \quad (2.5a)$$

in which,

$$S_k = \alpha_l (G_k + P_b - \rho \epsilon) \quad (2.5b)$$

Conservation equation for the dissipation rate of turbulence kinetic energy, ϵ :

$$\frac{\partial}{\partial x}(\rho_l \alpha_l u \epsilon) + \frac{\partial}{\partial y}(\rho_l \alpha_l v \epsilon) + \frac{\partial}{\partial z}(\rho_l \alpha_l w \epsilon) = \frac{\partial}{\partial x}(\alpha_l \frac{\mu_e \partial \epsilon}{\sigma_\epsilon \partial x}) + \frac{\partial}{\partial y}(\alpha_l \frac{\mu_e \partial \epsilon}{\sigma_\epsilon \partial y}) + \frac{\partial}{\partial z}(\alpha_l \frac{\mu_e \partial \epsilon}{\sigma_\epsilon \partial z}) + S_\epsilon \quad (2.6a)$$

in which,

$$S_\epsilon = \alpha_l \left[\frac{C_1 \epsilon G_k - C_2 \rho \epsilon^2}{k} \right] + (P_b \epsilon / k) \alpha_l \quad (2.6b)$$

G_k appearing in Eqs.(2.5) and (2.6) is the volumetric rate of turbulence generation and for a three dimensional Cartesian co-ordinate system, can be expressed as:

$$G_k = 2 \mu_T \left[\left(\frac{\partial u}{\partial x} \right)^2 + \left(\frac{\partial v}{\partial y} \right)^2 + \left(\frac{\partial w}{\partial z} \right)^2 \right] + \mu_T \left[\left(\frac{\partial u}{\partial y} + \frac{\partial v}{\partial x} \right)^2 + \left(\frac{\partial v}{\partial z} + \frac{\partial w}{\partial y} \right)^2 + \left(\frac{\partial w}{\partial x} + \frac{\partial u}{\partial z} \right)^2 \right] \quad (2.7)$$

The effective viscosity, μ_e , appearing in Eqs.(2.2) to (2.7) is defined as: $\mu_e = \mu_T + \mu_l$, in which,

$$\mu_T = \frac{C_\mu \rho k^2}{\epsilon} \quad (2.8)$$

The five empirical constants of the $k-\epsilon$ model viz., C_1 , C_2 , C_μ , σ_k and σ_ϵ were assigned to their standard values [31]. These are summarised in Table-2.2. As seen from the above, flow and turbulence model equations are mutually coupled.

Table-2.2:Values of constant used in a k- ϵ model.

C_1	C_2	σ_k	σ_ϵ	C_μ
1.43	1.92	1.00	1.30	0.09

2.3.3 Equation of motion of the gas phase

The effect of gas injection in the tundish and hence the motion of the gas bubbles in the bulk phase liquid has been carried out via a Langrangian approach, in which the trajectories of the individual bubbles are stochastically determined in space by solving three differential equations in time. The appropriate form of Newton's second law of motion that describes the bubble motion, can be represented along the three relevant coordinates, x (longitudinal), y (vertical) and z (transverse) according to:

Longitudinal direction, x:

$$(1 + 0.5 \frac{\rho_l}{\rho_g}) \frac{dV_{B,x}}{dt} = - \frac{3\mu_l}{4d_b^2 \rho_g} C_D Re (V_{B,x} - U) + \frac{\rho_l}{\rho_g} [V \frac{\partial u}{\partial y} + U \frac{\partial u}{\partial x} + W \frac{\partial u}{\partial z}] \quad (2.9)$$

Vertical direction, y :

$$(1 + 0.5 \frac{\rho_l}{\rho_g}) \frac{dV_{B,y}}{dt} = - \frac{3\mu_l}{4d_b^2 \rho_g} C_D Re (V_{B,y} - V) + 1.5 \frac{\rho_l}{\rho_g} [V \frac{\partial v}{\partial y} + U \frac{\partial v}{\partial x} - W \frac{\partial v}{\partial z}] + (1 - \frac{\rho_l}{\rho_g}) g \quad (2.10)$$

and transverse direction, z:

$$(1 + 0.5 \frac{\rho_l}{\rho_g}) \frac{dV_{B,z}}{dt} = - \frac{3\mu_l}{4d_b^2 \rho_g} C_D Re (V_{B,z} - W) + 1.5 \frac{\rho_l}{\rho_g} [V \frac{\partial w}{\partial y} + U \frac{\partial w}{\partial x} + W \frac{\partial w}{\partial z}] \quad (2.11)$$

The three corresponding kinematic relationships, which define the trajectories of bubbles

within the two dimensional flow domain are:

$$\frac{dx}{dt} = V_{B,x} \quad (2.13)$$

$$\frac{dy}{dt} = V_{B,y} \quad (2.12)$$

and,

$$\frac{dz}{dt} = V_{B,z} \quad (2.14)$$

The instantaneous drag coefficient, C_D , in the Eqs.(2.9) to (2.11) was evaluated using an experimentally determined correlation[32] for oblate spheroid / spherical capped bubbles:

$$C_D = \frac{0.622}{\left[\frac{1}{E_o} + 0.235 \right]} \quad ; \quad (500 < Re < 5000) \quad (2.15)$$

Furthermore, Re in Eqs.(2.9) through (2.11) is the Reynolds number, and is estimated on the basis of absolute magnitude of the relative velocity vector, i.e.

$$Re = \rho_l d_b \left[\frac{U_b - U_r}{\mu_l} \right] \quad (2.16)$$

Similarly in Eqs.(2.9) through (2.11), U , V and W are the instantaneous components of fluid motion, and were estimated by summing up the relevant mean velocity components (u , v and w) with the corresponding fluctuating velocity components assuming turbulent fluctuations are essentially isotropic and obey a Gaussian probability distribution function. For example,

$$U = u + \Psi \left(\frac{2k}{3} \right)^{\frac{1}{2}} \quad (2.17)$$

where ψ is a normally distributed random variable and varies between -1 and 1. Thus during the rise of the bubble through the liquid, the velocity fluctuations were estimated stochastically and were assumed to remain constant for a time period, equivalent to the eddy life time, τ . The life time of an eddy, during which a characteristic velocity fluctuation was assumed to persist, is estimated from the turbulence theory according to[32] :

$$\tau = 0.195 \frac{k}{\epsilon} \quad (2.18)$$

2.3.4 Estimation of gas volume fraction

Figure(2.1) illustrates a typical section of the grid network and a bubble trajectory intercepting the Eulerian grid system. Once the bubble population in the flow domain is predicted from solution of the bubble sub-model equations, gas voidages can be readily estimated from the principle of volume continuity, according to :

$$\alpha_g = \frac{\text{volume of gas}}{\text{volume of control volume}} = \frac{Q_t(N+1)\Delta t}{2\Delta V_{cv}} \quad (2.19)$$

Further more, liquid volume fraction, α_l , can be easily determined from the above since, $\alpha_g + \alpha_l = 1.0$.

2.3.5 Estimation of the interphase drag and the turbulence production due to bubbles

The volumetric flow rate of turbulence generation via the bubbles, P_b , embodied in the k- ϵ model can be represented as :

$$P_b = C_b \frac{Q_t}{N\Delta V_{cv}} \sum \int \frac{3\mu_l C_D Re}{4d_b^2} (V_B - U_f)^2 dt \quad (2.20)$$

where, V_B is the resultant bubble velocity and U_f is the resultant fluid velocity. C_b in Eq.2.20

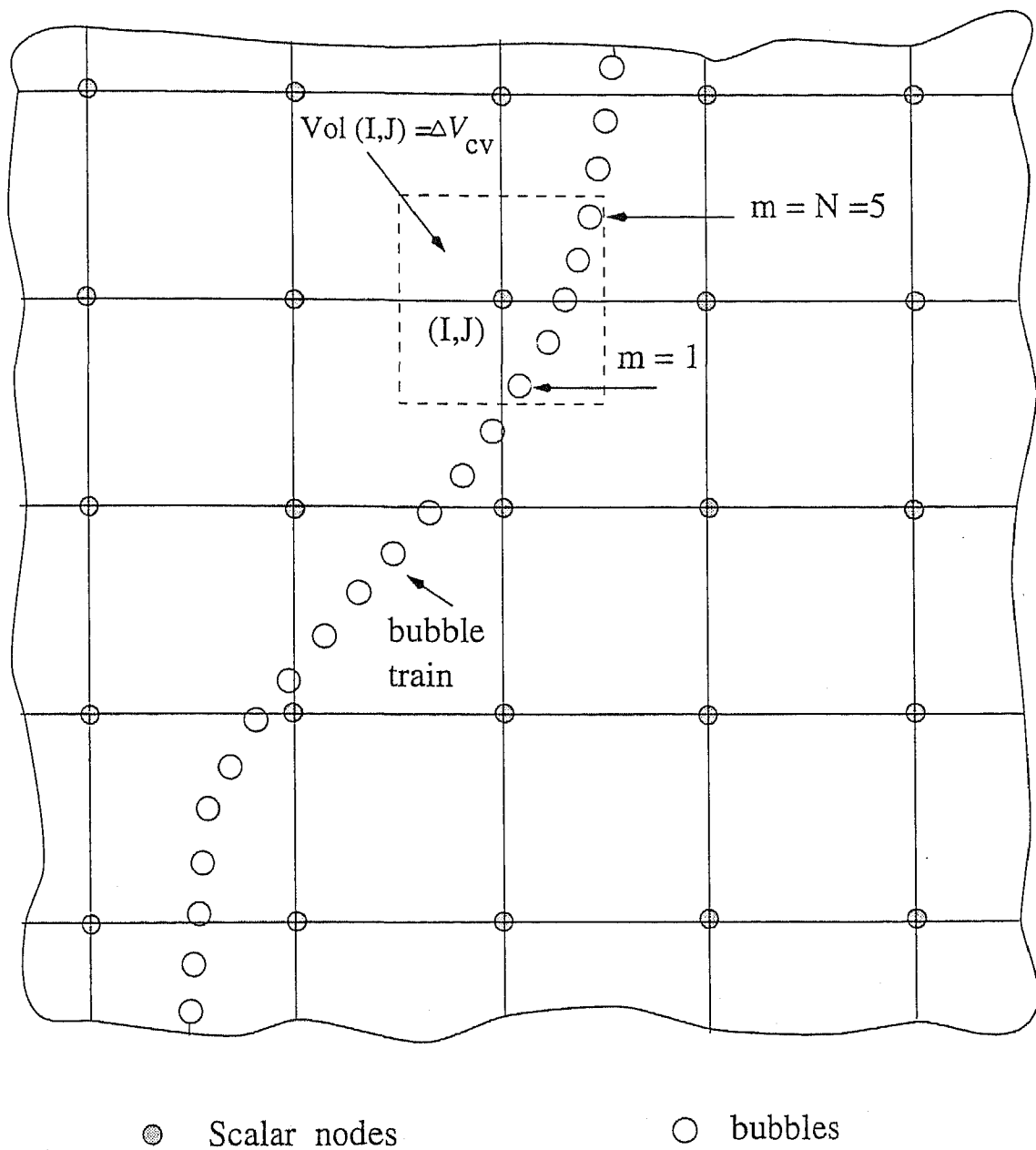


Fig. (2.1): Schematic of a section of Eulerian grid network intercepted by a bubble trajectory (2D - representation).

is a constant and takes a value between 0 and 1. The value of C_b depends on the physical characteristic of the two phase plume (e.g., bubble population, bubble size etc.). The constant C_b is normally determined by trial and error.

Similarly, the momentum exchange terms F_x , F_y , and F_z can be evaluated assuming that drag forces experienced by bubbles act with equal magnitude but opposite directions in the liquid phase. The expressions for F_x , F_y , and F_z can be represented in the compact tensorial notation as :

$$F_t = \frac{Q_t}{N \Delta V_{cr}} \sum \int \frac{3\mu_t C_D Re}{4d_b^2} (V_{B,t} - U) dt \quad (2.21)$$

2.3.6 Equation of tracer dispersion

As pointed out previously the residence time distribution (RTD) characteristic of a tundish can be studied mathematically by solving an appropriate species conservation equation. Thus, following a pulse addition the appropriate conservation equation of the added tracer can be described in Cartesian co-ordinate system in terms of the following transient convection-diffusion equation:

$$\frac{\partial}{\partial t}(C_t) + \frac{\partial}{\partial x}(uC_t) + \frac{\partial}{\partial y}(vC_t) + \frac{\partial}{\partial z}(wC_t) = \frac{\partial}{\partial x}(D_e \frac{\partial C_t}{\partial x}) + \frac{\partial}{\partial y}(D_e \frac{\partial C_t}{\partial y}) + \frac{\partial}{\partial z}(D_e \frac{\partial C_t}{\partial z}) \quad (2.22)$$

in which, D_e is the effective diffusivity defined as: $D_e = D_l + D_T$, where D_l is the molecular diffusivity and D_T is the eddy diffusivity. The latter, can be directly equated to the turbulence kinematic viscosity assuming turbulent Schmidt number to be approximately unity i.e., $\mu_T / (\rho D_T) = 1$ (valid for a wide range of engineering problems).

2.4 The boundary conditions

Fig.(2.2) shows the schematic of a tundish for mathematical simulation in the present study. The set of boundary conditions applied on the governing equations with relevance to the given

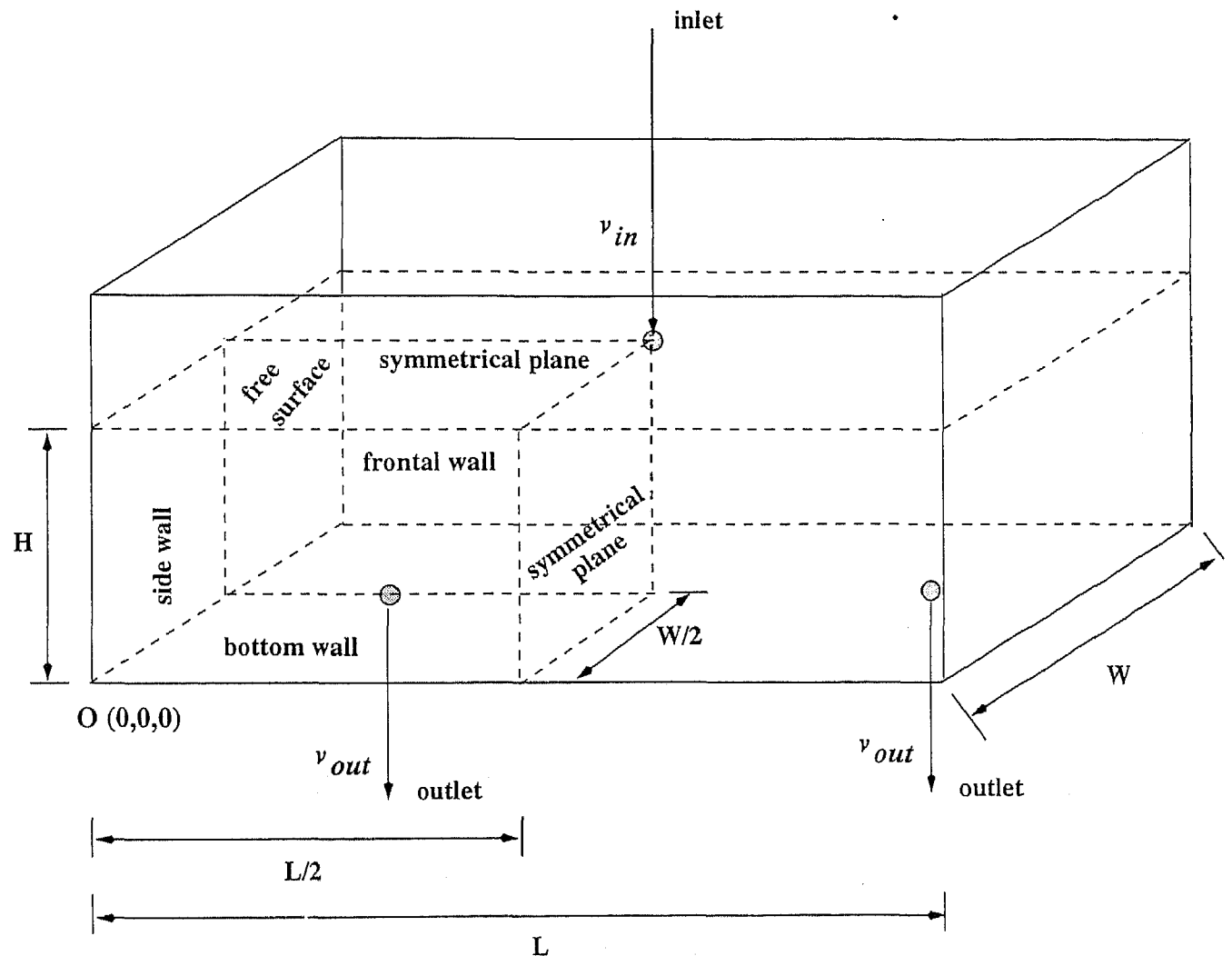
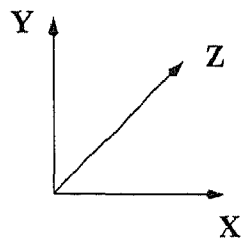


Fig. (2.2) : Schematic of the one quarter of the tundish taken for computation.

tundish can be represented as:

(i) At the free surface (in the north direction) zero shear is assumed to be transmitted for the velocity components. Zero gradient of k and ϵ were specified at the free surface. In conjunction with these, vertical component of flow is set to zero.

Mathematically,

At $y = H$, $0 \leq x \leq L/2$ and $0 \leq z \leq W/2$,

$$v = 0, \partial u / \partial y = \partial w / \partial y = 0, \partial k / \partial y = \partial \epsilon / \partial y = 0$$

(ii) No slip condition for the velocity components was specified at the solid walls. The values of k and ϵ were set at zero at the wall.

At the bottom wall, $y = 0$, $0 \leq x \leq L/2$ and $0 \leq z \leq W/2$,

$$u = v = w = 0, k = \epsilon = 0.$$

At the side wall, $x = 0$, $0 \leq y \leq H$ and $0 \leq z \leq W/2$,

$$u = v = w = 0, k = \epsilon = 0.$$

At the frontal wall, $z = 0$, $0 \leq y \leq H$ and $0 \leq x \leq L/2$,

$$u = v = w = 0, k = \epsilon = 0.$$

(iii) Gradients of all the velocity components at the symmetry plane are taken as zero and together with zero gradient of k and ϵ .

At the central longitudinal symmetrical plane, $z = W/2$, $0 \leq y \leq H$ and $0 \leq x \leq L/2$,

$$\partial u / \partial x = \partial v / \partial y = \partial w / \partial z = 0, \partial k / \partial y = \partial \epsilon / \partial y = 0$$

At the central transverse symmetrical plane, $x = L/2$, $0 \leq y \leq H$ and $0 \leq z \leq W/2$,

$$\partial u / \partial x = \partial v / \partial y = \partial w / \partial z = 0, \partial k / \partial y = \partial \epsilon / \partial y = 0$$

In addition to these, computations were carried out by force fitting the following conditions in the numerical solution scheme.

(iv) Inside the pouring stream,

$$u = w = 0, v = v_{in}$$

(v) At the exit nozzle,

$$u = w = 0, v = v_{out}, \partial k / \partial y = \partial \epsilon / \partial y = 0$$

The near wall regions have two major characteristics that distinguish them from the bulk flow [31,35]:

- i. steep non-linear gradient in the flow properties, and
- ii. levels of Reynolds number are sufficiently low for local isotropy of small scale turbulence to prevail.

Hence, the basic turbulence model becomes inapplicable in these regions and alternate representation must be sought. In the present study wall function procedure [31,35] has been used. The method is based on one-dimensional fluid flow, and assumes that the velocity profile in the near wall region is given by the universal logarithmic wall law which can be represented as :

$$\frac{u}{u_*} = \frac{1}{\kappa} \ln (y^* E) \quad (2.23)$$

where u is the velocity parallel to the wall and u_* ($= \sqrt{(\tau_w / \rho)}$) is the friction velocity, κ is the van Karmen constant and E is the roughness parameter typically taken as 9 for hydraulically smooth walls. y^* is a dimensionless wall distance and is defined as :

$$y^* = \frac{(y u_* \rho)}{\mu} \quad (2.24)$$

where y is the normal distance from the wall. This law has been applied to a point whose y^* value is greater than 11.63. This is schematically shown in Fig.(2.2). In the y^* region specified above the Reynolds stresses are constant and the wall stresses, τ_w can be calculated as :

$$\tau_w = \rho C_\mu^{0.5} k \quad (2.25)$$

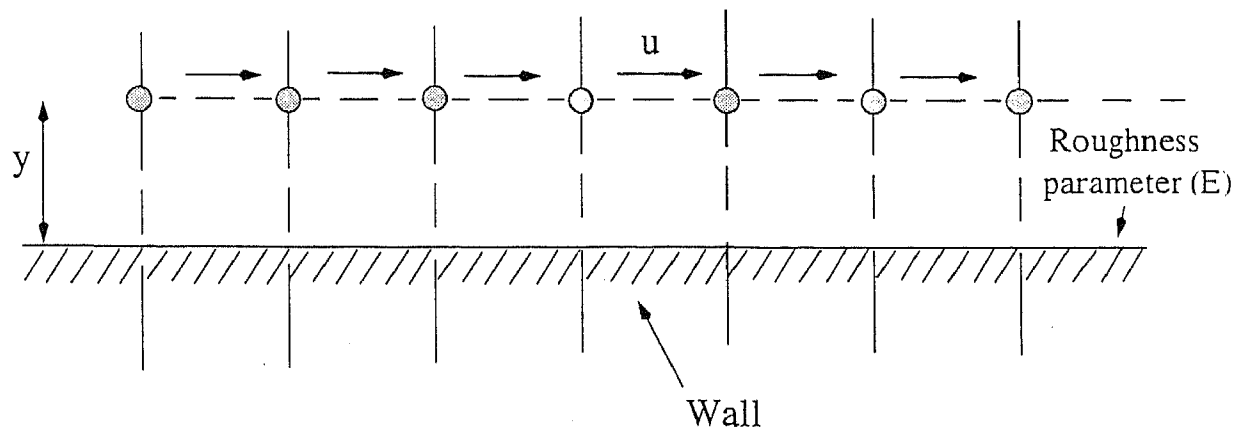


Fig. (2.3) : Schematic representation of procedure aplplied for the near wall region on flow variable and turbulence parameter.

Further, in the near wall region the convection-diffusion of $(\underline{u}\underline{u})$ is negligible. This implies that the rate of production of turbulent kinetic energy k is equal to its dissipation. Such considerations lead to:

$$\frac{k}{u_\tau^2} = \frac{1}{(\sqrt{C_\mu})} \quad (2.26)$$

This relation is normally used as an boundary condition for k in the two equation $k-\epsilon$ model. Similarly the boundary condition for ϵ can be expressed as :

$$\epsilon = \frac{u_\tau^3}{\kappa y^*} \quad (2.27)$$

The two preceding relationships are to be applied to a near wall node whose y^+ is greater than 11.63.

For concentration field calculation zero flux boundary condition is imposed on all the solid surfaces,symmetrical planes and the free surface. In addition to this, the following condition i.e.,

$$\text{at } t = 0, C_i = C_i^o$$

was applied to Eq.(2.22) as an initial condition, where, C_i^o is tracer concentration (tracer having the same density as the bulk liquid was considered) in the system at $t=0$. It is instructive to note here that one way coupling between Eq.(2.22) and the flow and turbulence model equations allows flow computation to precede the calculation of tracer dispersion. Using the converged flow field, the $C_i(x,y,z,t)$ field was predicted. From the predicted concentration at the outlet as a function of time, t , the C -curve was constructed.

2.5 The General Differential Equation

The general structure of the relevant differential equations (Eqs.(2.1) to (2.6)) describing the conservation of mass and momentum and that of the $k-\epsilon$ Model of turbulence indicate that all the dependent variables of interest obey a generalised conservation principle. If the general variable is denoted by ϕ , the general differential equation can be written as:

$$\frac{\partial}{\partial t} (\rho \phi) + \operatorname{div} (\rho u \phi) = \operatorname{div} (\tau \operatorname{grad} \phi) + S_\phi \quad (2.28)$$

The four terms in the general differential equation, are the transient term, convection term, the diffusion term (Γ is the diffusion coefficient) and the source term, S_ϕ . The quantities Γ and S are specific to a particular meaning of ϕ . Depending on the general variable ϕ , an appropriate meaning will have to be given to the diffusion coefficient Γ and the source term S . For the present set of governing equations this is summarised in Table-2.3.

Table-2.3 : Definition of Γ , ϕ and S of Eq.(2.28).

Conservation of	ϕ	Γ	S_ϕ
Mass	1	0	0
Momentum	u	μ_e	Eq.(2.2.a)
	v	μ_e	Eq.(2.3.a)
	w	μ_e	Eq.(2.4.a)
Turbulent kinetic energy	k	μ_e/σ_k	Eq.(2.5.a)
Dissipation rate of kinetic energy	ϵ	μ_e/σ_ϵ	Eq.(2.6.a)
Concentration	C_i	μ_e/ρ	Eq.(2.22)

Hence, the procedure of casting any particular differential equation into the general form Eq.(2.28) requires manipulation of the equation so that the convection and diffusion terms conform to the standard form. The coefficient of $\operatorname{grad} \phi$ is taken as the expression for Γ and the remaining terms on the right hand side are collectively defined as the source term S . Since, all the equations for mass, momentum transport, turbulence related phenomena and species conservation can be thought of a particular case of general equation Eq.(2.28) consequently, we need to concern ourselves with the numerical solution of Eq.(2.28) only.

2.6 The Grid Arrangement

A portion of the three dimensional grid is shown in Fig.(2.4). For the grid point P , points E and W (east and west respectively) are its x-direction neighbours, while N and S (north

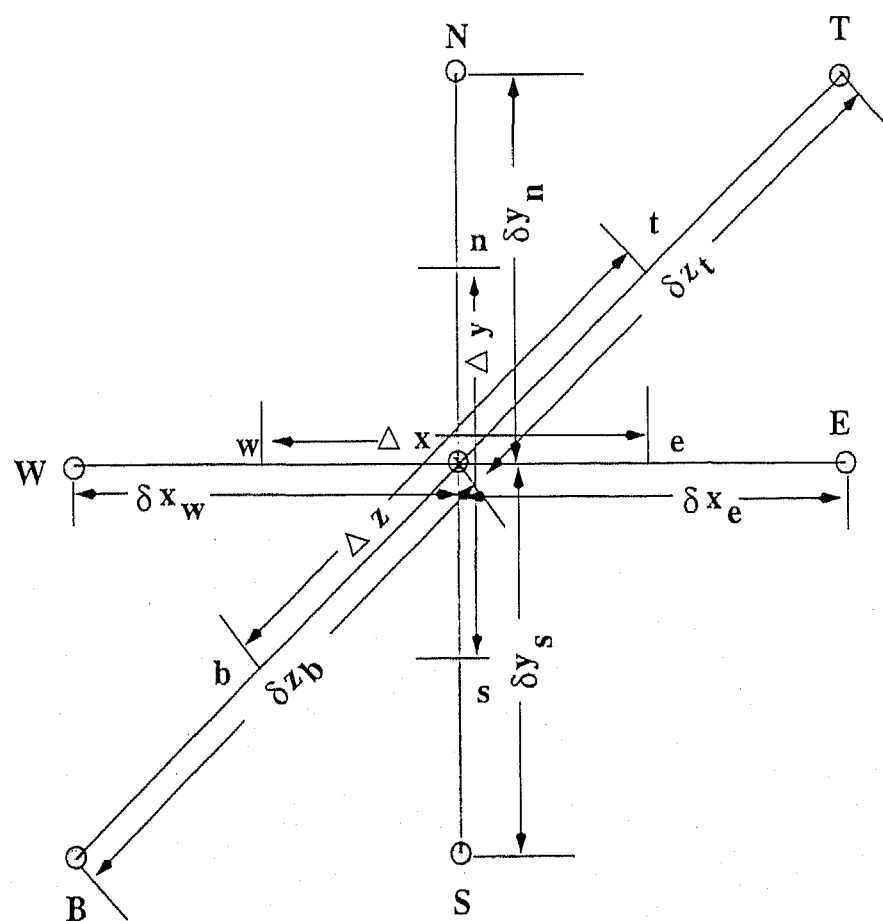
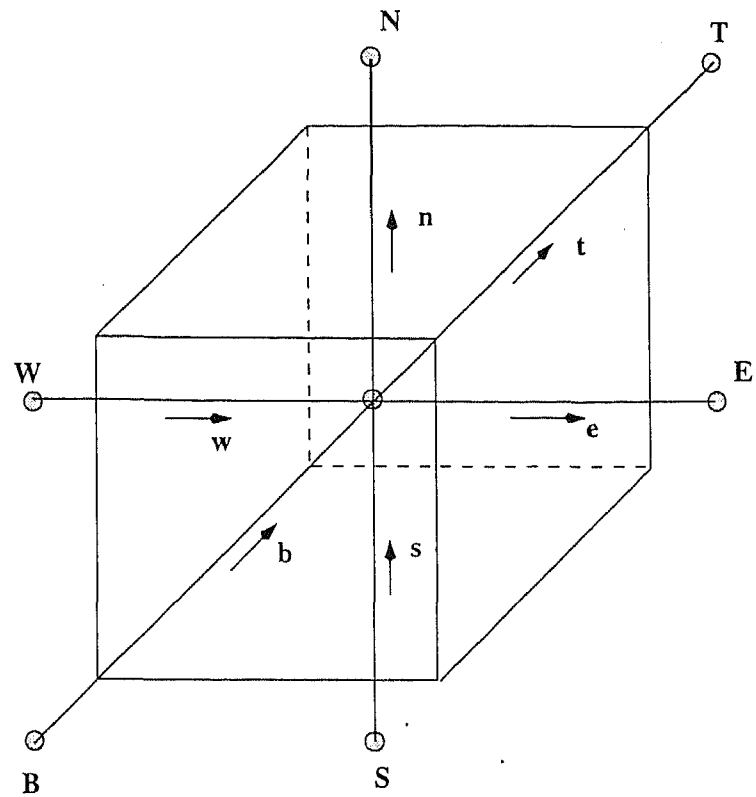
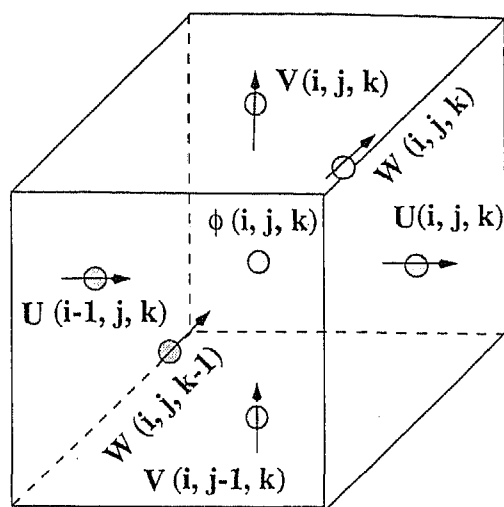
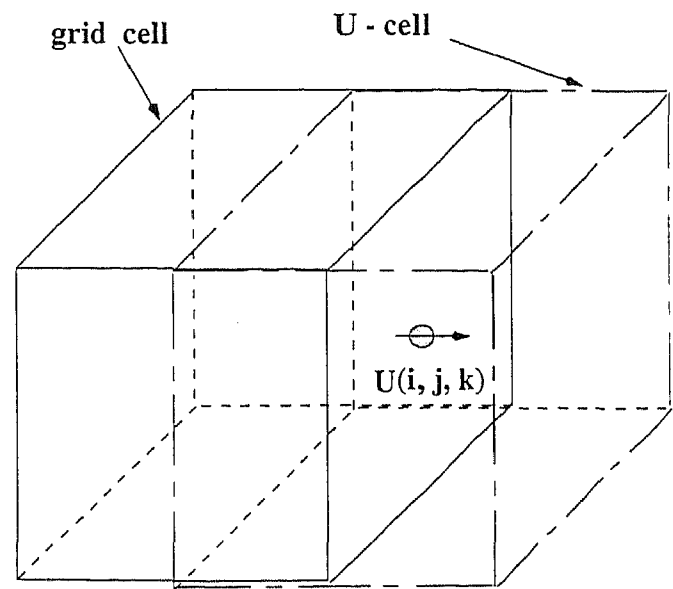


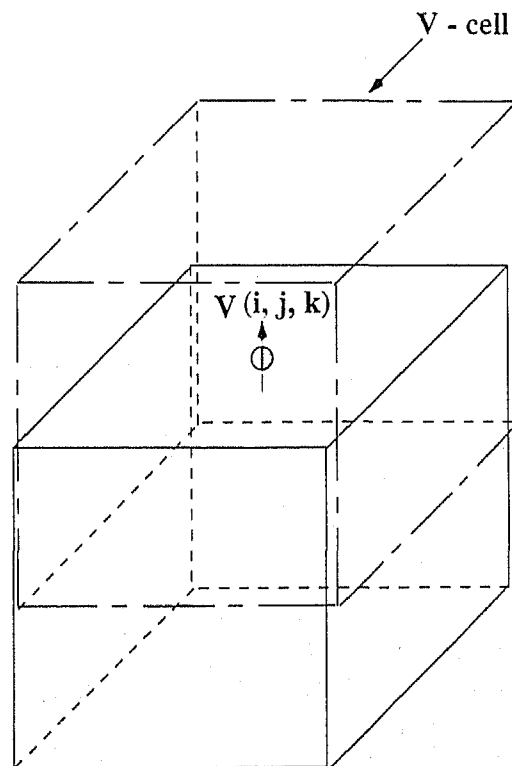
Fig. (2.4): A typical three dimensional, scalar control volume and various nomenclature used in the cartesian co-ordinate system.



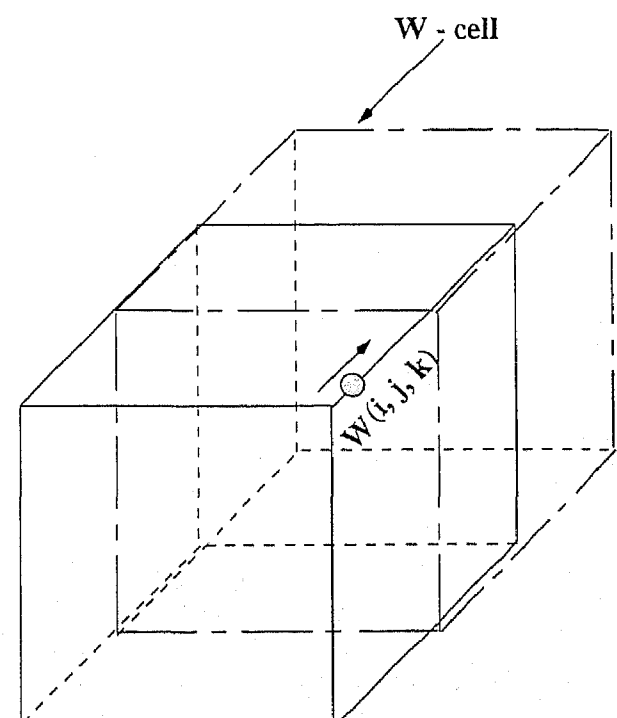
A Grid Cell



A U - Cell



A V - Cell



A W - Cell

Fig. (2.5) : Scalar and staggered control volumes in three dimensional Cartesian co-ordinate system

and south respectively) are the y-direction neighbours and T and B (top and bottom respectively) are the neighbours in the z-direction. The whole flow domain has been divided into a number of such non-overlapping control volumes. Staggered control volumes have been considered for the velocity components u , v and w . Fig.(2.5) represents the different staggered control volumes at which the discrete values of the velocities are located. These values represent the averages over the respective control volumes. Scalar variables i.e., p , k , μ_e , ρ and ϵ are stored at the grid nodes, while the velocities u , v and w are stored midway between the main grid nodes. The velocities are located where they are needed for the calculation of the convective fluxes of scalar variables.

2.7 The Numerical Solution Procedure

A control volume based finite difference procedure [34] has been adopted in the present study to solve the governing equations numerically. The solution is initiated by discretizing the domain in a large number of non-overlapping control volumes. The governing equation is integrated around all such control volumes to yield a system of algebraic equations. called the discretization equation [34]. The governing equations Eqs.(2.1) to (2.8) have both first and second order derivatives. These terms are numerically integrated using the concept as applied to a combined convection-diffusion problem incorporating the hybrid differencing scheme proposed by Patankar [34]. The pressure-velocity interlinkage in Eqs.(2.2) to (2.4) have been solved by an implicit finite difference procedure referred to as *SIMPLE* [34] (Semi-Implicit Method for pressure linked equations). A typical discretization equation for the general differential equation (2.29) can be written as :

$$A_p \phi_p = A_E \phi_E + A_W \phi_W + A_N \phi_N + A_S \phi_S + A_T \phi_T + A_B \phi_B + A_p^o \phi_p^o + S_C . vol \quad (2.29)$$

in which, A_p , is the centre point coefficient while A_E , A_W , A_N , A_S , A_T and A_B are the neighbour point (three dimensional) coefficients, representing the combined effect of fluid convection and diffusion. $A_p^o \phi_p^o$ is zero for steady state problems. Further, S_C represents the constant component of the linearized source term (viz., $S = S_c + S_p \phi_p$) while the slope has been embodied in the expression of A_p , the centre point coefficient.

The centre point coefficient A_P is represented as :

$$A_P = A_E + A_W + A_N + A_S + A_T + A_B + A_P^o - S_p \cdot vol \quad (2.30)$$

Thus, in a system of n internal control volumes, n number of similar algebraic equations (viz., Eq.(2.30) are obtained. Further, since the discretization equations are obtained from the same governing equation Eq.(2.28), the former therefore embodies the same conservation principle as the latter one. This is an important feature of the control volume based formulation as against the routine Taylor series numerical solution procedure.

Prior to the solution of the discretization equations the boundary conditions are also transformed into equivalent numerical form. Boundary conditions are only applied to control volumes located at the domain boundaries. Discretization equations are derived by the same procedure as mentioned. In essence, the incorporation of a boundary condition involves the modification of A_P and/or the source terms of the discretization equations of the boundary control volumes .

The resultant set of discretization equations for both boundary and internal nodes were solved using the Tri-Diagonal Matrix Algorithm (*TDMA*) adopting a line by line solution procedure. In this, a particular grid line, say in z -direction, is chosen and assuming the dependent variable (ϕ) to be guessed in the x and y directions, the problem is thus reduced to a pseudo-one-dimensional situation and subsequently solved by *TDMA*. This was applied to all the grid lines in one direction and the entire process was repeated for the other two space directions to obtain a tentative solution of the dependent variable , ϕ . This typically constituted one iteration. The total number of iterations required was decided by the convergence criteria adopted, which in the present study was defined according to :

$$\sum \sum \sum [A_p \phi_p - (\sum A_{nb} \phi_{nb} + S_C \cdot vol)] < \epsilon_\phi \quad (2.31)$$

in which,

$$A_{nb} \phi_{nb} = A_E \phi_E + A_W \phi_W + A_N \phi_N + A_S \phi_S + A_T \phi_T + A_B \phi_B \quad (2.32)$$

The triple sum in Eq.(2.31) represents the summation over the entire three dimensional domain. Under relaxation of dependent variable was employed to achieve/enhance convergence. If ϕ_p^* is the value from the previous iteration of the dependent variable ϕ_p (ϕ_p implies ϕ evaluated at a point P) and α is the under relaxation factor then the change in the value of ϕ_p can be slowed down from iteration to iteration by the following mathematical treatment [34] :

$$\phi_p = \phi_p^* + \alpha \left(\frac{\sum a_{nb} \phi_{nb} + b}{A_p} - \phi_p^* \right) \quad (2.33)$$

in which, ϕ_p^* the value of ϕ in the previous iteration.

Under relaxation factors for the problem chosen were determined by trial and error. Typically, under relaxation factor of 0.5 was applied to u , v and w and while a value of 0.7 was used for the turbulence parameters, k and ϵ . No under relaxation factor was used for the calculation of concentration field.

2.8 Modelling of the inclined tundish wall and flow modification devices

To this end, the well known cell porosity technique of Moult and coworkers[36] have been applied. In this, the numerical calculation domain is considered to be perfectly rectangular and therefore, the grid is laid assuming the tundish to be rectangular Fig.2.6 (a). Subsequently, the inclined walls (e.g., the exact tapered tundish geometry) are superimposed on the numerical calculation domain, so as to produce the true flow domain Fig2.6.(b). These are shown schematically in Fig.(2.6). There, as seen, the intersection of the inclined tundish walls with the numerical grid results into two different kinds of control volumes in the numerical calculation domain. Active control volumes and inactive control

volumes. Inactive control volumes are completely out side the flow domain (shown with a dot at the centre in Fig.2.6(b)), Active control volumes while are either partly or completely within the flow domain. For the latter type of control volumes (e.g., completely within the flow domain and thus, entirely filled with liquid), the full form of the discretisation equation (which is the algebraic equivalent of the partial differential equations, written below, for example, for a general variable ϕ) is applicable, viz.,

$$A_P \phi_P = A_E \phi_E + A_W \phi_W + A_N \phi_N + A_S \phi_S + A_T \phi_T + A_B \phi_B + S_C .vol \quad (2.34)$$

However, for the control volumes which are partly within the flow domain and partly outside, the coefficients of the discretisation equation are modified in such a way that only the correct, available control surfaces are applied to the calculation of convective and diffusive fluxes . Referring to Fig.(2.7) , thus, a set of blockage ratios or cell porosity factors can be estimated (from knowing the tundish inclination and the characteristics of the grid system) and these can be subsequently applied to modify the coefficients of the discretisation equations Eq.(2.34) appropriately. For a typical three dimensional control volume partly in the flow domain and partly outside (see Fig.2.7), one can therefore, define a set of six different blockage ratios for the six faces of the control volume. On the basis of such, the following set of modified coefficients, applicable to such control volumes, can be conveniently estimated, viz.,

$$A_{E, \text{new}} = A_{E, \text{old}} [1 - b_E]$$

$$A_{W, \text{new}} = A_{W, \text{old}} [1 - b_W]$$

$$A_{N, \text{new}} = A_{N, \text{old}} [1 - b_N]$$

$$A_{S, \text{new}} = A_{S, \text{old}} [1 - b_S]$$

$$A_{B, \text{new}} = A_{B, \text{old}} [1 - b_B]$$

$$A_{T, \text{new}} = A_{T, \text{old}} [1 - b_T]$$

In the set of above expressions, b 's are the blockage ratios in different directions (as characterised by the subscript).

An interesting situation arises, when all the blockage ratios for a given control volume assume a value of unity. This implies that the control volume is essentially outside the

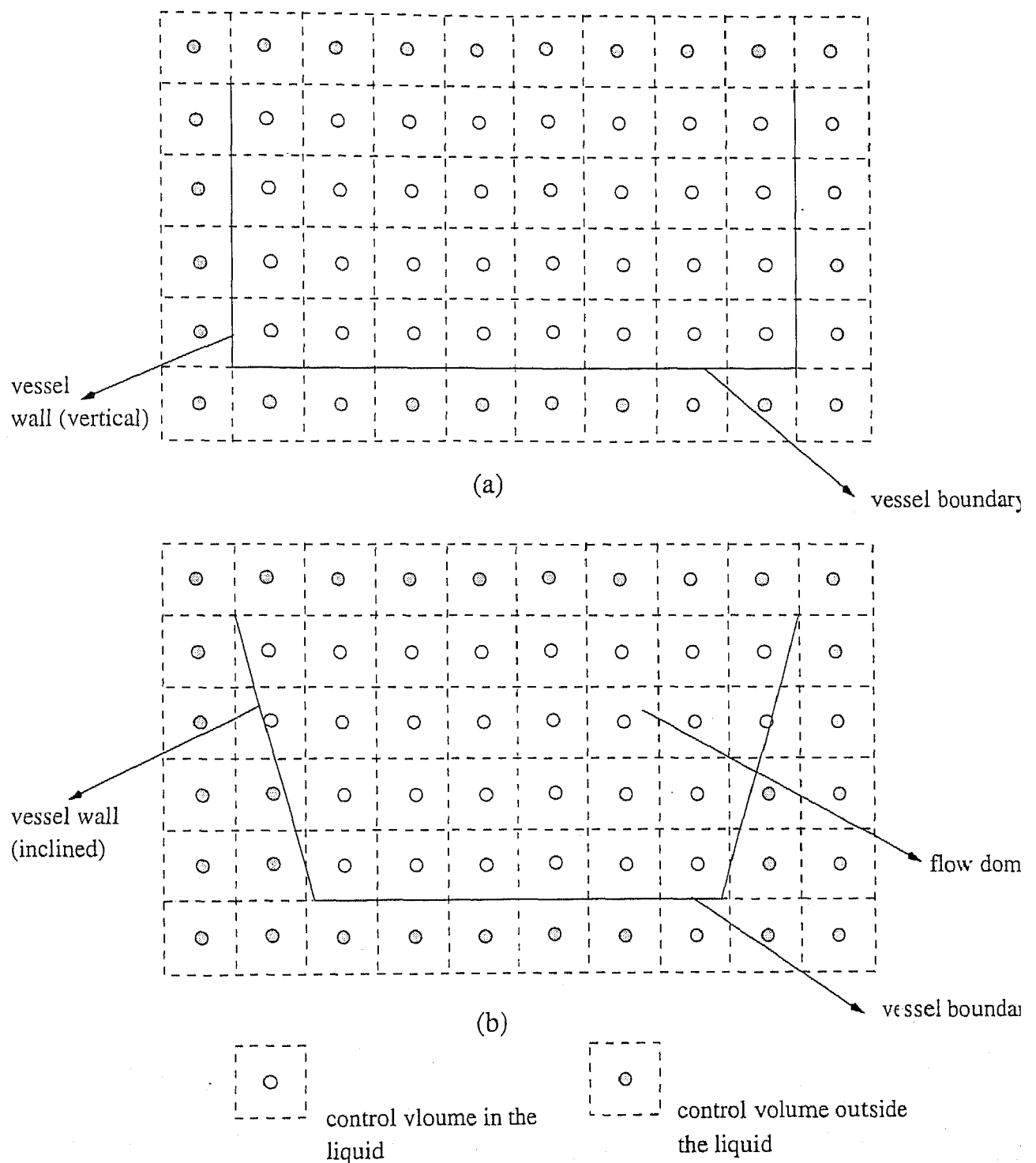


Fig. (2.6) : The characteristics of calculation and flow domains in terms of the finite difference grid.
 (a) calculation domain (b) flow domain

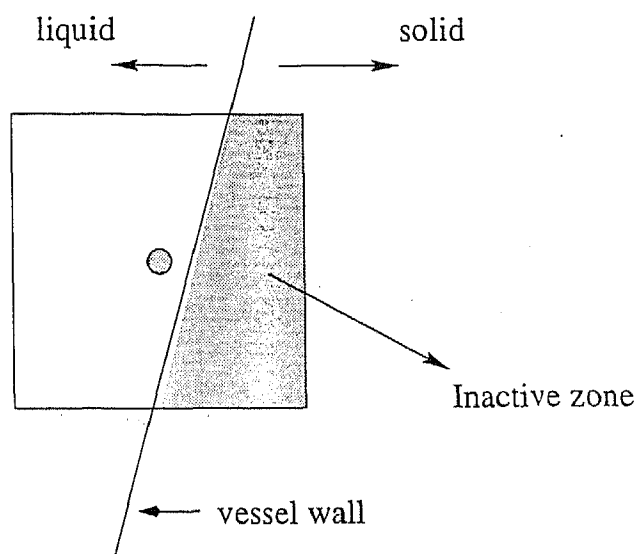


Fig. (2.7) : A control volume cut by the vessel wall (2-D representation).

flow domain and therefore inactive, as far as its influence on the predicted results is concerned. Under such a condition, the control volume or the characteristic grid node is completely isolated from the calculation domain by re-defining the components of the source terms, S_p and S_c as follows:

$$S_c = 10^{30} * \text{the desired value}$$

$$\text{and, } S_p = -10^{30}$$

Through such a practice, zero value of the dependent variables can be fixed at all the inactive control volumes. Similar approaches were adopted to model the flow control devices (dams, weirs etc.) which are essentially inactive portion of the flow domain. Standard wall function procedures were applied on both the faces of the flow control devices which are normal to the longitudinal direction, x.

2.9 The computer program

The concept of casting all governing differential equations to a general differential equation has been outlined Section-2.5. Consequently, a general purpose computer program was developed to solve Eq.(2.28). The flow diagram of the three dimensional model developed is shown in Fig.(2.8).

The basic structure of the present combined Langrangian-Eulerian procedure has been:

- i. The total flow is equally divided between a preconsidered number of trajectories. On the basis of such, flow rate (Q_t) per trajectory is estimated.
- ii. The equations for bubble motion are solved for each of the trajectories and then superimposed on the Eulerian grid. From these, overall distributions of α_l , F_x , F_y and F_z etc. estimated.
- iii. Estimated α_l , F_x , F_y and F_z are incorporated into the equations of the continuous phase (viz., the liquid) and solved iteratively by embodying the *SIMPLE* procedure of Patankar and Spalding [34].

- iv. At the end of a predetermined number of iterations of the liquid phase equations, the trajectories of the bubbles are recalculated using the prevalent flow and turbulence fields.
- v. Based on this the distribution of α_l , F_x , F_y and F_z etc. were updated. The above steps are repeated till the converged velocity field and bubble trajectories are obtained.
- vi. Using converged velocity fields, the concentration is calculated as a function of time.

For single phase calculations (viz. no gas injection), steps (iii) through (vi) were only considered assigning a value of unity to α_l .

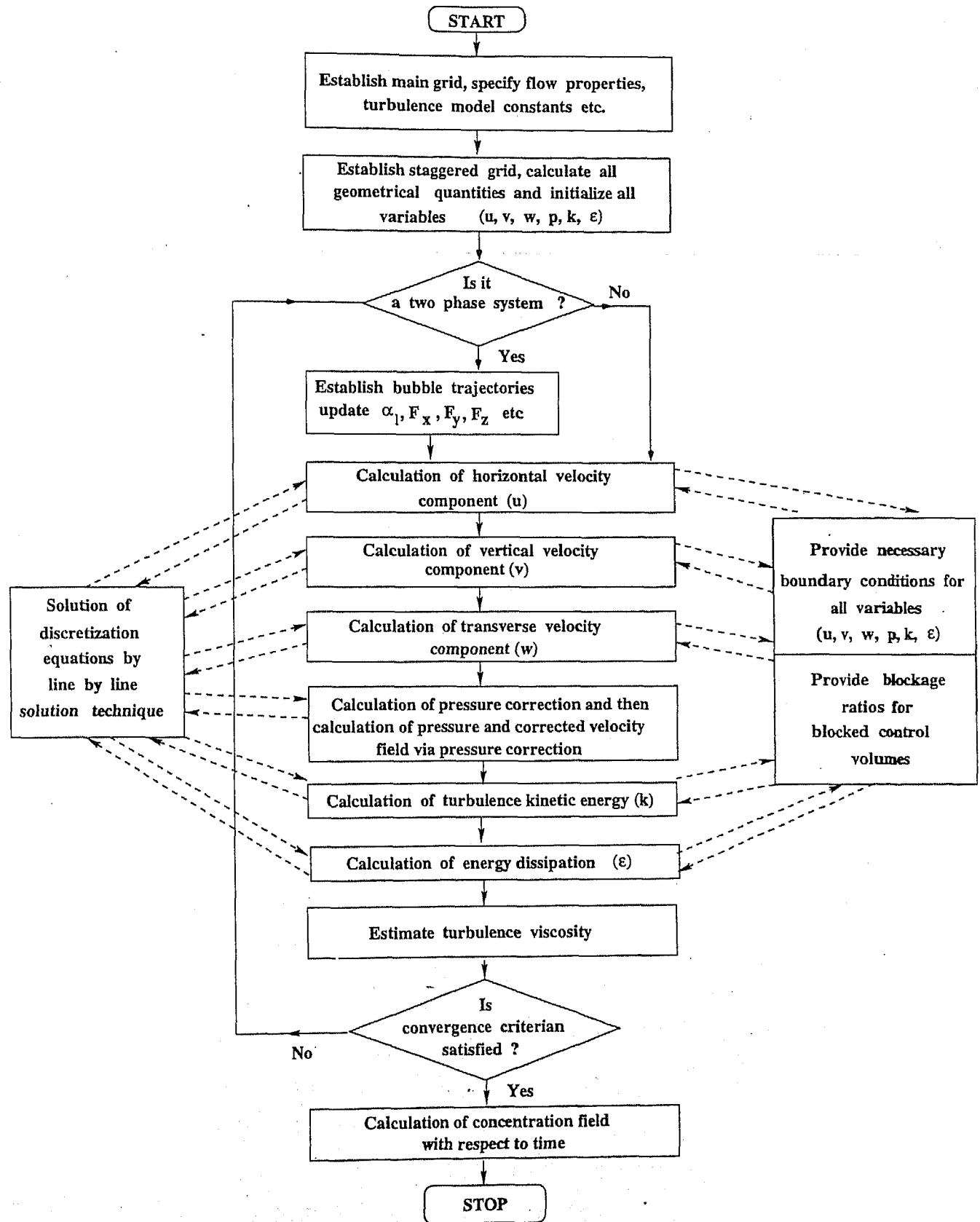


Fig. (2.8) : The flow diagram of the computer model

CHAPTER 3

RESULTS AND DISCUSSION

In the previous chapter, the salient features of the two phase, three dimensional turbulent flow model were presented. This chapter is concerned with the validation of the three dimensional two phase model and application of the model to fluid flow and Residence Time Distributions (RTD) in different tundish designs.

3.1 Assessment of the computational procedure developed

The adequacy and appropriateness of the steady state, three dimensional, two phase turbulent flow model was assessed by carrying out some standard three dimensional flow simulation tests. This included, (i) flows in enclosed cavity with one of the walls moving, (ii) entrance length v. Reynolds number calculation in ducts of square cross-section and (iii) prediction of bubble rise in a stagnant fluid. These calculations were carried out under laminar flow condition (by setting $\mu = \mu_e$ and modifying S_u , S_v and S_w appropriately in the flow equations). These are summarised below in detail.

3.1.1 Laminar flow in an enclosed cubic cavity

Steady, laminar, single phase flow in three dimension can be conveniently represented by the Navier-Stokes equations presented already. Thus, considering $\mu_e = \mu$, $\alpha_1=1.0$ and $S_u = S_v = S_w = 0$ in the calculation procedure, fluid flow in a cubic cavity ($l = 1\text{m}$, $\rho = 1 \text{ kg/m}^3$ and $\mu = 0.01 \text{ kg/m.s}$) was predicted numerically considering one of the two horizontal cavity walls moving with a velocity of 1m/s (e.g., $Re=100$) in the positive x direction. The boundary conditions for the test problem included, a zero velocity (no slip) on all the stationary walls. However, the influence of the moving wall was incorporated via a viscous drag acting on the fluid in contact with the moving wall. In this one of the walls of the cubic cavity was made to move with a velocity of 1m/s in the positive x

direction as shown in Fig.3.1. The remaining five solid walls were considered to be stationary. In order to define the boundary conditions for the given problem exactly, a zero velocity (no slip) condition was applied on the stationary walls. In addition to this, to incorporate the influence of the moving north wall on the fluid flow, the general discretization equation for the dependent variable u , (the x component of motion), i.e.,

$$A_p u_p = A_E u_E + A_W u_W + A_Y u_N + A_S u_S + A_T u_T + A_B u_B + S_c \quad (3.1)$$

was modified for the boundary control volumes lying in the immediate vicinity of the moving wall according to :

$$A_p u_p = A_E u_E + A_W u_W + A_S u_S + A_T u_T + A_B u_B + S_c^* \quad (3.2)$$

where, $S_c^* = A_n u_n + S_c$ and u_n is the given velocity of the moving wall(= 1 m/s).

The predicted flow on the central vertical XY plane (at $z=0.5$ m), transverse vertical YZ plane(at $x=0.5$ m) and transverse horizontal plane at ($y=0.5$) have been shown in Figs 3.2a through 3.2c. These flow fields are in good qualitative agreement with the equivalent computational results of Hwar and coworkers[37].

To illustrate this further, the predicted variations of the horizontal velocity component, u along the central vertical line and that of the vertical velocity component along the horizontal centre line are shown in Fig 3.3 There, equivalent results reported by Hwar and coworkers[37] have also superimposed for the sake of a direct comparison. Near perfect agreement between present and earlier estimates is readily apparent in Fig.3.3. It is important to mention here that results presented in Figs. 3.2 and 3.3. were derived using a $31 \times 31 \times 31$ uniform grid system which was essentially found to produce a grid independent solution.

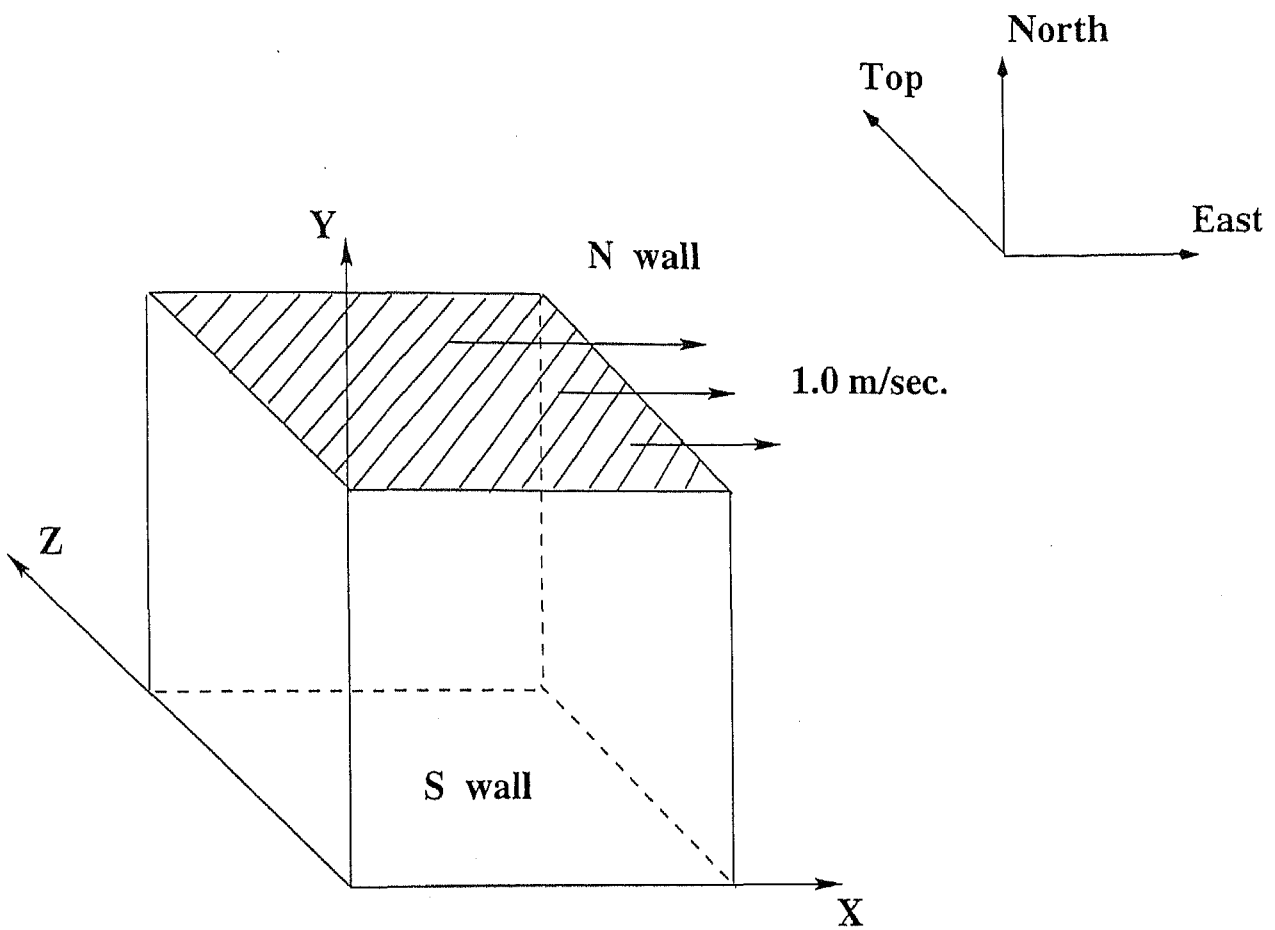
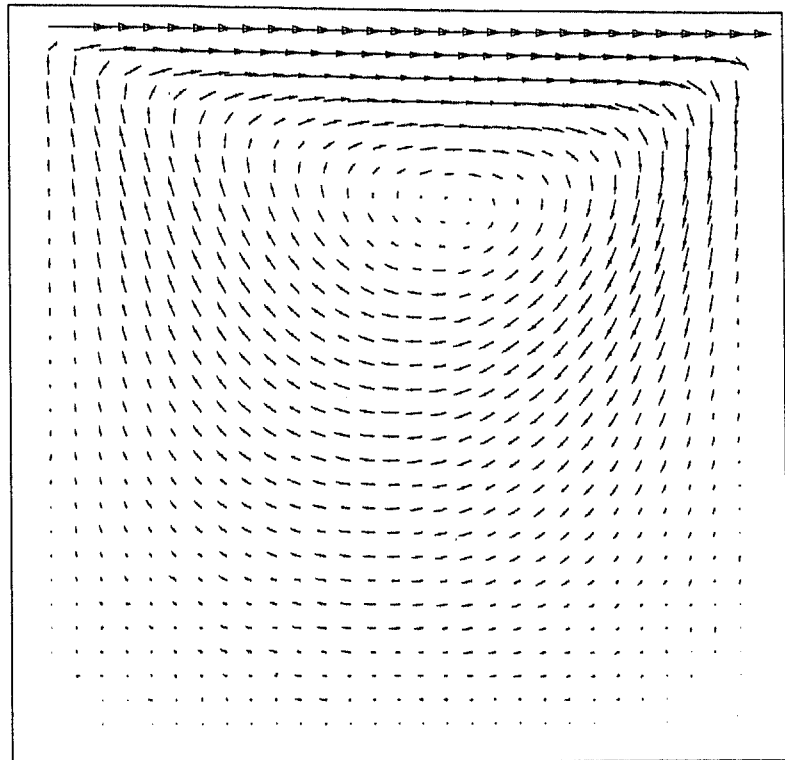


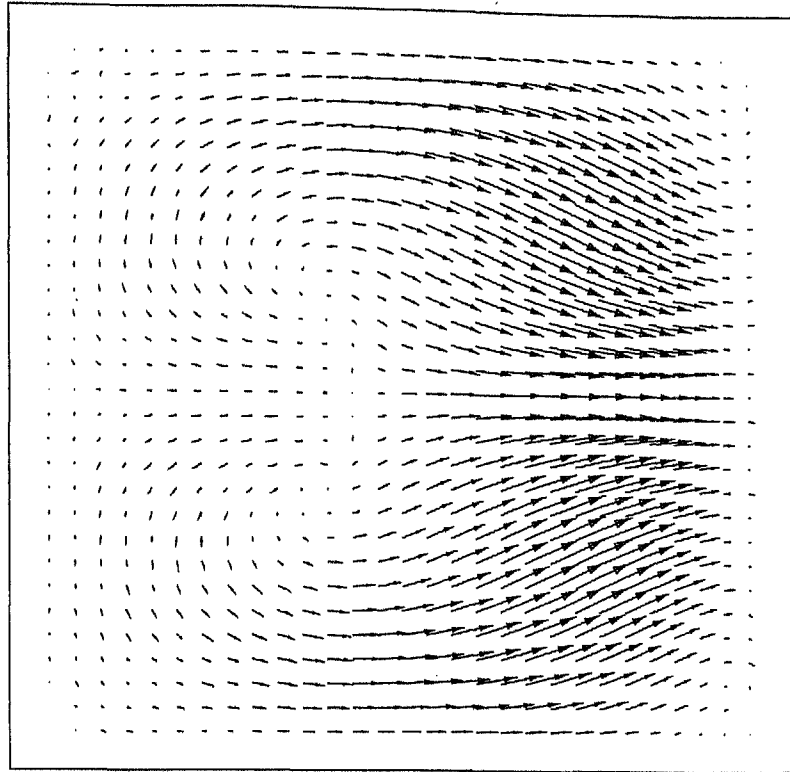
Fig. (3.1) : Schematic of the cubic cavity with one of the walls moving.



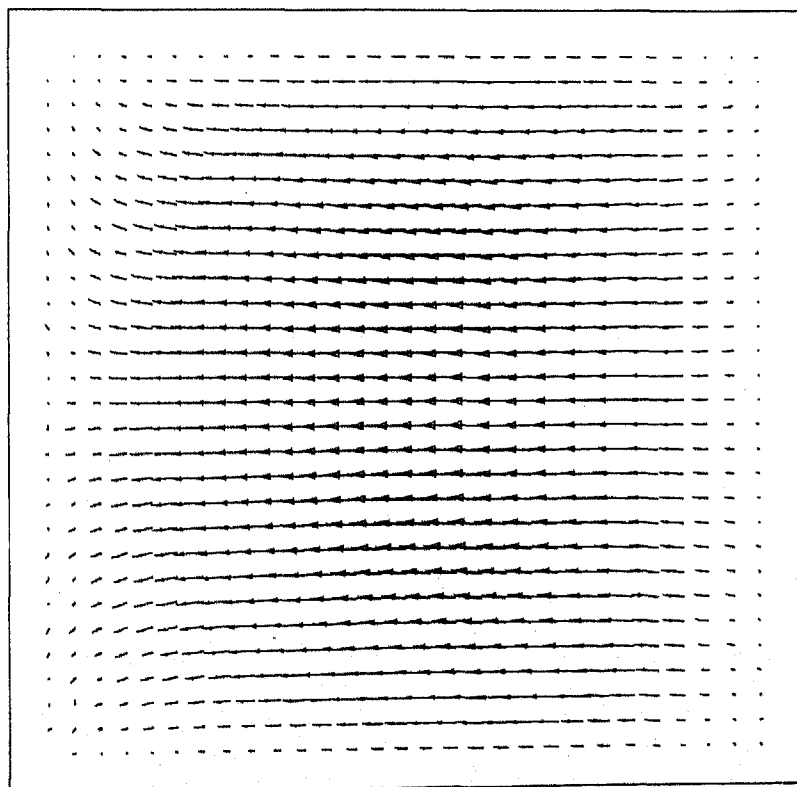
1.0 m s^{-1}



Fig. (3.2a) : Predicted velocity field in longitudinal vertical plane at z/W of 0.5 for cubic cavity test ($Re=100$)



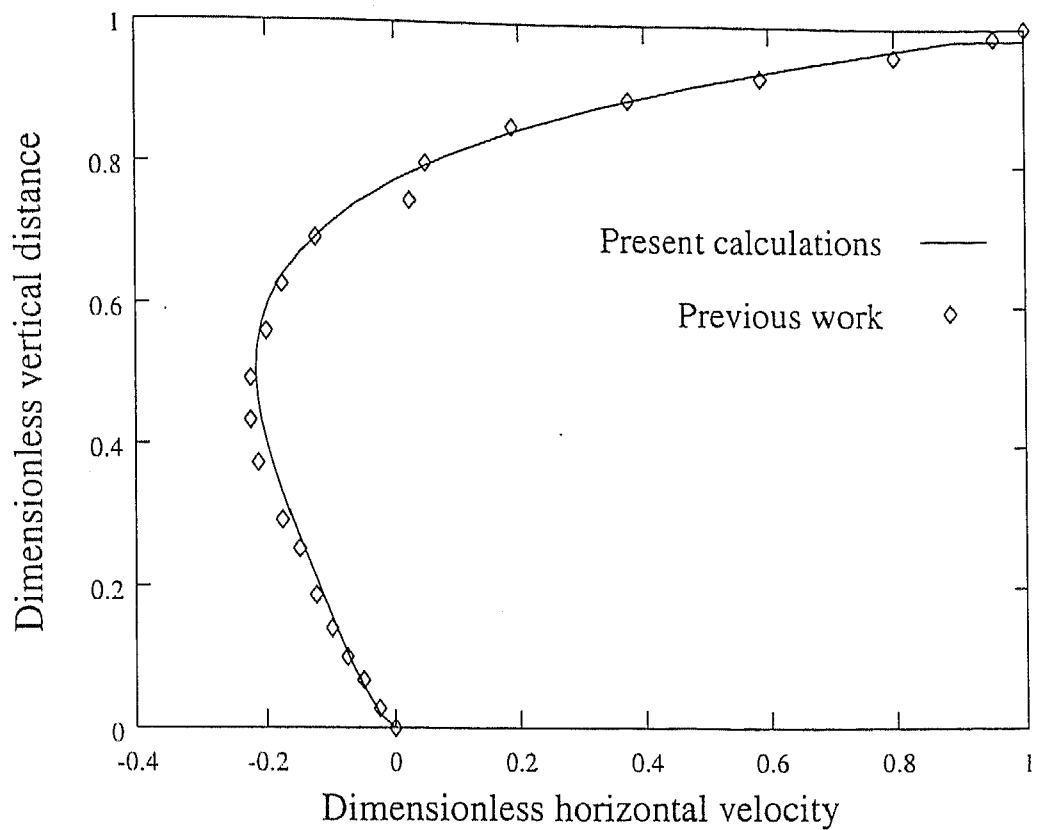
(a)



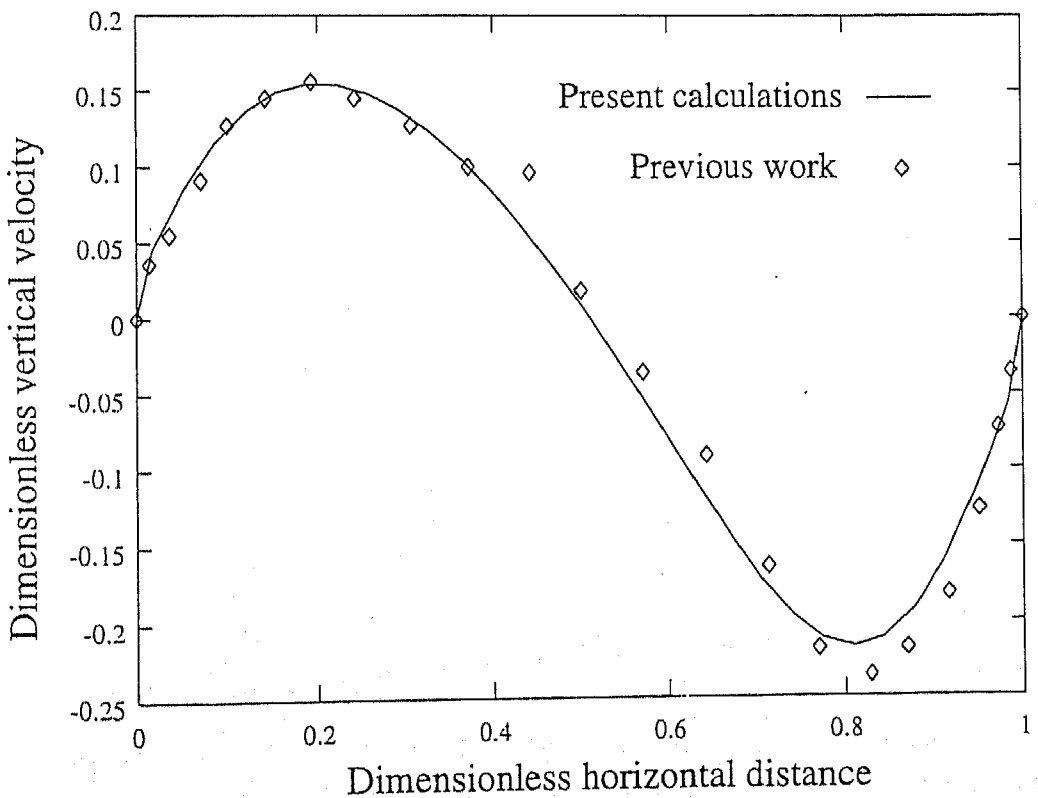
(b)

Fig. (3.2b) : Predicted velocity field for cubic cavity test (Re=100)

- (a) transverse vertical plane at $x/L=0.5$
- (b) transverse horizontal plane at $y/H=0.5$



(a)



(b)

Fig. (3.3) : Cubic cavity velocity profile for (Re=100)

(a) vertical centre line

(b) horizontal centre line

3.1.2 Entrance length prediction for laminar flow

When a flow enters a duct (internal flow bounded by walls) the viscous effects grow and boundary layer on the duct wall develops. The boundary layers eventually meet along the centreline and from this point onwards, the thickness of the boundary layers remain invariant in the streamwise direction. This is shown in Fig.(3.4) [38]. As seen, there is an entrance region where a nearly inviscid upstream flow converges and enters the tube. Viscous boundary layers grow downstream, retarding the axial flow $u(x,r)$ at the wall and thereby, accelerating the centre core flow to maintain the incompressible, continuity requirement. At a finite distance from the entrance, the boundary layers merge and the inviscid core disappears. The tube flow then is entirely viscous, and the axial velocity adjusts slightly further until at $x = L_e$, it no longer changes with x (no acceleration) and is said to be fully developed, i.e. $u = u(r)$ only. Downstream of $x = L_e$ the velocity profile as well as the wall shear stress is constant, and the pressure drop varies linearly with x , for both laminar and turbulent flows (see Fig.3.4).

Dimensional analysis [38] shows that the Reynolds number is the only parameter affecting entrance length. Thus,

$$\frac{L_e}{D} = g \left(\frac{\rho V D}{\mu} \right) = g (Re) \quad (3.3)$$

For laminar flow [39], the accepted correlation for entrance length in ducts is :

$$\frac{L_e}{D} = K Re \quad (3.4)$$

Where k is a constant of proportionality, the value of which, depends on the cross-section of the duct, e.g. for ducts with circular cross section, $k = 0.06$. In the present work entrance lengths were calculated for ducts with square cross-section Fig.(3.5) for laminar flow condition.

The dimension of square cross-section (D) was varied between 1×10^{-2} to 3×10^{-2} m

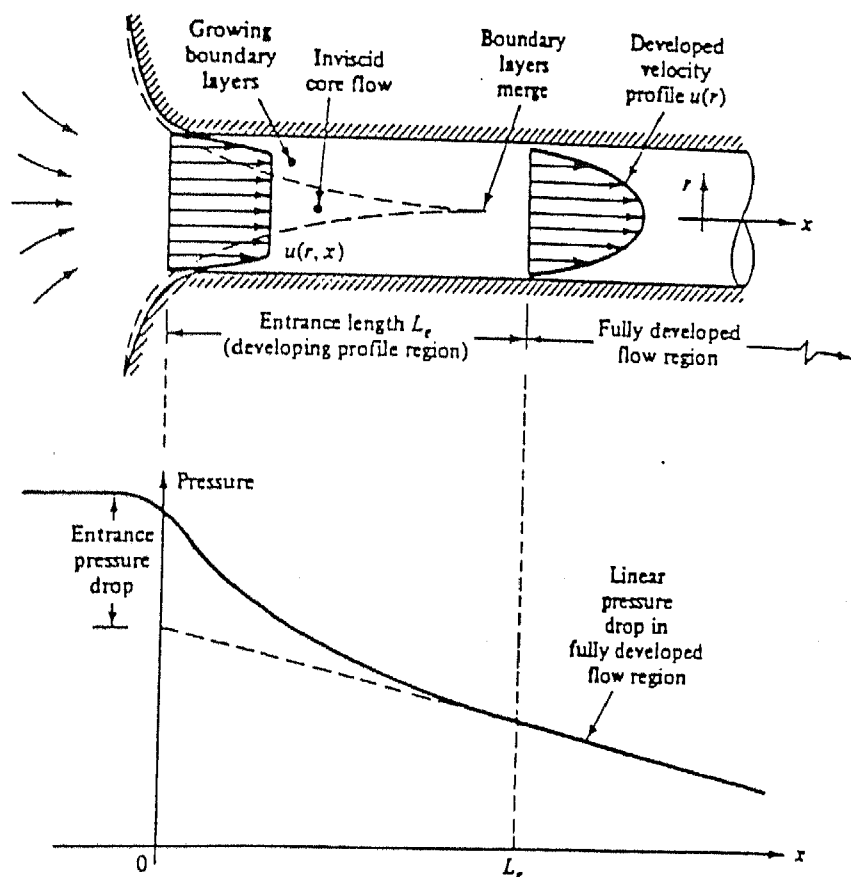


Fig.(3.4) : Schematic of the developing velocity profiles and pressure changes in the entrance of a duct flow.

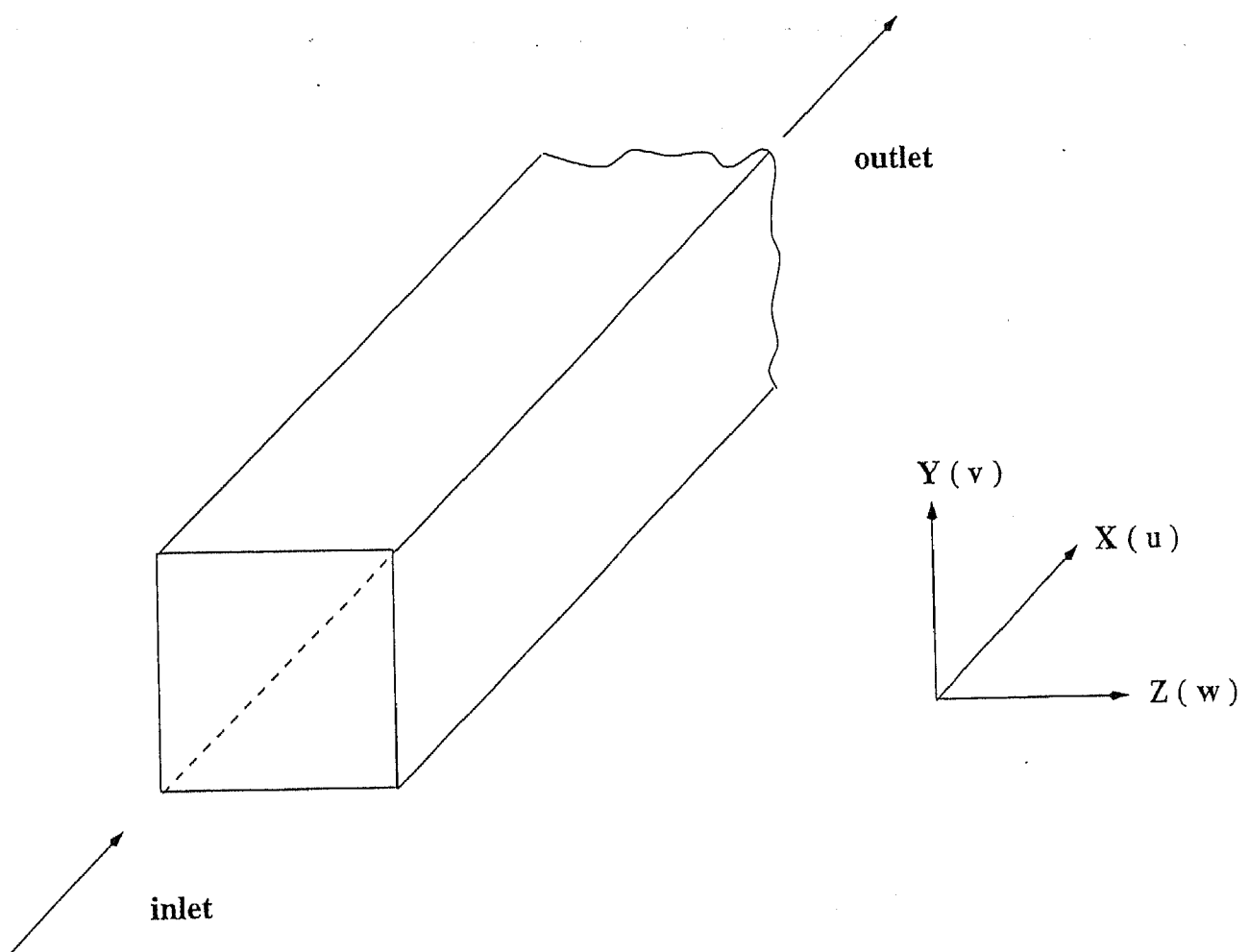


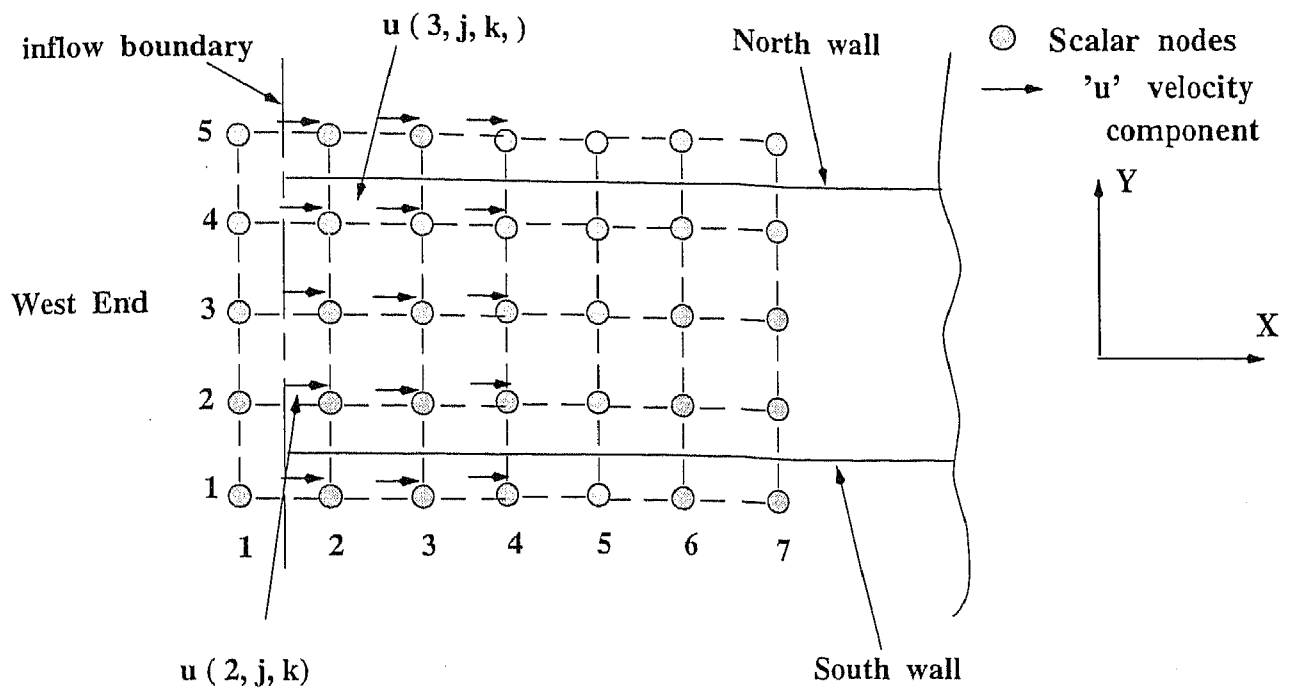
Fig. (3.5) : Schematic of a duct with a square cross-section and the relevant coordinate axis to the problem.

(dimensions in the y and the z direction). Dimension of the duct in the x direction (the direction of main flow) was defined such that $x \gg L_e$. Zero velocity (no slip) boundary conditions were specified for north, south, top and the bottom walls. Inflow and outflow boundary treatments were specified at the inlet (west) and outlet (east) planes respectively. Fig. 3.6 represents a two dimensional grid arrangement near the entry and the exit planes. Since, u velocity (x component of motion) is known at the inlet plane, consequently, a numerical treatment analogous to that presented in Section-3.1.1 can be applied to accommodate the exact inflow boundary condition into the calculation procedure. For all the grid points P lying adjacent to the outflow boundary, the coefficient A_E is set to zero i.e. Peclet number is made sufficiently large ($P_E \rightarrow \infty, A_E \rightarrow 0$) to make the behaviour locally one way in this region. In addition to this, the average exit velocity is specified at the outflow boundary on the basis of overall continuity which is updated from iteration to iteration by setting $u(ni,j,k) = u(ni-1,j,k)$.

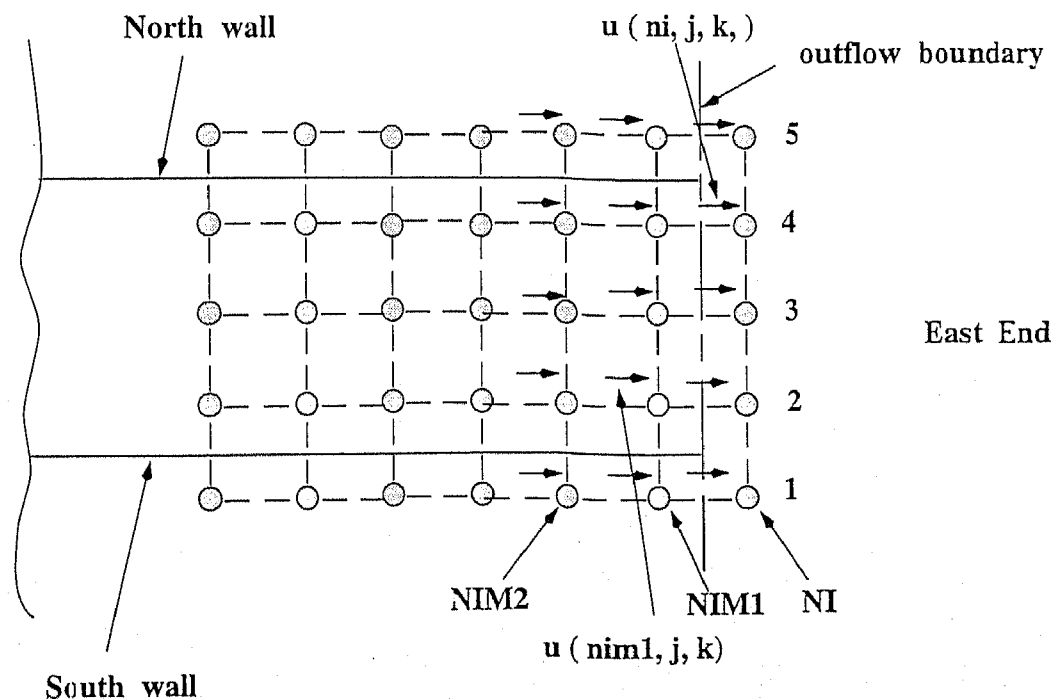
Reynolds numbers (e.g., ∞ inlet velocity) were varied arbitrarily between 25 to 180 and the flow field within the duct was predicted as a function of inlet Reynolds number. From the predicted results, entrance lengths were estimated graphically by plotting the centreline velocity as a function of x . Entrance lengths thus estimated were non-dimensionalised (by dividing L_e by D) and plotted against the inlet Reynolds number. This is shown in Fig.(3.7). As shown a straight line was obtained between the two, satisfying the requirement dictated by in Eq.(3.4) (e.g., $L_e / D \propto Re$).

3.1.3 Prediction of bubble rise in a stagnant fluid

Assigning zero fluid velocity and turbulence in flow and turbulence model equations and considering a classical drag coefficient value of $8/3$, the rise velocities of four different sized spherical cap air bubbles in water were estimated numerically following the computational procedure outlined already. An arbitrary vertical velocity was applied to Eq.(14) as the initial condition. The results as one would normally anticipate, indicated that the bubbles attain their terminal rise velocity within a short distance from above the point of injection. A comparison between numerically predicted terminal rise velocity and those



Inflow boundary treatment



Outflow boundary treatment

Fig. (3.6) : The procedure adopted for modelling the inflow and outflow boundary conditions for the prediction of entrance lengths.

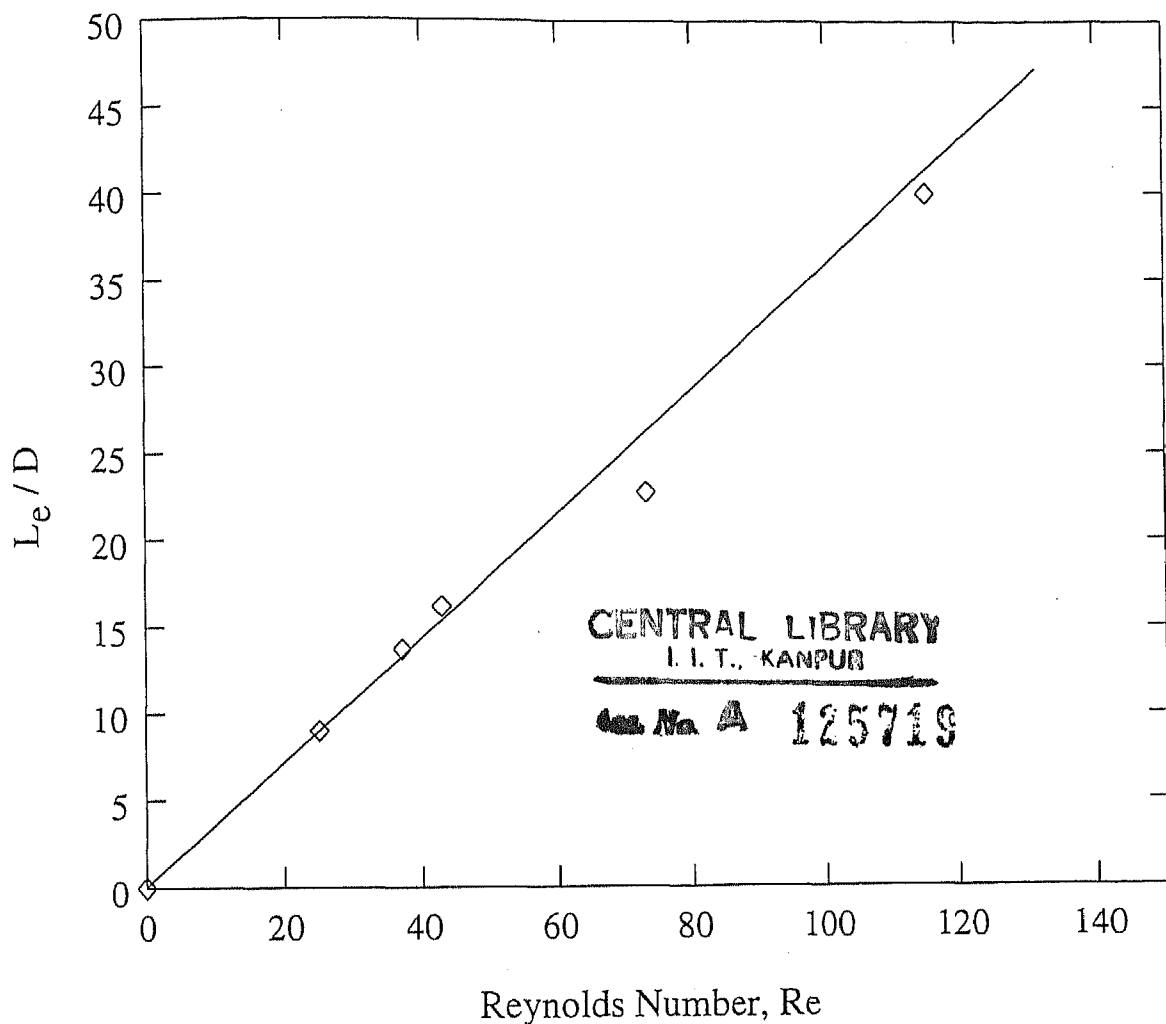


Fig. (3.7) : Predicted entrance lengths (L_e / D) as a function of the inlet Reynolds number.

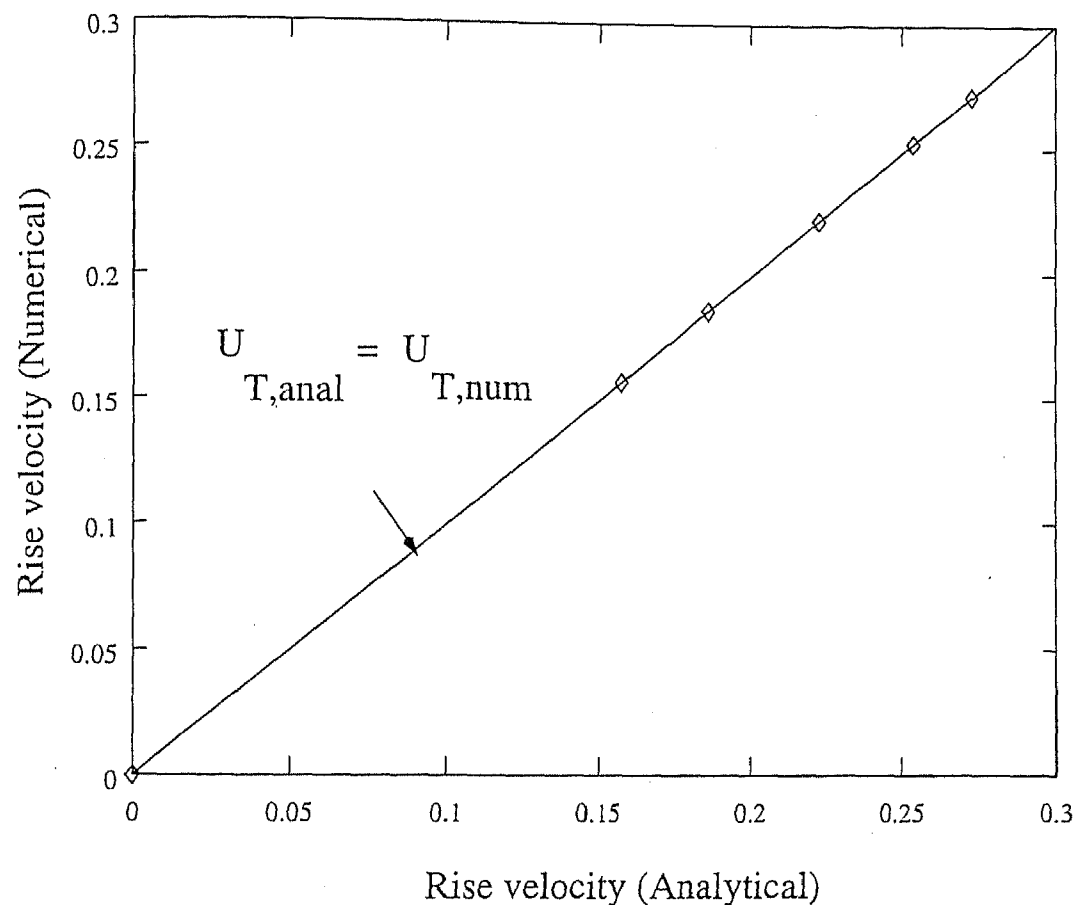


Fig. (3.8) : Comparision of analytical and numerical estimated terminal rise velocities of four different sized spherical bubbles in water.

obtained on the basis of the following expression[32].

$$U_T = 0.711 \sqrt{\frac{gd_b \Delta \rho}{\rho_l}} \quad \dots\dots(3.5)$$

is illustrated in Fig.3.8. There, perfect agreement between the analytical and numerical estimates is at once apparent. Results presented so far evidently demonstrate the adequacy and appropriateness of the calculation procedure outlined in the preceding section.

In addition to the aforesaid three tests, some other numerical experiments were also carried out (viz., turbulent flow over a flat plate, cubic cavity with two parallel moving walls [40]. These have also appear to confirm the reliability of the present computational procedure developed.

3.2 Modelling of flow and Residence Time Distributions in steelmaking tundish system

The two phase, three dimensional turbulent flow model was applied to investigate flow and RTD in three different tundish designs. These included, (i) a single strand slab casting tundish, (ii) a two strand slab casting tundish and (iii) a six strand delta shaped billet casting tundish respectively. These are summarised below in detail.

3.2.1 Flow and RTD in a single strand tundish

As a starting case, fluid flow and RTD distribution behaviour in a water model tundish with single inlet and outlet and no flow control devices has been analysed computationally. The side walls of the tundish were tapered while the frontal walls were perfectly vertical. The characteristic design features of the model tundish are summarised in Table 3.1 .A schematic of the tundish is shown in Fig. (3.9).

Table-3.1: Characteristic parameters of the single strand model tundish [8].

Parameter	Numerical value
Fluid	Water, ($\mu=0.001 \text{ kg m}^{-1}\text{s}^{-1}$, $\rho=1000 \text{ kg/m}^3$)
Base length, m	1.0
Width (at base), m	0.30
Height, m	0.37
Liquid depth, m	0.26
Shape	rectangular with sloping walls (15°)
No. of strands	one
Ladle shroud diameter, m	0.022
Volumetric flow rate, m^3/s	1.55×10^{-4}
Inlet Reynolds number	9.0×10^3

Computations were performed using a nonuniform grid covering the whole tundish. A grid system of $38 \times 13 \times 13$ was chosen for the x (longitudinal), y (vertical) and the z (transverse) directions respectively. Under-relaxation factors of 0.5 for velocities and 0.7 for turbulence quantities were adopted. Details of the under-relaxation procedure employed has already been summarised in Chapter 2. A typical execution took almost 10,000 iteration and this required about 300 *min* of *CPU* for flow field to converge. Approximately, 150 *min* of *CPU* time was involved for the concentration to reach steady state level. All computations were carried out in the *HP-9000* series machine at IIT, Kanpur.

The predicted three dimensional flow field in the single strand tundish is shown in Figs. 3.10 through (3.12) via a series of two dimensional plots. Figure (3.10) shows flow at different

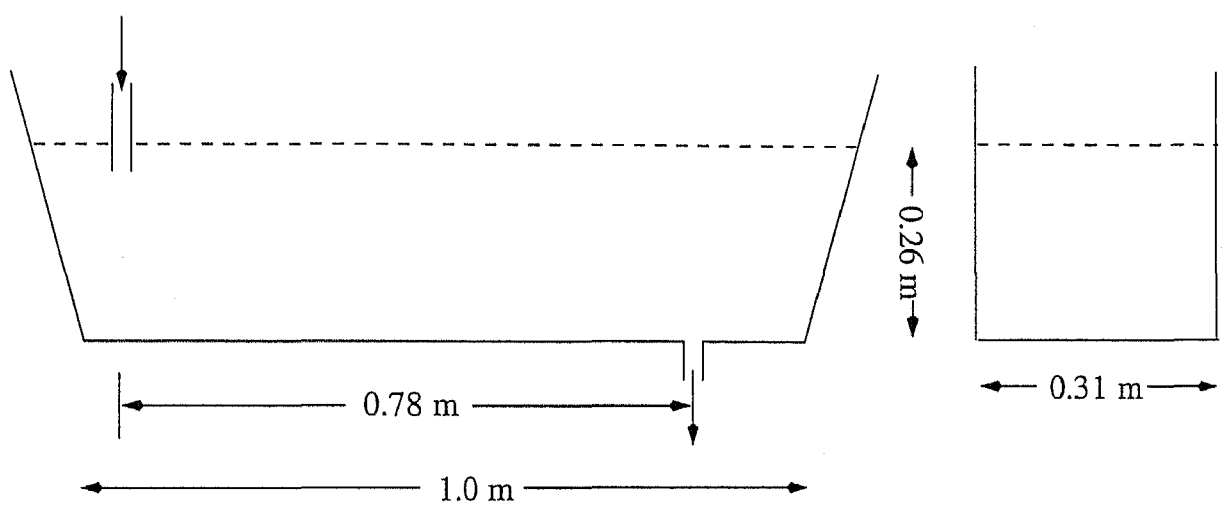
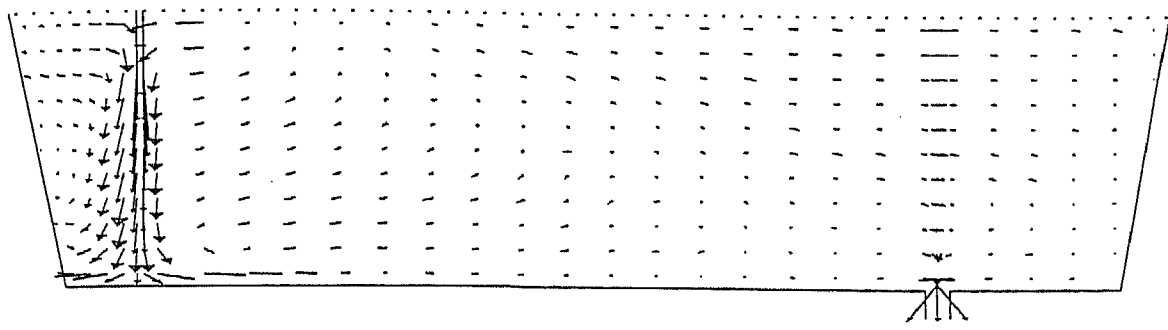


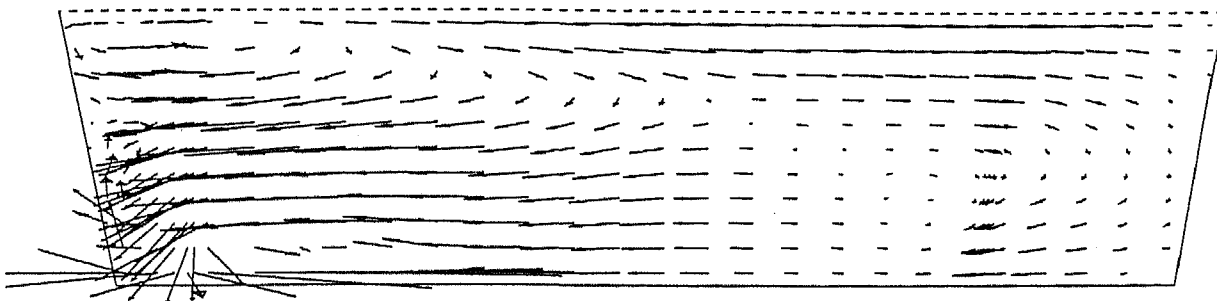
Fig.(3.9) : Schematic of the single strand model tundish dimensions[8].

elevations in the transverse horizontal planes (X-Z planes). There the bottom most figure (3.10d) corresponds to the flow on a horizontal plane that is closer to the tundish base, while the upper most plot (3.10a) corresponds to the flow in the vicinity of the free surface. Referring to Fig.3.10, it is seen that the jet following its impingement on to the tundish base spreads radially along all directions. Further more, while the flow closer to the vertical frontal wall is directed primarily towards the exit nozzle, in contrast shows a flow reversal along the central line of the particular plane. In the vicinity of the exit nozzle, a sink like vortex can be observed which is due to drainage effect. As one moves towards the free surface, this flow characteristic (flow pattern on plane (a)) changes and more liquid is seen approaching the input stream from towards the right of the vessel. Finally, near the free surface flow pattern again shifts where surface flow primarily directed towards the exit nozzle is observed. It is important to note here that predicted flow on the horizontal planes exhibit symmetry with respect about the horizontal centreline.

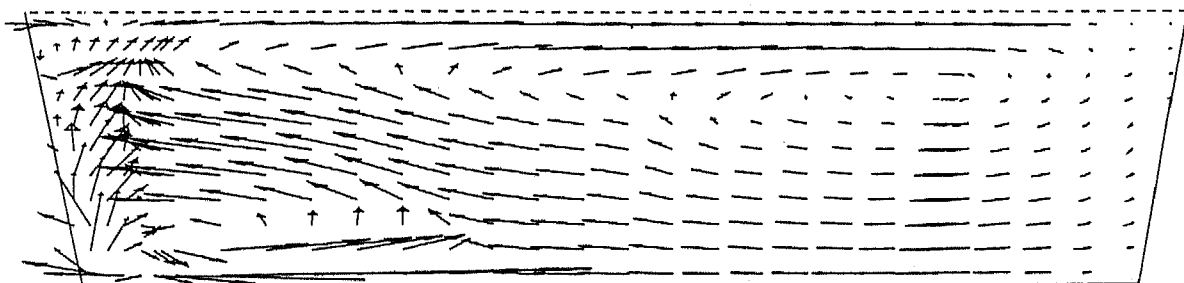
In Fig. 3.11 predicted flows on four different vertical planes are shown. because the tundish is symmetrical about the central vertical plane consequently flow on the frontal half has been shown in Fig.3.11 . On the central vertical plane Fig.3.11a, it is seen that the jet upon entry, entrains surrounding fluid and undergoes considerable expansion before impinging on to the base of the tundish. Towards the left of the incoming jet, a distinct recirculatory loop is seen (created by the confinement of the jet by the tundish vertical and side walls). Towards the bottom of the same plane, the flow is seen to be first directed towards the orifice . However at some horizontal distance from the inlet plane, the flow is seen to be reversed. The flow pattern changes drastically as one visits various planes from the centreline to the proximity of the frontal vertical wall. In Figs.3.11(b) and 3.11(c) considerable amount of fluid is seen to be moving towards the jet impinging area. Further more, the surface directed flow becomes more intense near the frontal vertical wall (e.g., as one moves down from Fig.3.11(a) to 3.11(d). Similarly, in Fig. 3.12, flow patterns along the transverse vertical planes are shown. This, shows the distinct recirculatory loop created by the confinement of the jet between the two frontal walls particularly, in the proximity of the input stream.



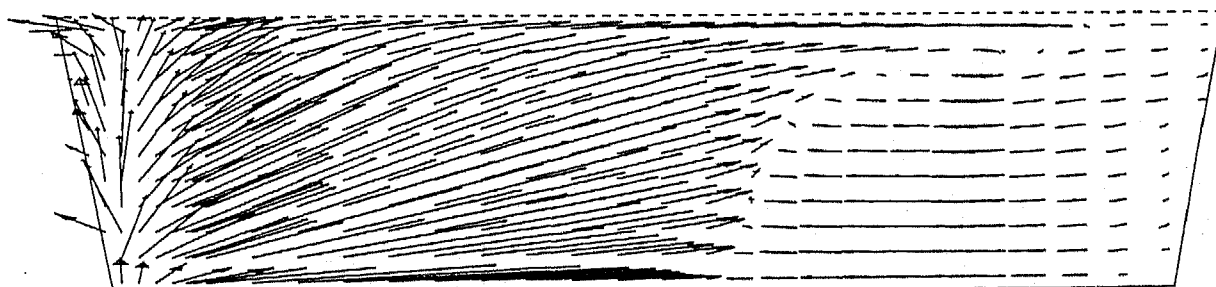
(a)



(b)



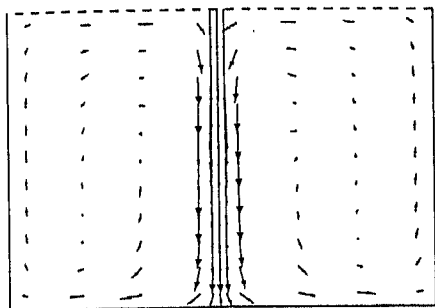
(c)



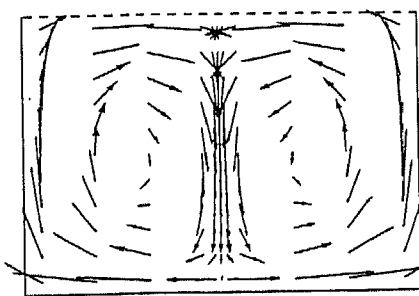
(d)

0.4 m/s
→

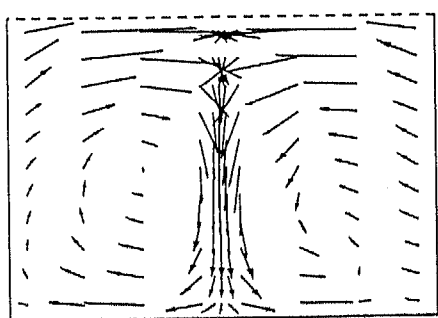
Fig.(3.11) : Predicted flow field in single strand tundish in longitudinal vertical planes at dimensionless distances (z/W) of (a) 0.5 (b) 0.1 (c) 0.19 (d) 0.045



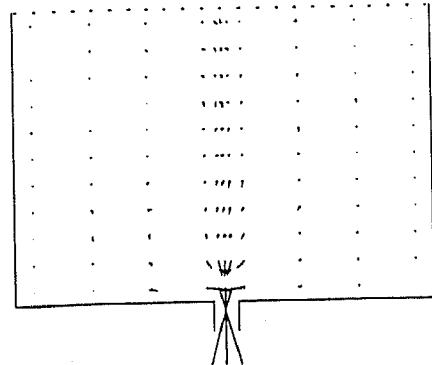
(a)



(b)



(c)



(d)

0.4 m/s
→

Fig.(3.12) : Predicted flow field in single strand tundish in the transverse plane at dimensionless distance (x/L) of (a) 0.11 (b) 0.28 (c) 0.67 (d) 0.78

As pointed out already, the Residence Time Distribution characteristics in the model tundish was investigated through numerical solution of the convection- turbulent diffusion equation summarised already in Chapter 2. In this, at time $t = 0$, the inlet control volume was made full of tracer of the same density as that of bulk liquid phase (e.g., water) and the concentration of the tracer was then computationally monitored as a function of time at the control volume passing through the exit nozzle and one control volume vertically above it. The concentration of tracer at these these locations was subsequently non-dimensionalised using the average concentration that the tracer would assume in the vessel, if the later were perfectly mixed in the absence of any drainout ($C_o = (mass_{tracer}/Volume_{fluid}) = 0.02 \text{ kg/m}^3$). Similarly, time was also non-dimensionalised using the nominal holding time Eq.(1.1) of the fluid in the vessel (t_r). The result thus obtained (C/C_o vs. t/t_r) was then plotted to get the desired C-curves. In Fig.(3.13), the C-curves obtained computationally for the control volume just above the exit nozzle is shown. There as seen, the tracer is initially of negligible concentration at the exit stream, but it quickly increases to a maximum, before showing a gradual fade out. These features of the RTD curve is a characteristic of the metallurgical tundish systems and is similar to those reported by numerous other investigators [8,12,18].

The minimum breakthrough time, the time at which peak concentration is reached and the mean residence time were calculated from the "C" curve. Mean residence time has been calculated using eq(1.2). On the other hand, minimum break through time and Peak concentration time were deduced from visual examination of the predicted C curve. Residence Time Distribution characteristics thus obtained have been compared directly in Table 3.2 which also contains corresponding experimental measurements reported by Singh and Koria. There, excellent agreement between prediction and experiment is readily apparent.

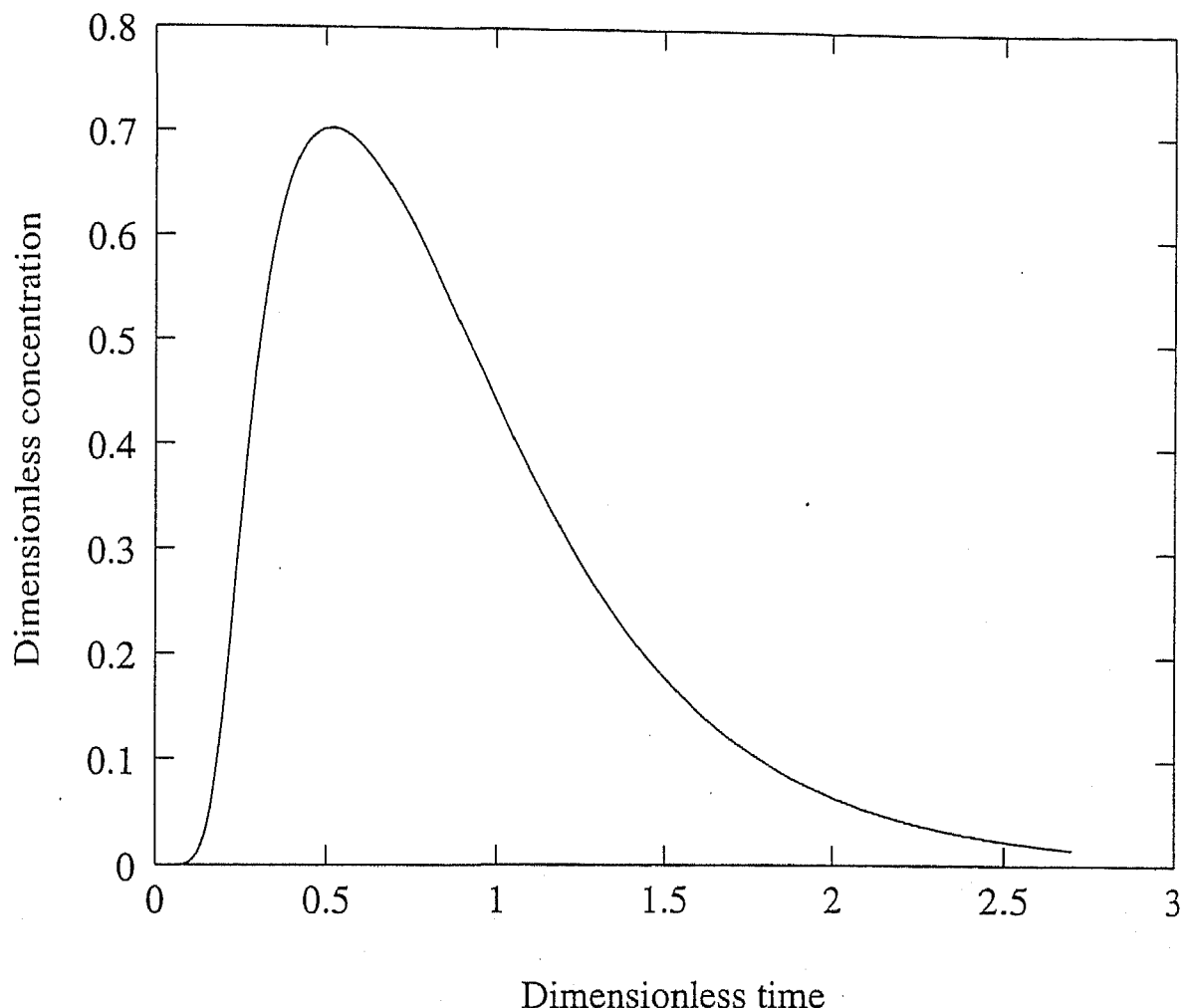


Fig.(3.13) : RTD in single strand tundish

Table 3.2 : Characteristics of the RTD in the single strand tundish and their comparison with equivalent measurements reported in the literature[8].

RTD Characteristics	Predicted value, s	Experimental value, s
Minimum break through time	25	31
Peak concentration time	285	262
Average residence time	489	444

3.2 Flow and RTD in a two strand slab casting tundish

Table 3.3: Characteristic parameters of the two strand model tundish (13) .

Parameter	Numerical values
Fluid	Water, ($\mu=0.001 \text{ kg m}^{-1}\text{s}^{-1}$, $\rho=1000 \text{ kg/m}^3$)
Base length, m	1.2
Width (at top), m	0.2
Width at the base ,m	0.154
Liquid depth, m	0.14
Shape	rectangular (~10° inclined)
No. of strands	two
Tundish nozzle diameter, mm	10
Volumetric flow rate, m^3/s	0.93×10^{-4}
Inlet Reynold's Number	9.43×10^3

Three different configurations of the two strand tundish were used for numerical computations. In each configuration, the operating parameters were kept identical to those summarised in Table 3.3. Schematics of the three configuration are shown in Fig.3.14. Owing to symmetry, computations were restricted to only one quarter of the tundish. A 32x12x13 grid system was applied to seek the numerical solution. Details of the computed results obtained together with discussion are summarised below.

In Figs.3.15 through 3.16 flow fields in the absence of any flow modification devices are shown through a series of two dimensional plots. In Fig.3.15, flow fields are presented for three different vertical planes. There, the central vertical plane shows strong downward fluid motion in the vicinity of the jet entry location. In the remaining of the plane, fluid is relatively stagnant gaining momentum again in the proximity of the exit nozzle. Furthermore, the flow velocities particularly towards the bottom of the tundish are seen to be aligned in a direction towards the exit nozzle for some distance only. However, as one approaches the frontal wall, the intensity of the exit nozzle directed flow increases substantially Fig.3.15(c). These characteristics of the flow are qualitatively very similar to those presented earlier for the single strand tundish . This is to be expected since there is no significant geometrical difference between a single strand and one half of a two strand tundish in a qualitative sense.

In Figs. 3.16(a) through (c), flow pattern in three different horizontal planes have been shown for the operating conditions summarised in Table 3.3.. This shows that the jet following its impingement on the tundish base, flows outwards . A portion of the jet flows towards the frontal wall and then rises up (see also Fig.3.15(c)) while the remaining portion of the jet flows preferentially towards the exit nozzle. As one moves towards the free surface this characteristics of the flow pattern changes substantially and ultimately near the free surface flow is seen to be directed towards the jet entry region. In the horizontal planes, except for the immediate vicinity of the inlet stream, flow is seen to be relatively sluggish.

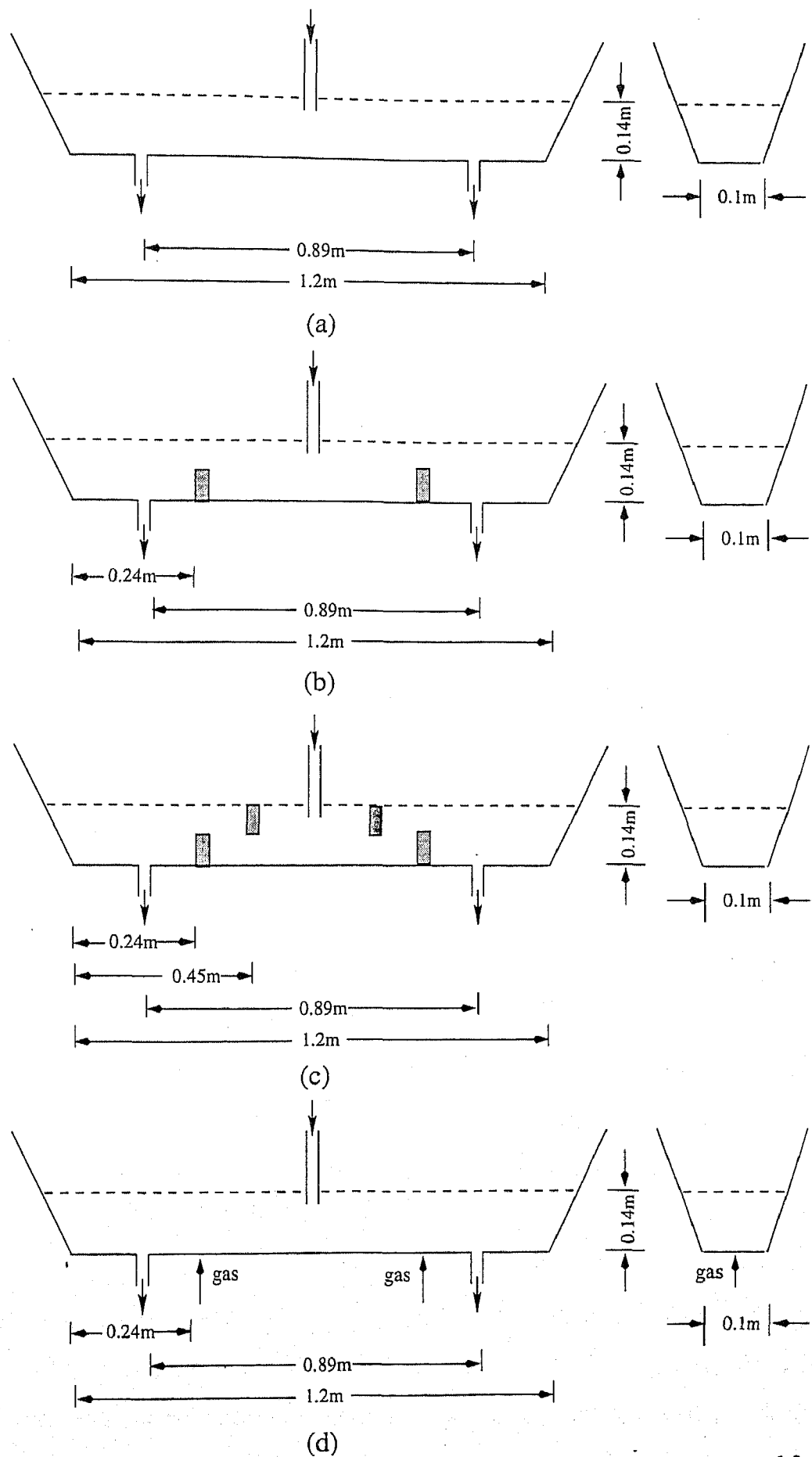


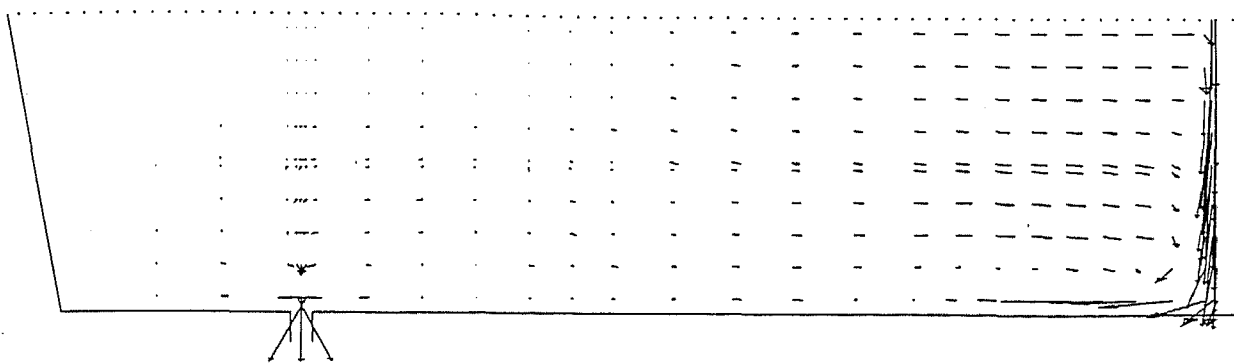
Fig.(3.14) : Schematic of three different configurations of the two strand tundish used for numerical simulation (a) without baffle (b) with a dam (c) with a dam and a wier (c) with a bubbler in place of dam

In Fig.3.18, flow field in three different vertical planes are shown for the two strand tundish with a dam placed at a distance of 0.36m from the central plane of symmetry . These figures show that the flow pattern, particularly between the inlet stream and the dam is not much affected by the presence of the dam within the flow domain. However in the vicinity of the dam and beyond, the flow pattern appears to have changed with respect to an equivalent unbaffled situations. Similarly, in Fig.3.18(a) through (c) flow patterns in three different horizontal planes are shown. There, flow fields on those planes above the dam are practically identical to those presented earlier for an equivalent no-baffle situation. The dam seems to have no influence on the flow patterns generated on the horizontal planes particularly in regions bounded by the the inlet steam and the dam. This is to be expected since the dam is located much down stream of the inlet nozzle.

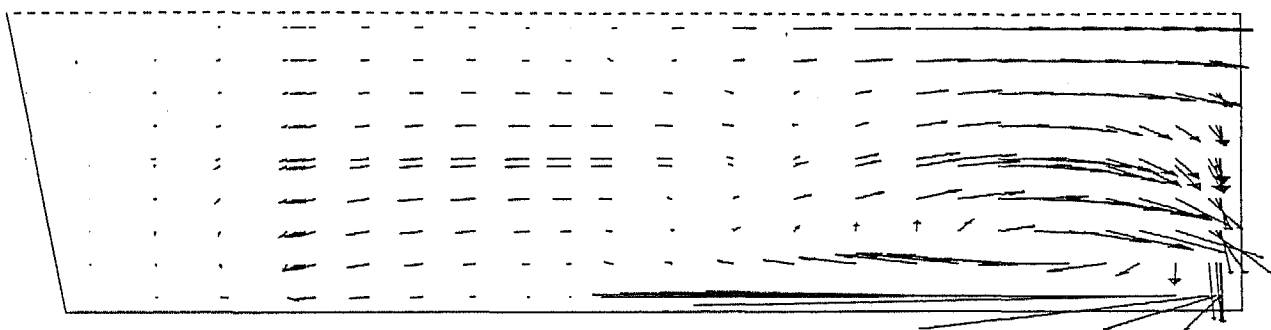
In Figs. (3.19) through (3.20) flow fields in the two strand tundish with a dam and a weir is shown. The weir as seen from these figures appear to influence the predicted results considerably because of its proximity to the jet entry location. Interestingly, large flow velocities coupled with appreciable fluid turbulence is seen to be primarily restricted between the region bounded by the inlet stream and the weir, which is desirable feature as far as tundish hydrodynamics are concerned.

Finally, flow fields were computed in the two strand tundish with gas ($Q= 2$ lit/ min) stirring through a plug located at the base of the vessel. These were carried out in the absence of any flow modification devices. Predicted flow patterns are shown in Figs 3.21 through 3.22. There the general features of the flow is very similar to those presented earlier for an equivalent no baffle situation. Only in the proximity of the bubbler, some noticeable changes in the flow intensity can be seen and bubbler forms recirculatory motions on its either sides.

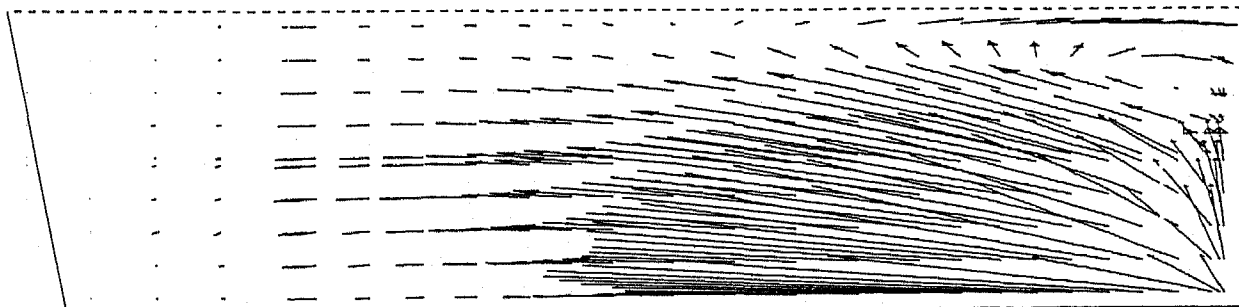
Corresponding predicted Residence Time Distribution characteristics (see Fig.3.23) are shown in Table 3.4 for the four different cases . There, predicted minimum break through time, time at which peak concentration is reached and the average residence time have been summarised. It is clear that the dam and the dam+weir configuration tends to increase the



(a)



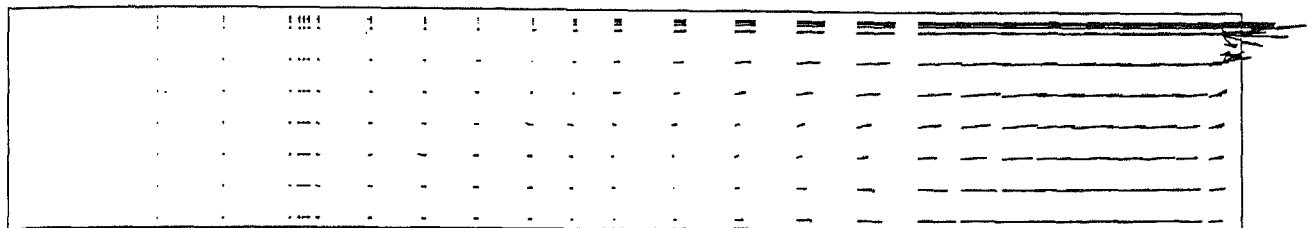
(b)



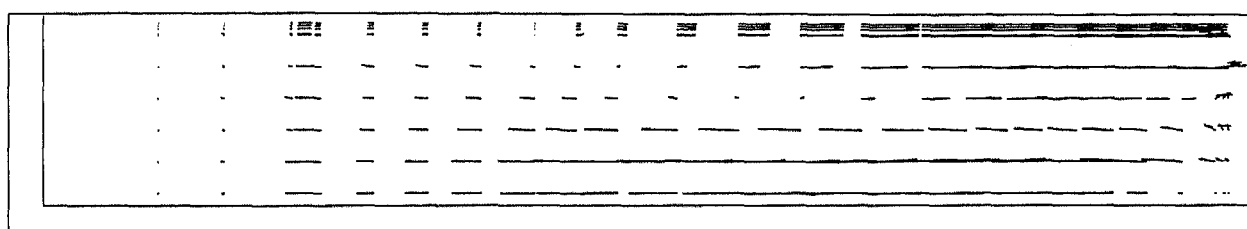
(c)

0.3 m/s

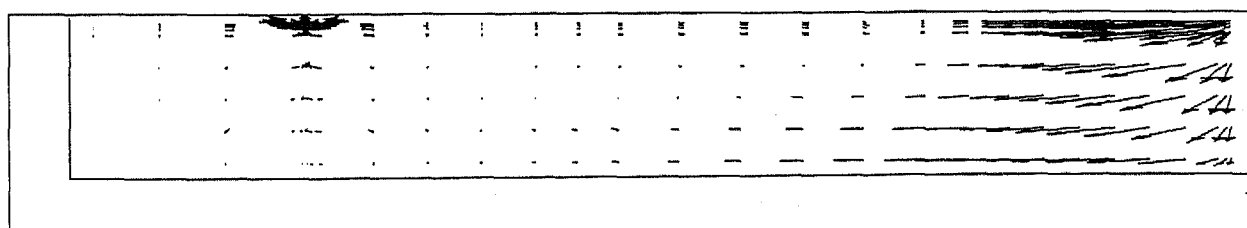
Fig.(3.15) : Predicted flow field in the two strand symmetrical tundish without baffle in the longitudinal vertical planes at dimensionless distance (z/W) of (a) 0.99 (b) 0.70 (c) 0.34



(a)



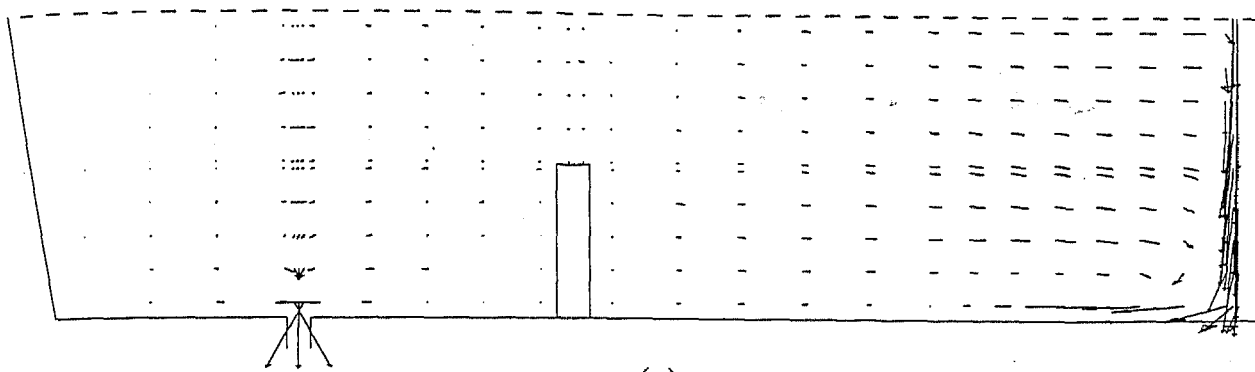
(b)



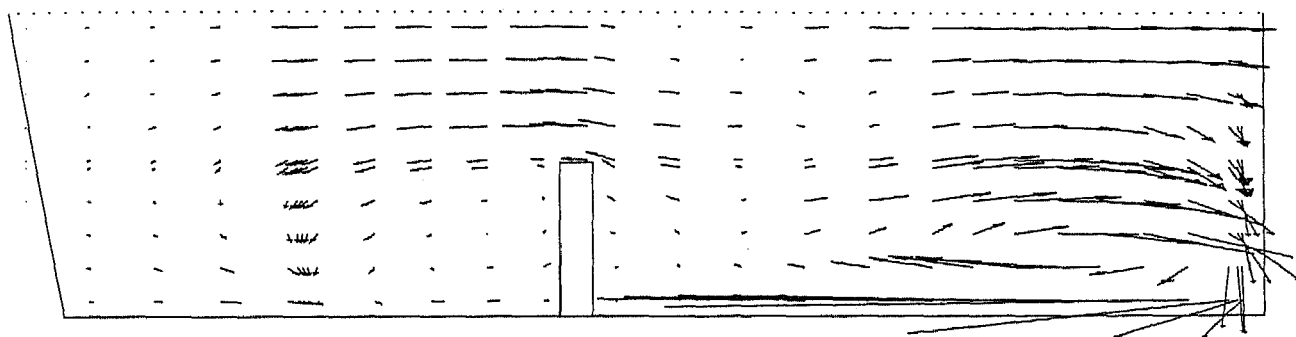
(c)

0.011 m/s

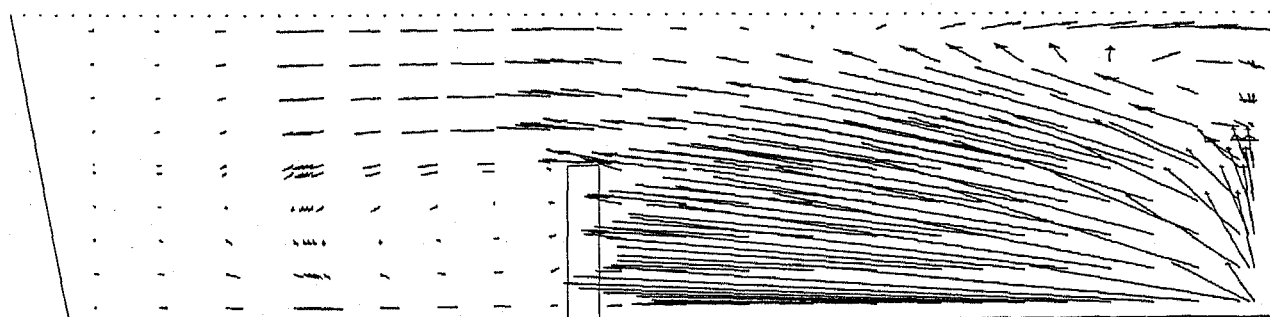
Fig(3.16) : Predicted flow field in the two strand symmetrical tundish without baffle in the horizontal transverse planes at different dimensionless height (y/H) of (a) 0.99 (b) 0.50 (c) 0.05



(a)



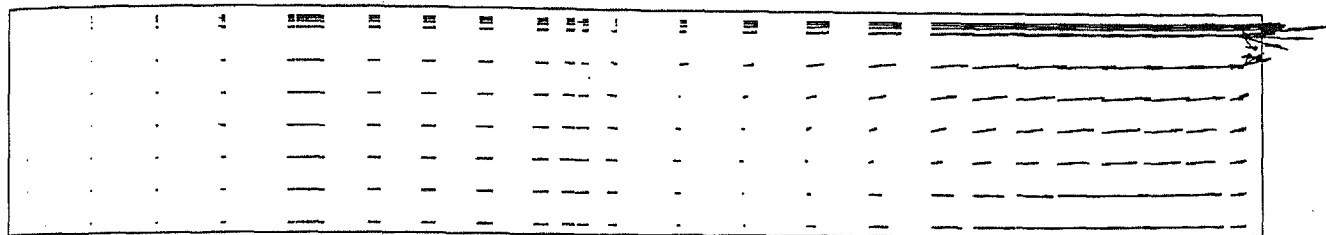
(b)



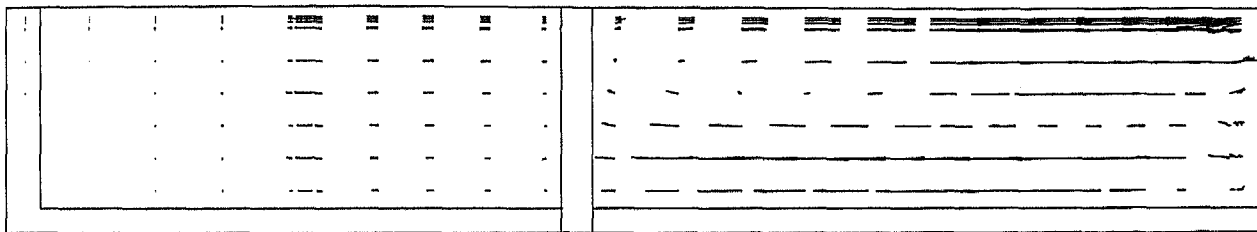
(c)

0.3 m/s

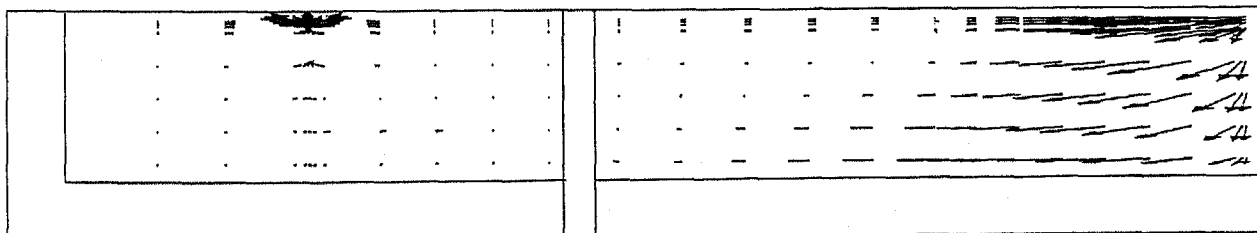
Fig.(3.17) : Predicted flow field in the two strand symmetrical tundish with a dam in the longitudinal vertical planes at dimensionless distance (z/W) of (a) 0.99 (b) 0.70 (c) 0.34



(a)



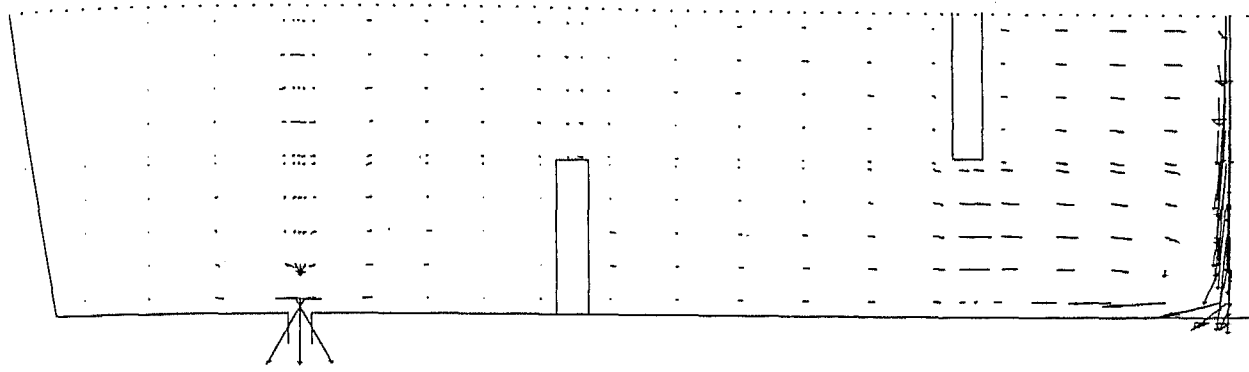
(b)



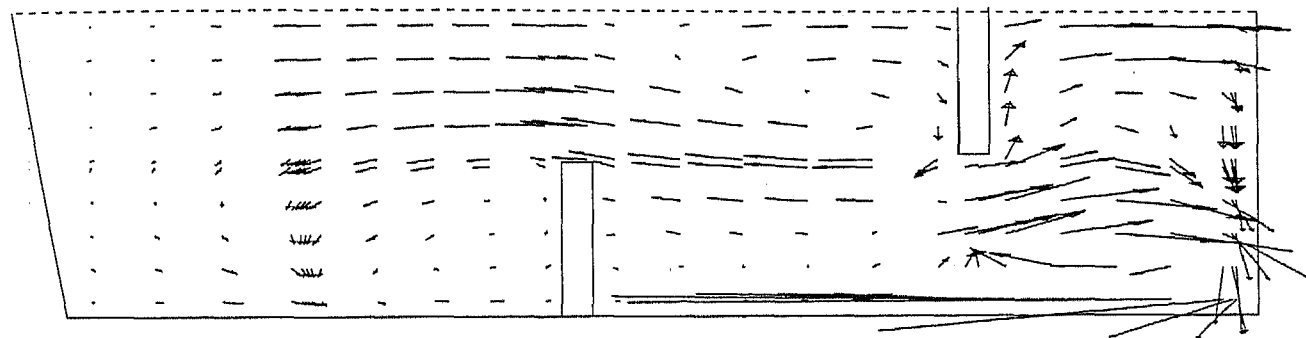
(c)

0.011 m/s

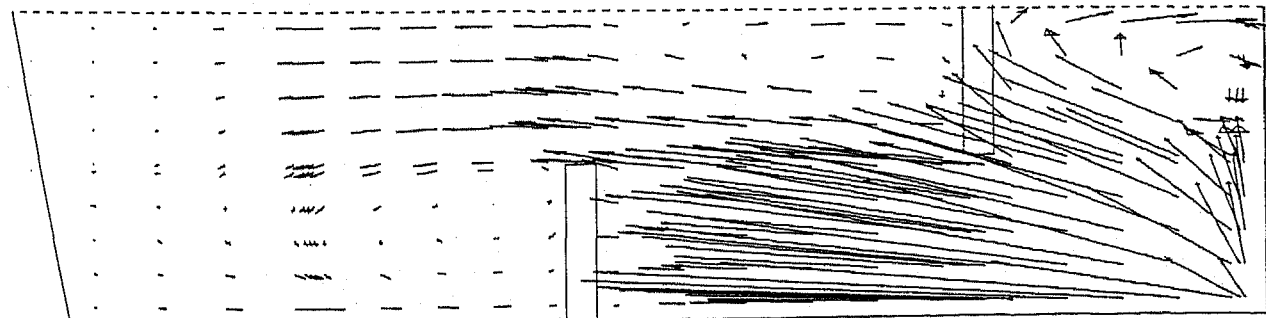
Fig(3.18) : Predicted flow field in the two strand symmetrical tundish with a dam in the horizontal transverse planes at different dimensionless height (y/H) of (a) 0.95 (b) 0.49 (c) 0.05



(a)



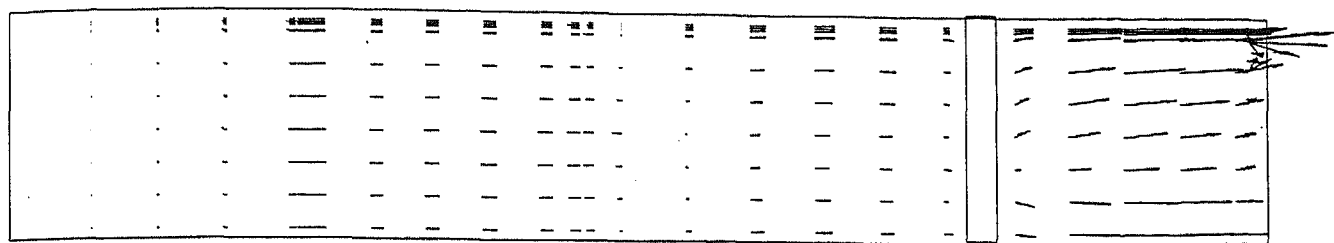
(b)



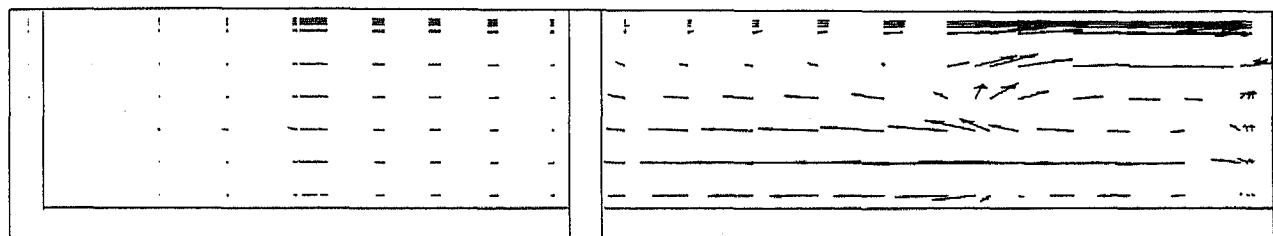
(c)

0.3 m/s

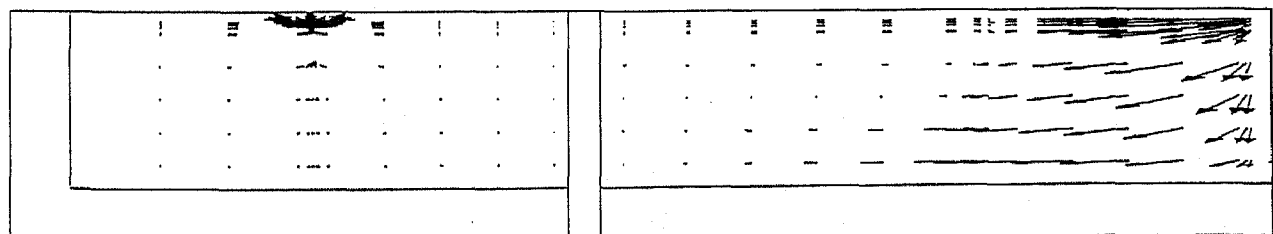
Fig(3.19) : Predicted flow field in the two strand symmetrical tundish with a dam & a wier in the horizontal transverse planes at different dimensionless height (y/H) of (a) 0.99 (b) 0.70 (c) 0.34



(a)



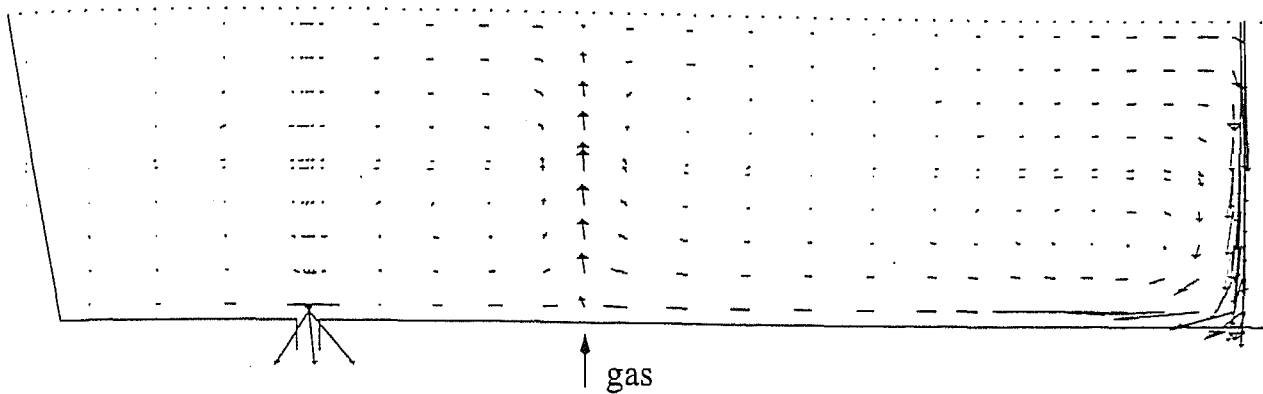
(b)



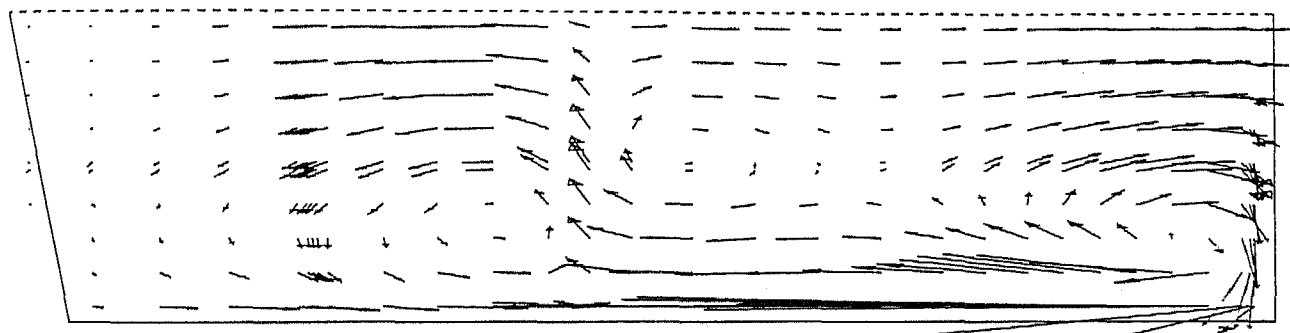
(c)

0.011 m/s
→

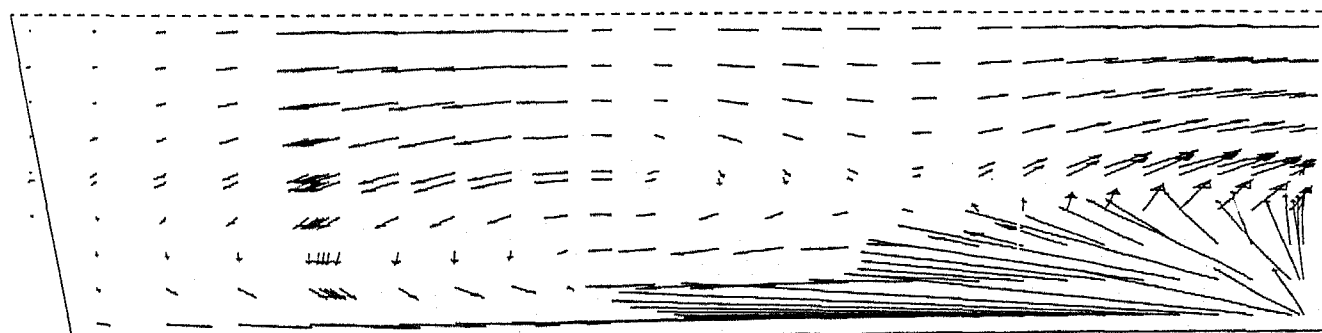
Fig. (3.20) : Predicted flow field in the two strand symmetrical tundish with a wier and a dam in horizontal transverse planes at different dimensionless heights of (a) 0.95 (b) 0.49 and (c) 0.05.



(a)



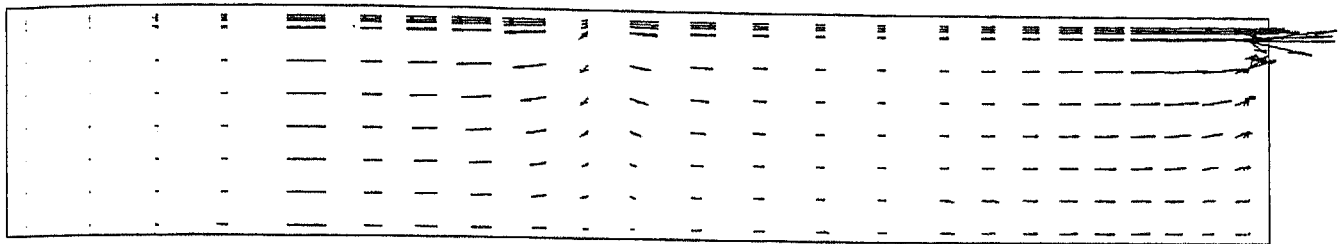
(b)



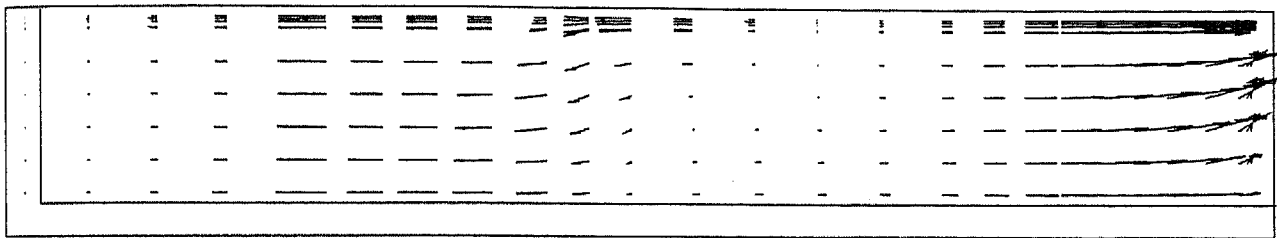
(c)

0.3 m/s

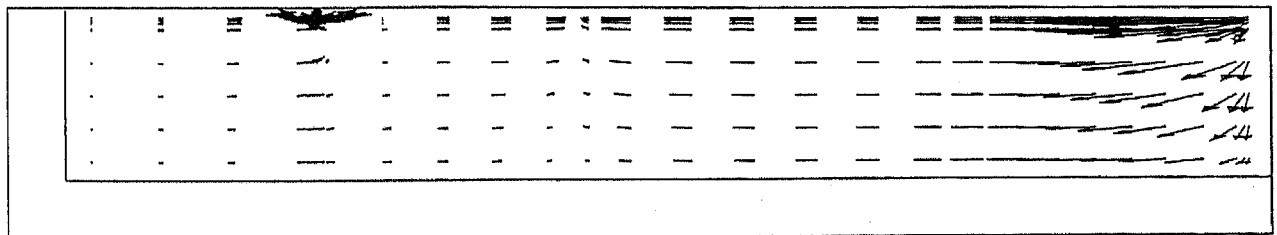
Fig.(3.20) : Predicted flow field in the two strand symmetrical tundish with a bubbler in the longitudinal vertical planes at dimensionless distance (z/W) of (a) 0.99 (b) 0.70 (c) 0.34



(a)



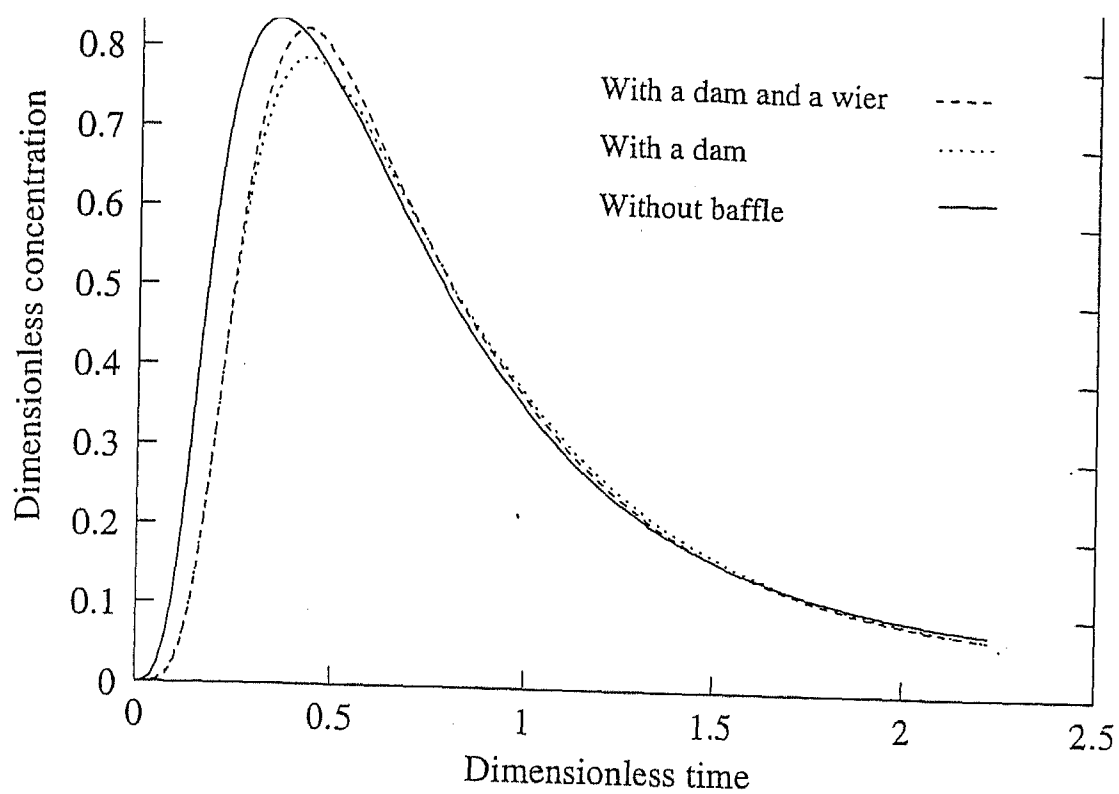
(b)



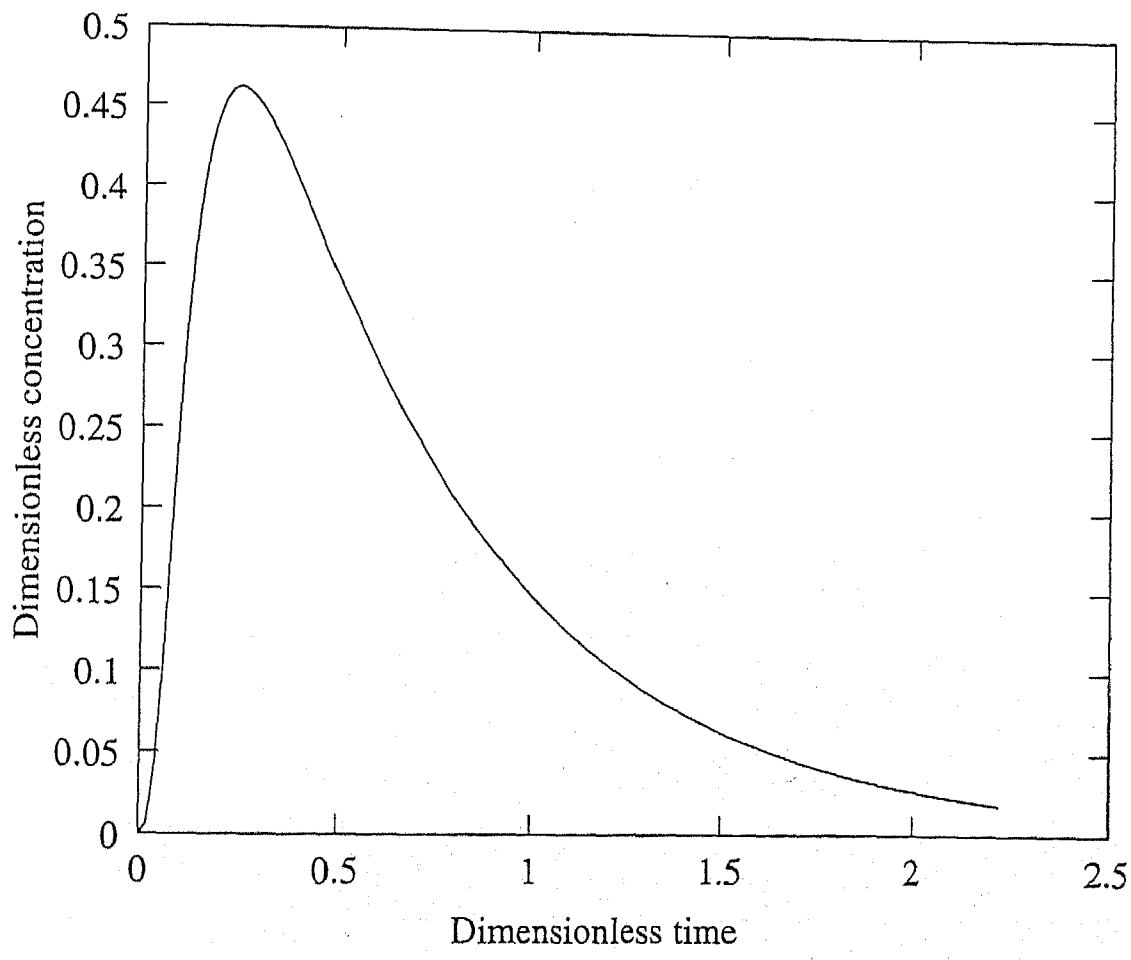
(c)

0.011 m/s

Fig(3.21) : Predicted flow field in the two strand symmetrical tundish with a bubbler in the horizontal transverse planes at different dimensionless height (y/H) of (a) 0.95 (b) 0.50 (c) 0.05



(a)



Dimensionless time

(b)

Fig.(3.22) RTD for two, strand tundish for four different case (a) without baffle (b) with a dam (c) with a weir and a dam (d) with a bubbler located in place of a dam

residence time of the fluid in the tundish as one would normally anticipate. Significantly, the bubbler seem to serve no purpose as far as increase of residence time of fluid in the tundish are concerned. In fact gas stirring needs to be applied in conjunction with flow modification devices to obtain the necessary benefits. This is however left for a future study.

For the three configurations the dead volume, dispersed plug volume and complete mixing volumes were calculated from the eqs. 1.3 to 1.5 and compared with the equivalent experimental values and a good agreement can be observed.

Table 3.4 : Residence Time distribution characteristics in the two strand tundish as a function of various configurations

Configuration of the tundish	RTD characteristics	Numerical values, s
Without baffle	Minimum break through time	5
	Peak concentration time	110
	Mean residence time	200
with a dam only	Minimum break through time	14
	Peak concentration time	115
	Mean residence time	213
with a weir and a dam	Minimum break through time	14
	Peak concentration time	115
	Mean residence time	211
with a gas bubbler	Minimum break through time	06
	Peak concentration time	40
	Mean residence time	141

Table 3.5 : Comparision of flow characteristics of two strand tundish with experimentally observed values.

Configuration of the tundish	Flow characteristics	Predicted values (%)	Experimenta -l values (%)
Without baffle	dead volume	26	29
	dispersed plug volume	19	3
	complete mixing volume	55	68
With a dam only	dead volume	21	7
	dispersed plug volume	23	7
	complete mixing volume	56	86
With a weir and a dam	dead volume	22	15
	dispersed plug volume	23	8
	complete mixing volume	55	77

3.3 Flow and RTD in the six strand billet casting tundish

Finally flow and RTD simulation were carried out in a delta shaped six strand billet casting water model tundish. Schematics of the six strand tundish is shown in Fig. 3.24. The operating characteristics of the six strand tundish are summarised in Table 3.5. Computations were performed using a nonuniform grid covering the the half of the tundish because of symmetry . The grid set of $40 \times 15 \times 20$ were chosen for the x (longitudinal), y (vertical) and the z (transverse) directions respectively. A typical execution involving 8000 iteration required about 350 min of CPU time for flow field to converge and an additional 200 min of CPU time for the concentration field to attain steady state.

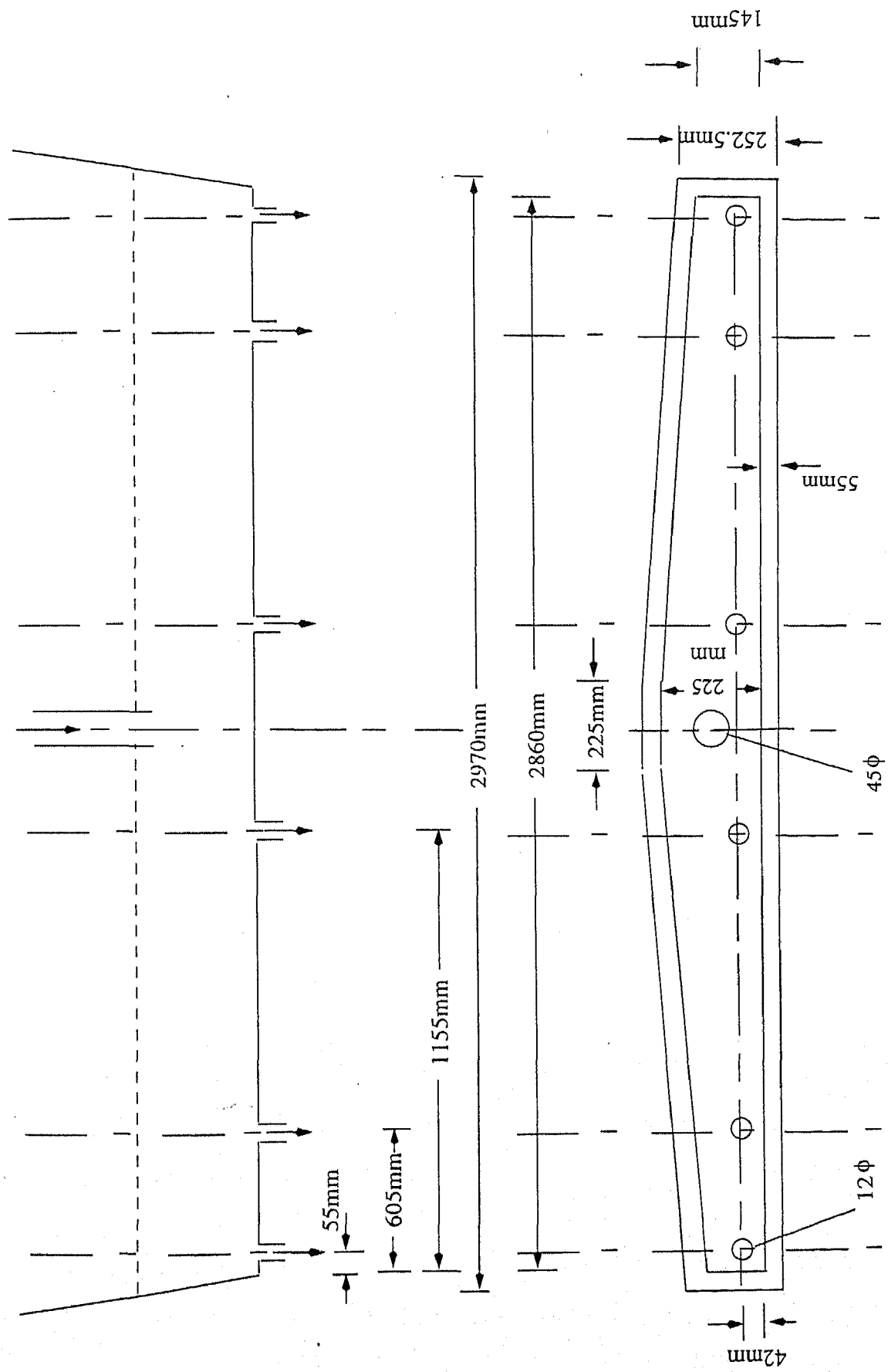


Fig. (3.23) Schematic of the six strand tundish with all dimensions

Table 3.6 : Characteristic parameter of the six strand delta shape water model tundish.

Parameter	Numerical values
Fluid	Water, ($\mu=0.001 \text{ kg m}^{-1}\text{s}^{-1}$, $\rho=1000 \text{ kg/m}^3$)
Base length, m	2.86
Width (at base), m	0.145 at side walls and 0.225 at the centre
Height, m	0.330
Liquid depth, m	0.275
Shape	delta shape with sloping walls (10^0)
No. of strands	six
Ladle shroud diameter, m	0.040
exit nozzle dia, m	0.012
Volumetric flow rate, m^3/s	6.0×10^{-4}

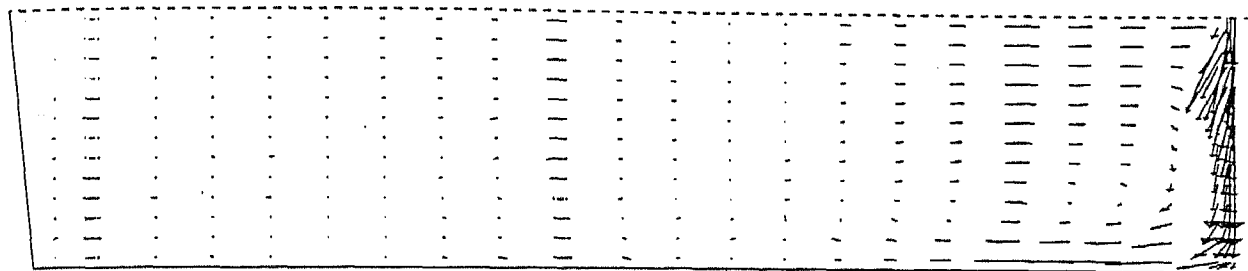
Details of the results and analyses on predicted flow and RTD are presented below.

The velocity profiles near the frontal wall is predominantly towards the outlet side which is due to large drainage effect associated with the three outlets (Fig.3.25d). There some part of fluid is seen to be directed towards the free surface due to entrainment of the liquid by the down coming jet and this forms a recirculatory motion to the right. Fluid velocities on the plane passing through the outlets are very weak elsewhere except in the proximity of the outlets(Fig.3.25c) and a very weak recirculation can be observed close to bottom

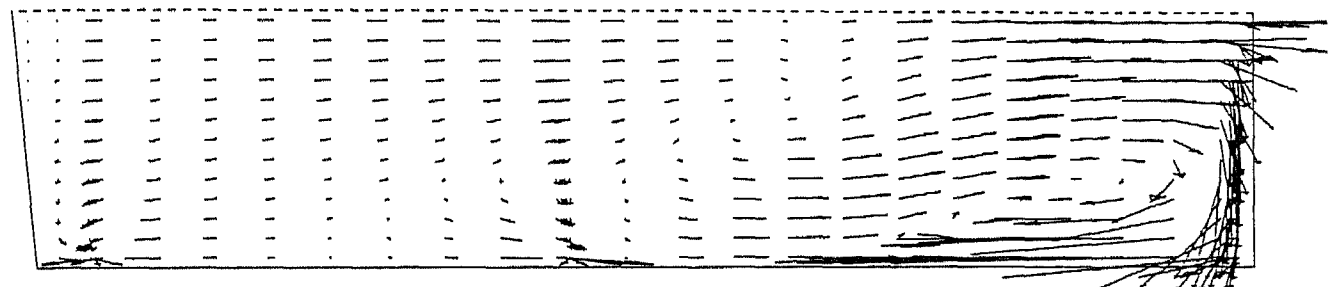
wall and at the inlet stream. As seen from Fig. (3.29b) entrainment has become quite strong as is evident from fluid flowing towards the inlet jet close to free surface in the right half of the tundish. While in the left part of the tundish we can see fluid comes from the free surface to the bottom because of the drainage effect of the outlets. As seen in Fig.(3.25a), which has the inlet stream the fluid is stagnant everywhere except in the region of inlet jet, where a strong recirculation can be observed because of combined entrainment effect of inlet jet and drainge effect of the outlets.

In transverse horizontal planes, close to bottom Fig(3.26d) flow is predominantly towards the exit nozzles. The incoming jet strikes at the base of the tundish and spreads radially outwards. More fluid flows towards the frontal wall because of the drainage effect of the outlets. Fluid velocities are weak near exit nozzles # 2 and # 3 which are further from the flow inlet. As one moves from the bottom plane towards the free surface the reversal of the fluid flow reversal can be witnessed. In Fig.(3.26b) on the right of the tundish, in the middle of the tundish the flow is mainly towards the inlet jet because of the etrainment, whereas in the region close to the walls and to the left of the tundish the flow is towards the exit side. As we move towards the free surface, to the left of the tundish the flow is predominantly towards the exit side and to the right the flow is mainly towards the inlet jet with high velcities, because of the large entrainment effect.

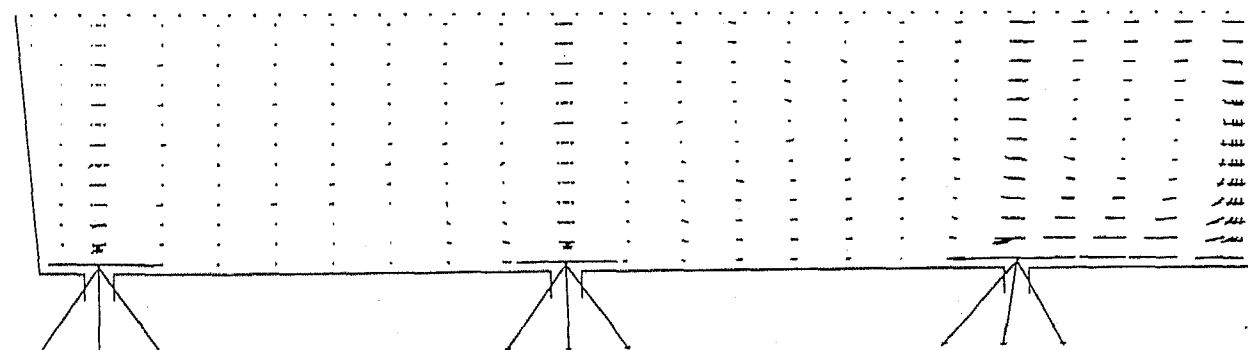
Fig.(3.27), shows the RTD characteristics of the given configuration. Table (3.7) shows the comparision of minimum breakthrough time of prdicted and experimentaly observed values. Only minimum breakthrough for three outlets have been compared with the experimentaly observed values, as only those experimental values were available by the time this study was completed. As we can see that we have excellent agreement of the two. As expected the minimum break through times for exit #1 is the shortest while the same for exit nozzle #3 is the largest. This is to be expected since the exit nozzle # 1 is closest while exit nozzle #3 is farthest from the inlet stream.



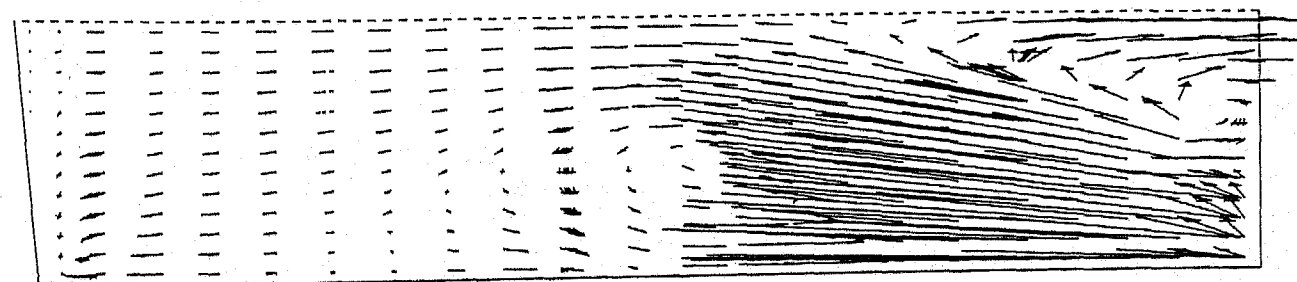
(a)



(b)

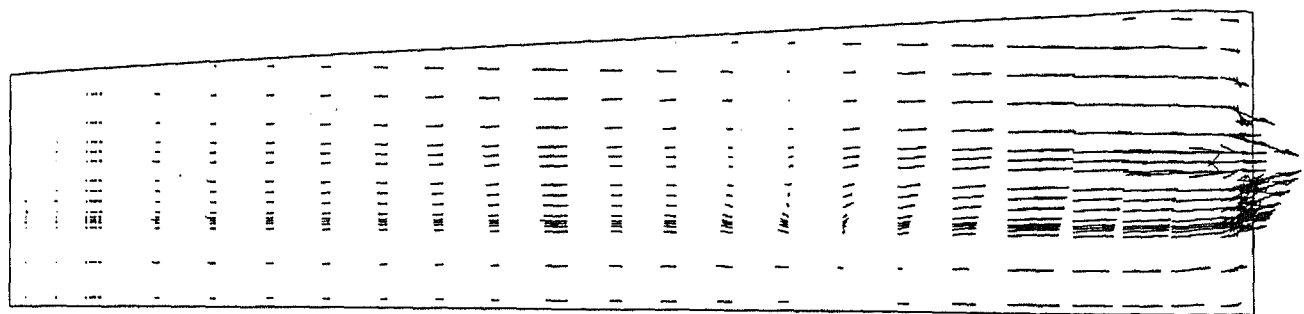


(c)

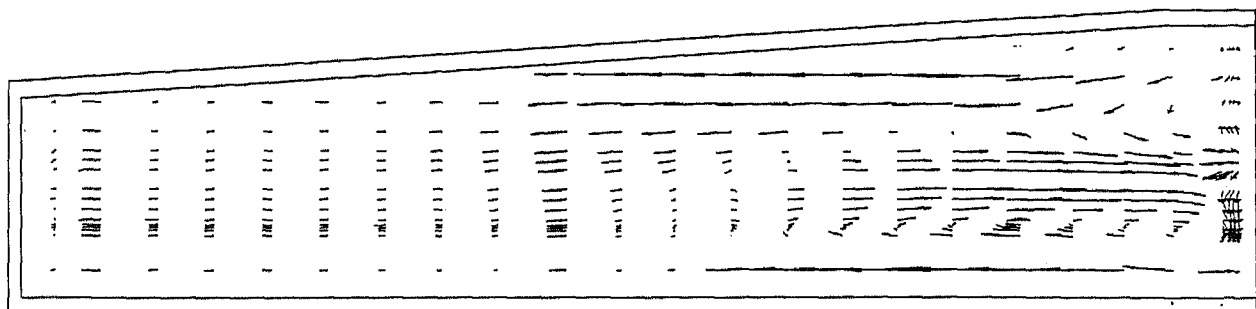


(d)

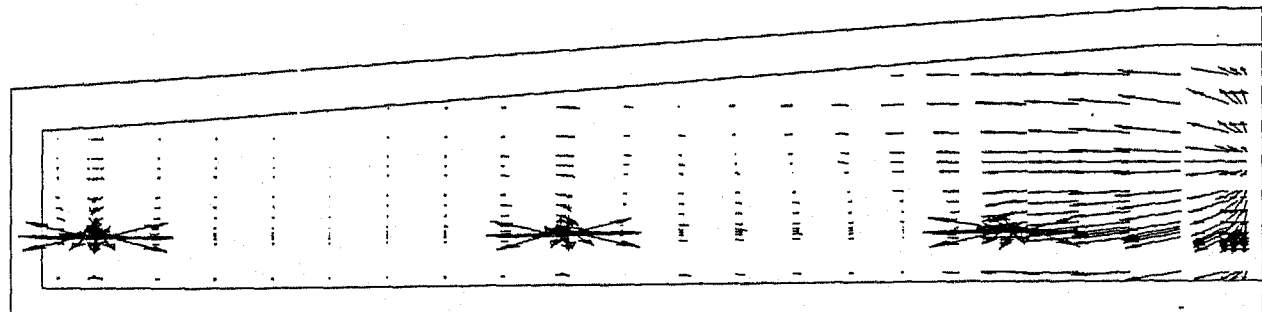
Fig.(3.24) Predicted flow field in six strand full scale tundish (no baffle) in longitudinal vertical planes at dimensionless distance z/W of (a) 0.40 (b) 0.3 and (c) 0.4(d) 0.15



(a)



(b)



(c)

Fig.(3.25) Predicted flow field in six strand water model tundish (no baffle) in transverse horizontal planes at dimensionless height y/H of (a) 0.05 (b) 0.50 (c) 0.95

0.60 m/s

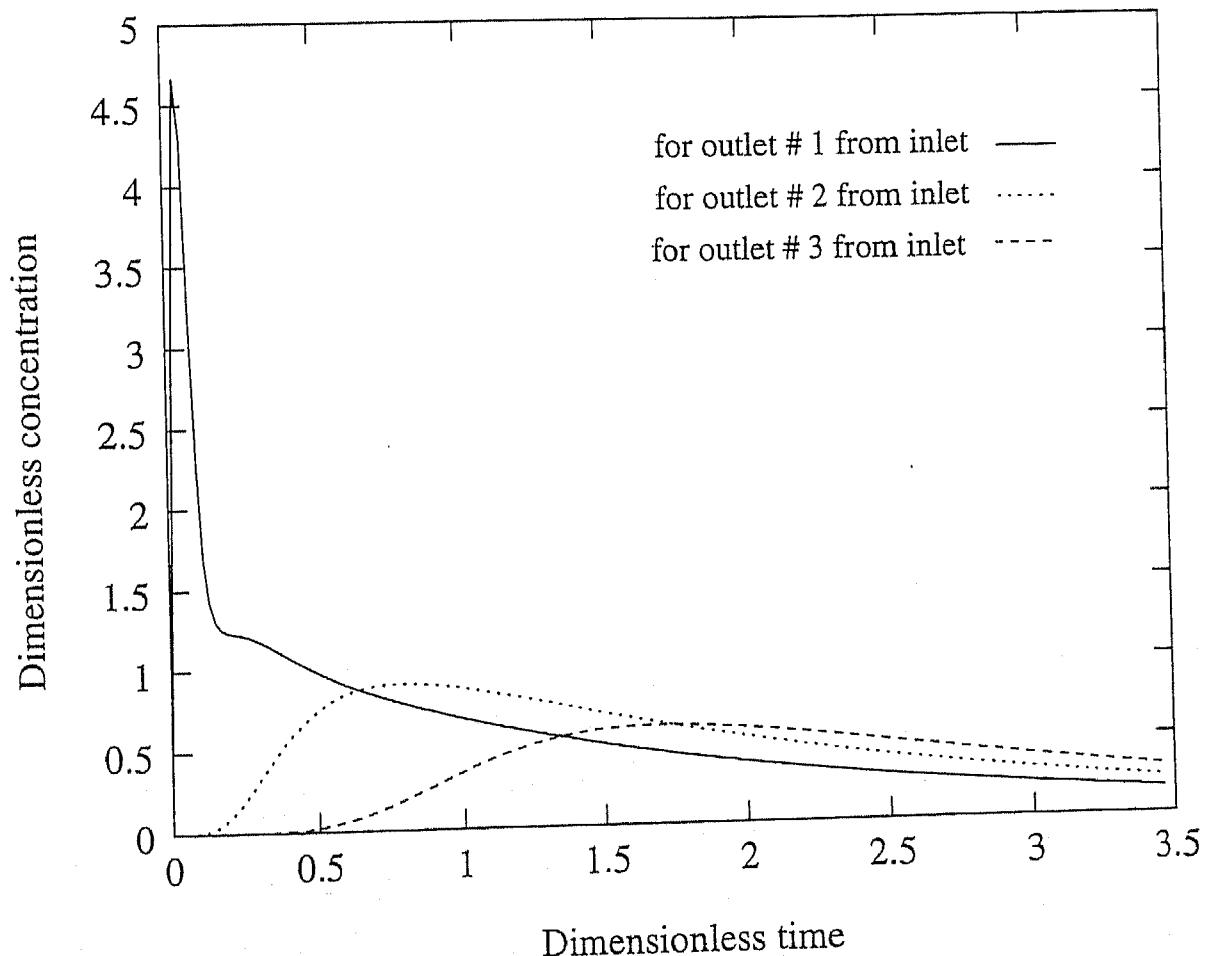


Fig.(3.26) Comparison of RTD for six strand delta shaped tundish without baffle for different outlets

Table 3.7 : Comparision of predicted and experimentally observed values of minimum breakthrough times for different outlets of six strand delta shaped water model tundish

Exit nozzle	RTD characteristics	Prdiected values	Experimental values
1	Minimum break through time	2 sec	4 sec
2	Minimum break through time	18 sec	20 esc
3	Minimum break through time	100 sec	120 sec

CHAPTER 4

CONCLUDING REMARKS

The following three major conclusions can be derived from the present study:

- (i) A steady state, three dimensional, two phase, turbulent flow calculation procedure has been developed in Cartesian coordinate system adopting the control volume based finite difference procedure in conjunction with the *SIMPLE* algorithm of Patankar and Spalding. The calculation procedure developed has been tested against several bench mark solutions to essentially demonstrate its adequacy and appropriateness.
- (ii) The model has been modified through incorporation of cell porosity technique for flow and RTD simulation in three different designs of tundish which are most commonly encountered in the steelmaking industry.
- (iii) RTD predictions for all tundish geometries have been compared with equivalent experimental results published in the literature and good agreement has been achieved.

CHAPTER 5

RECOMMENDATIONS FOR FUTURE WORK

The scope of the present work can be further expanded considering the following:

- (i) The two phase, three dimensional, turbulent flow model which has been developed in the present work can be suitably modified to carry out equivalent computations in polar co-ordinate system. The code can then be used to simulate a variety of metallurgical processes such as, asymmetric gas injection in vessels, side blown converters, *R.H* degassers and so on.
- (ii) The influence of temperature variations on fluid flow (free convection affects) has been neglected in the present study. Integration of heat transfer aspects to the present model will enable it to predict the affect of temperature losses or auxiliary heating on fluid flow. Similarly, appropriate form of Maxwell equations can be incorporated in the body force terms of the Navier-Stokes equation in the present model, to study the affect of magnetic field on fluid flow in metallurgical tundishes and its resultant influences on the tundish efficiency.
- (iii) The gas injection device is to be incorporated in conjunction with appropriate flow modification devices (dam and weir). Instead of a single bubbler, a set of bubblers is to be considered in the model to investigate the benefits of gas injection.
- (iv) Extensive numerical trials are to be carried out to study the influence of grid size, incremental time step and the distance of the near wall node on the predicted results. Similarly, under relaxation, solution of the discretisation equations etc. are to be looked at more rigorously to enhance the computational efficiency of the calculation procedure.

developed.

REFERENCES

1. A.W.D. Hills : Heat and Mass Transfer in Process Metallurgy, The Institute of Mining and Metallurgy, London, 1967.
2. J.Szekely : Metall. Trans. B, Vol 19 B (1988), p 525.
3. F. Kemeny, A. McLean, T. R. Meadowcroft and J. D. Young, Proc. Process Tech. Conf., 1981, Vol. 2, p. 232/45.
4. Y. Sahai and R. Ahuja, Iron and steel making, 1986, Vol. 13, p. 241.
5. T. Robertson and A. Perkins, Iron and steel making, 1986, Vol. 13, p. 241.
6. Y. Sahai and M. D. Burwal, Proc. Steelmak. Conf., 1992, p 469.
7. Liu Xintian, Zhou Yaohe, Shang Baolu, and Jiag Weiming , Ironmaking Steelmaking, Vol.19, 1992, p 221.
8. S. Singh and S. C. Koria Iron and steel making, 1993, Vol. 20, p. 221
9. S. Joo and R. I. L. Guthrie, Met. Trans. B, vol. 24B, 1993, p 755.
10. F. Shen, J. M. Khodadadi, S. J. Pien, and X. K. Lan, Met. Trans. Vol. 25B, 1994, p. 669.
11. D. Mazumdar, G. Yamanoglu, Ramani Shankarnarayanan and R.I. L. Guthrie, Steel Research, 66(1995), p. 14.
12. Y. Sahai and Toshihiko Emi, ISIJ Inter. 36(1996) No.6, p. 667.
13. D. Mazumdar, G. Yamanoglu, and Roderick I. L. Guthrie, Steel research, 68(1997), p. 293.
14. J. Szekely and N. El-Kaddah, Steelmaking Conference Proceeding, 1986, p.761
15. O. J. Illegbusi and J. Szekely, in "Mathematical Modelling of Metallurgical Processes", Ed. J.W.Evans et al., p.409
16. K. Y. M. Lai, M. Salcudean, S. Tanaka, and R. I. L. Guthrie, Met. Trans. B, vol 17b, 1986, p. 449
17. K. H. Tacke and J. C. Ludwig, Steel research 58 (1987), No. 6, p. 262
18. Y. He and Y. Sahai, Met. Trans. B, vol. 18B, 1987, p. 81.
19. O. J. Illegbusi and J. Szekely, Steel Research 59 ,1988, No. 9, p. 399.
20. O. J. Illegbusi and J. Szekely, Iron and steel making, 1989, Vol. 16, p. 110
21. O. J. Illegbusi and J. Szekely, Steel Research 62 ,1991, No. 9, p. 193.
22. J. L. Yeh, W. H. Hwang, and C. L. Chou, Iron and steel making, 1992, Vol. 19, p. 501
23. S. Chakraborty and Y. Sahai, Met. Trans., vol 23B, 1992, p. 135.

24. S. Chakraborty and Y. Sahai, Iron and steel making, 1992, Vol. 19, p. 488.
25. S. Chakraborty and Y. Sahai, Met. Trans., vol 23B, 1992, p. 153.
26. S. Joo and R. I. L. Guthrie, Met. Trans., vol 24B, 1993, p. 767.
27. B. Kaufmann, A. Niedermayr, H. Sattler and A. Preuer, Steel Research 64 ,1993, No. 4, p. 203.
28. O. J. Illegbusi,ISIJ Inter. (1994) , p. 732.
29. C. Damle and Y. Sahai, ISIJ Inter. (1995), p. 163.
30. J.Szekely: Fluid phenomena in Metal Processing, Academic Press, (1971).
31. B.E.Launder and D.B.Spalding: Comput. Methods Appl. Mechan. Eng., 3 (1974), 269.
32. R.Clift, J.R.Grace and M.E.Weber: Bubbles, drops and particles, Academic press, London (1978).
33. F.M.White : Fluid Mechanics, McGraw-Hill KogaKusha, Tokyo, (1979).
34. S.V.Patankar: Numerical Heat Transfer and Fluid Flow, Hemisphere publishing corporation, NewYork, (1980).
35. W.Rodi : Turbulence Models and Their Application in Hydraulics - A State of the Art Review, University of Karlsruhe, Germany, (1980).
36. Moult,A., Spalding,D.B. and Markatos, N.C.G., Trans. IchE, Vol.57(1979), p-14.
37. Hwar,C.K., Richard,S.H., and Thomas, D.T, Journal of computational Physics, Vol.70(1987),p-439..
38. F.M.White : Fluid Mechanics, McGraw-Hill KogaKusha, Tokyo (1979).
39. F.M.White : Viscous fluid flow, McGraw-Hill, NewYork, (1974).
40. Chaitanya Bhanu: M. Tech. Thesis, Jan. 1997, IIT,Kanpur.

A

125719

MME-1997-M-ROB-MAP



A125719